1972

Transient Analysis of Multiple Solid-Fluid Reactions in an Adiabatic Fixed Bed Reactor: Removal of Sulfur-Dioxide From Flue Glass.

Sydney Bourgeois V., Jr
Louisiana State University and Agricultural & Mechanical College

INFORMATION TO USERS

This dissertation was produced from a microfilm copy of the original document. While the most advanced technological means to photograph and reproduce this document have been used, the quality is heavily dependent upon the quality of the original submitted.

The following explanation of techniques is provided to help you understand markings or patterns which may appear on this reproduction.

1. The sign or "target" for pages apparently lacking from the document photographed is "Missing Page(s)". If it was possible to obtain the missing page(s) or section, they are spliced into the film along with adjacent pages. This may have necessitated cutting thru an image and duplicating adjacent pages to insure you complete continuity.

2. When an image on the film is obliterated with a large round black mark, it is an indication that the photographer suspected that the copy may have moved during exposure and thus cause a blurred image. You will find a good image of the page in the adjacent frame.

3. When a map, drawing or chart, etc., was part of the material being photographed the photographer followed a definite method in "sectioning" the material. It is customary to begin photoing at the upper left hand corner of a large sheet and to continue photoing from left to right in equal sections with a small overlap. If necessary, sectioning is continued again — beginning below the first row and continuing on until complete.

4. The majority of users indicate that the textual content is of greatest value, however, a somewhat higher quality reproduction could be made from "photographs" if essential to the understanding of the dissertation. Silver prints of "photographs" may be ordered at additional charge by writing the Order Department, giving the catalog number, title, author and specific pages you wish reproduced.

University Microfilms

300 North Zeeb Road
Ann Arbor, Michigan 48106

A Xerox Education Company

Transient Analysis of Multiple Solid-fluid Reactions in an Adiabatic Fixed Bed Reactor: Removal of Sulfur Dioxide from Flue Gases

A Dissertation

Submitted to the Graduate Faculty of the
Louisiana State University and
Agricultural and Mechanical College
in partial fulfillment of the
requirements for the degree of
Doctor of Philosophy

in

The Department of Chemical Engineering

by

Sidney V. Bourgeois, Jr.
B.S., Louisiana State University, 1968
M.S., Louisiana State University, 1970
May 1972

DEDICATION

This work is dedicated to my wife, Loraine, and my parents, Sidney, Sr. and Juanita.

ACKNOWLEDGEMENT

The author extends his sincere gratitude to Dr. Frank R. Groves, Jr. for his guidance and advice during the course of this research. Special thanks also go to Dr. Albert H. Wehe for the interest and guidance which he extended to the author.

Support for this work was provided by traineeships of the National Defense Education Act, National Science Foundation, and National Aeronautics and Space Administration and assistantships granted by the Chemical Engineering Department. The author also wishes to express his appreciation to the Dr. Charles E. Coates Memorial Fund of the L.S.U. Foundation, donated by Mr. George H. Coates, for financial assistance in the preparation of this dissertation.

Sincere thanks are also extended to Mr. Wayne Kraus for use of his general CALCOMP plotter subroutine and to Mrs. Eleanor Thibodeaux for her assistance in preparing this manuscript.

Finally, the author remains deeply indebted to the many sacrifices made by his wife.

TABLE OF CONTENTS

LIST OF TABLES

LIST OF FIGURES

ABSTRACT

A complex model capable of simulating the transient, non-adiabatic operation of fixed bed reactors involving multiple solid-fluid reactions has been developed. Numerical integration of the resulting differential equations was accomplished by a predictor-corrector technique which was programmed in FORTRAN IV computer language. Analysis of sulfur dioxide removal from flue gases was performed by utilizing this model.

The mathematical model was derived for the following irreversible gas-solid reactions:

$$Cu_2O + 1/2\ O_2 \rightarrow 2CuO \qquad \text{(oxidation)}$$

$$CuO + 1/2\ O_2 + SO_2 \rightarrow CuSO_4 \qquad \text{(sulfation)}$$

These reactions have industrial importance in the removal of sulfur dioxide from flue gases. The unreacted-shrinking-core mechanism describes the progress of these two reactions within the spherical porous particles which serve to pack the bed. The Cu_2O was assumed to be dispersed evenly throughout the pellets. All three intraparticle resistances to mass transfer and a film resistance to heat transfer at the pellet surface were considered. The latter resistance was adjusted to account for internal thermal conductivity of the patticles. Temperature gradients within the particles had to be neglected in order to achieve tractable particle energy balances. Pore diffusion was described by an effective diffusivity which accounts for both Knudsen and ordinary molecular diffusion.

Mass flow in the pores due to surface migration and pressure differences was neglected. Accumulation of mass within the pores can be safely ignored, but accumulation of energy within the particles was included. Chemical reaction rates were described by n^{th} order type expressions. The frequency factor, activation energy, dependency upon the sulfur dioxide concentration, the heat of reaction, and verification of the shrinking core mechanism have been reported in the literature along with the experimental data from which they were determined.

Axial transfer of heat and mass by forced convection and accumulation of heat and mass have been accounted for in the bulk gas phase. Transfer of heat and mass between the two phases is based on film coefficients. Diffusion of heat and mass and radial gradients in temperature and concentration were assumed negligible in the bulk gas. Provision for heat removal at the wall has been included, however. Due to the low concentration of oxygen and sulfur dioxide, the mass velocity was considered constant and Fick's law was utilized to describe pore diffusion.

The model consisted of partial differential equations describing the bulk gas phase material balances, solid reactant material balances, and bulk gas phase and pellet gas phase energy balances which incorporate the analytical solution for the pellet gas material balances. The rate of solid reactant consumption was expressed in terms of the rate of shrinkage of the shrinking cores within the particles. Variation of gas density and effective diffusivity with temperature was rigorously accounted for in the

pellet pores. Temperature variation of the other physical properties was assumed constant in the derivations, but were allowed to vary in the numerical integration procedure.

The characteristic transformation reduced the original system of partial differential equations to a set of equations with derivatives in each equation occuring in only one direction. The accuracy of the numerical technique was established by comparing numerical results with those obtained from an analytical solution for a limiting case.

Rate controlling factors during transient, adiabatic operation were the pore diffusion and chemical reaction in the sulfation zone of the particle and the particle thermal conductivity. Reactor performance was strongly influenced by the size of the pellets, inlet flue gas temperature, and initial pellet temperatures. The ability of the pellets to exchange heat between portions of the bed via the flue gas was shown to be important. Starting with Cu_2O in the bed rather than CuO led to increased temperature rises but slower initial consumption of the sulfur dioxide.

Under the proper conditions, removal of sulfur dioxide from flue gases by fixed beds of Cu_2O was feasible. Maximum pellet diameter of 1/4", minimum inlet flue gas temperatures of 400°C and minimum initial bed temperatures of 440°C should result in breakthrough times of 20 minutes and temperature rises of 100°C.

CHAPTER I

INTRODUCTION

The numerous and increasing use of fixed bed reactors in industry has created a concomittant rise in the utilization of fixed bed mathematical models. Practical applications for these models can be found in the analysis of experimental data, optimal control, and "a priori" design of fixed bed processes. A typical commercial design study might include scaleup, optimization and stability analyses. Models contain many factors which vary with bed dimensions, thereby lessening experimentation in the scaleup from pilot plant to commercial reactors. Optimization and stability analyses are also enhanced by accurate models. The transient response of a process to perturbations is required in obtaining quantitative conclusions with regard to stability, and a model facilitates the use of mathematically oriented optimization techniques. In the analysis of experimental data, a model may help explain an observed reaction rate in terms of basic kinetic mechanisms and transport phenomena. Proposed kinetic mechanisms are inserted in the model and a comparison between experimental results and model predictions determines their validity. The optimal control for a nonlinear fixed bed process can be obtained by simulation of the reactor under various control schemes. Thus the ability to predict the transient concentration and temperature profiles within fixed bed reactors is basic to their deisgn.

The purpose of this thesis is to study a fixed bed reactor of

The moving bed processes are discussed further in Section 2.3.2 of Chapter II.

Parsons et al (35) have compiled a voluminous work on the applicability of metal oxides for removing sulfur dioxide from flue gases. Economic analyses were performed on a fluidized bed process involving the following typical operating conditions:

sorber inlet temperature = 613°F = 323°C

sorber inlet SO_2 concentration = 0.003 mole fraction

sorber inlet pressure = 14.7 psia

sorber pressure drop = 4.28 in. H_2O

sorber outlet SO_2 concentration = 0.00015 mole fraction

regenerator inlet temperature = 1377°F = 747°C

This document (35) formed the basis for the article by Sladek et al (40). It contained thermodynamic screening to determine which metal oxides had the capacity to lower the SO_2 concentration to a specified level while forming a solid product which could be regenerated thermally by small amounts of energy. Further screening of oxides was accomplished by experimental studies to determine which of the thermodynamically favorable candidates had feasible rates of reaction. Only the oxides of copper and iron possessed rates of reaction rapid enough for significant solid conversion. Copper was utilized throughout the remainder of the study due to its better defined stoichiometry.

The sorption cycle of a fixed bed process based on operating features of the Shell process and the moving bed studies (35,40)

will be simulated in the present investigation. Critical parameters of interest are the maximum temperature rise in the bed and the exit SO_2 concentration. The sorption reactions are exothermic (see Appendix B-7), and the maximum temperature attained in the bed will have to be controlled to prevent degradation of the inert carrier and the sorbent. The exit concentration will be analyzed using breakthrough time. This is the elapsed time required for the exit concentration to reach a specified level after feed is introduced to the bed. When removing an impurity, the breakthrough concentration is usually determined by the maximum concentration specified for that component. Analysis of breakthrough is facilitated by use of breakthrough curves, which are graphs of exit fluid phase concentration versus time.

Also of interest when comparing alternate operations is the bed loading at breakthrough, which is the fraction of the solid phase utilized (sulfate versus oxide in this study). The bed loading can be related to the bed efficiency which is the cummulative fraction of SO_2 removed from the flue gas since its initial introduction in a sorption cycle.

Wen and Wang (49) state that the shrinking core mechanism describes SO_2 sorption accurately, and it will be utilized. The model will be derived as generally as possible so that it can be applied to other systems having similar reaction mechanisms.

The next chapter contains a discussion of fixed bed modelling techniques and the shrinking core mechanism, a review of the published fixed bed reactor models, and a survey of flue gas

sorption involving regenerable solids.

A derivation of the quasilinear partial differential equations which describe the transient operation of the fixed bed chemical reactor under study is presented in Chapter III. The equations are developed in a general manner, and then justifications for various simplifications are given. The characteristic transformations are also introduced in this chapter. Chapter IV discusses and presents solutions to these differential equations. A numerical solution algorithm based on the predictor-corrector technique is developed and an analytical solution based on the Legendre transformation is given for a special case (diffusion controlling the overall reaction rate). A comparison between the results of the numerical and analytical solutions and results for the solution of the general case are presented in Chapter V. The effects of inlet and initial conditions, flow rate, pellet diffusion, and bed and pellet dimensions are investigated.

CHAPTER II

LITERATURE SURVEY

2.1 Fixed Bed Modelling

To model a process rigorously, one must incorporate as many of the important physical phenomena involved as possible. A model for a fixed bed chemical reactor might include axial and radial energy and mass transfer due to forced convection and/or diffusion of the fluid, interparticle heat transfer by conduction and radiation, film transfer of heat and mass through the boundary layer surrounding the pellets, intraparticle heat conduction and mass diffusion, and the chemical reaction on the solid surface.

These phenomena and their interactions are illustrated in Figure 1. Parallel lines in either the pellet phase or the fluid phase consisting of the intersticial voids between pellets indicate that the transfer phenomena identified by these lines occur in parallel. In other words, they can occur simultaneously, whereas the intrapellet and film transfer phenomena occur in series. The mass or energy must be transferred across the film resistance in order for the pore diffusion mechanism to transfer the fluid or energy to or from the interior reaction site. In some cases, the chemical reaction and diffusion within the pellet occur in parallel rather than in series as shown in Figure 1, which means that chemical reaction occurs homogeneously throughout the pellet rather heterogeneously at a particular reaction site within the pellet respectively. The transfer of sensible energy due to the bulk movement of mass is also included in the diagram. Although not accounted for in this

Figure 1. Modes of Energy and Mass Transfer in Fixed Bed Reactors.

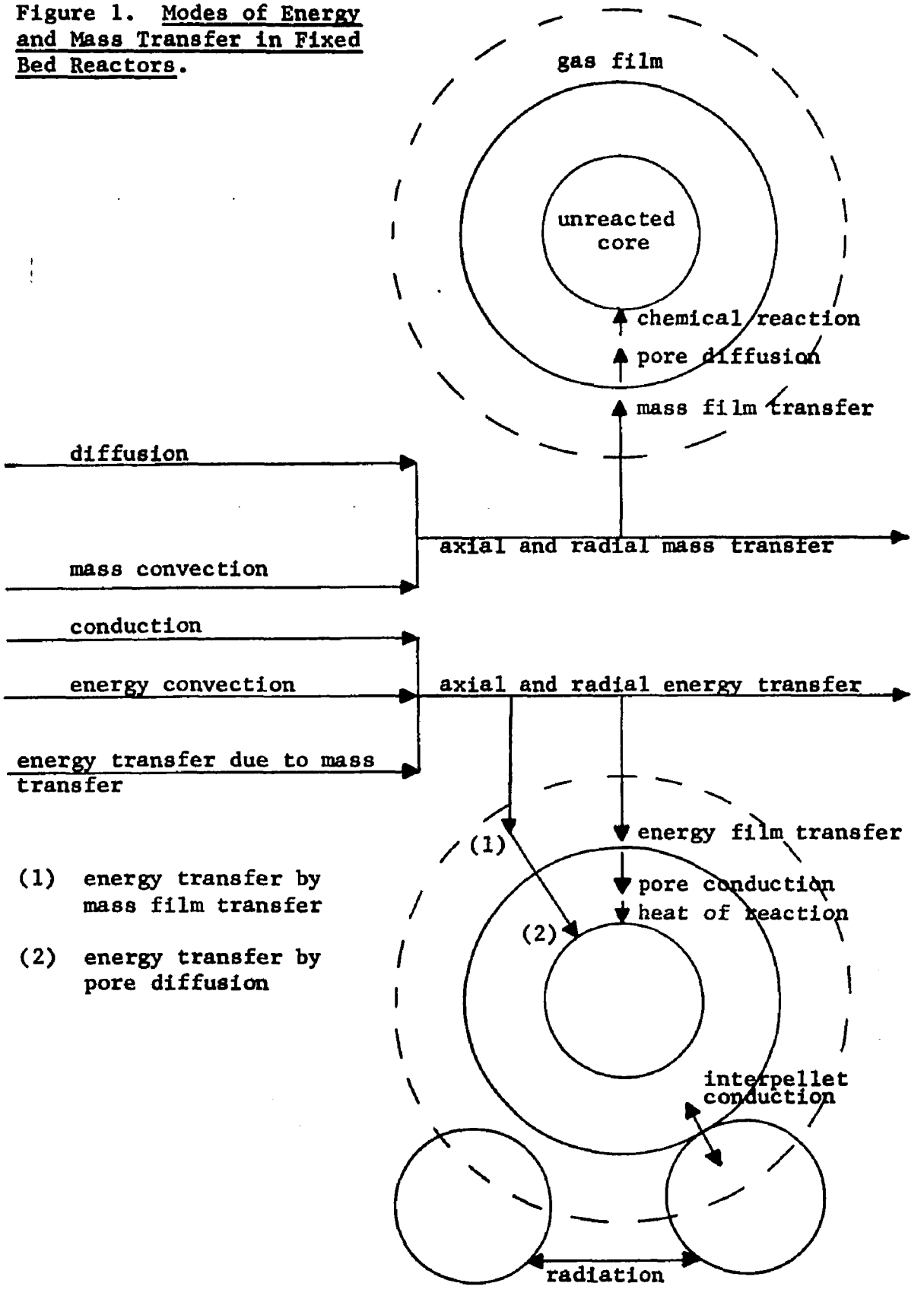

(1) energy transfer by mass film transfer

(2) energy transfer by pore diffusion

figure, the accumulation of energy and mass in both the pellet phase and the bulk fluid phase are other important physical phenomena which must be accounted for in certain applications of fixed bed reactors.

The manner in which the reaction proceeds inside of the porous solid phase may also be a significant factor in the performance of the reactor and special attention must be directed to incorporate this phenomenon into the model. The interaction of the diffusion and chemical reaction determine this solid reaction mechanism. For solid-fluid reactions, Wen (46) has classified the mechanisms and termed the two limiting cases as heterogeneous reaction and homogeneous reaction. In the former, the zone of reaction inside the pellet is restricted to the interface between the inner unreacted solid reactant and the outer product or "ash" layer. The shrinking core model of Yagi and Kunii (20,46) accurately describes this case which occurs when the porosity is small or the chemical reaction rate is rapid compared to the diffusion. Conversely, when the porosity of the solid is large and the solid reactants are distributed homogeneously throughout the solid phase, reactions between the fluid and solid occurs homogeneously throughout the solid. This regime Wen terms the homogeneous reaction. In actuality a combination of these two extremes may exist, as a particle may initially undergo homogeneous reaction and later convert to the shrinking core.

In addition to accuracy, the model has to be practical and tractable. It is relatively easy to account for all of the aforementioned rate processes and develop a very complex model,

but such a model is useless if the resulting system of equations is unsolvable. Thus, the goal of the reactor design engineer is to obtain a balanced model. The optimum arrangement is the most complete model which can be solved with an economical amount of equipment and time while simultaneously matching the performance of the pilot-plant or commercial reactor.

The mathematical simulation of fixed beds can be approached in a variety of ways. Lamb and Wilhelm (18) have classified fixed bed models into either the deterministic or stochastic categories with the former including the continuum and discrete approaches. In the continuum approach, the model consists of partial differential equations which are developed by applying the energy, mass and/or momentum conservation balances to appropriate differential elements of the bed. The fluid properties in the intersticial pellet voids are considered to vary continuously throughout the bed when deriving conservation equations in the bulk fluid phase. The fluid properties are taken as constant along the length of a pellet, however, when considering conservation balances in the pores of the solid packing (two phase models). In some cases, the bed is assumed to be composed of one pseudohomogeneous phase (36), and effectiveness factors are utilized to adjust the true reaction rate for intraparticle and film effects (one phase models). When the heat and mass transfer resistances at the pellet surface are significant, separate balances on the solid and fluid phase are necessary however. The most widely used and accurate discrete approach is the mixing cell or finite stage model first developed

by Kramers and Alberda (18) for one space dimension and later generalized by Deans and Lapidus (10) for the two-dimensional case. The mixing cell theory approximates a packed, tubular vessel by a sequence of finite, stirred tanks or cells - it considers interstices between pellets as a series of interconnected perfectly mixed stages.

Each cell is considered to be ring-shaped with length and width approximately equivalent to the pellet dimensions. They are arranged concentrically and in longitudinal layers with each successive longitudinal layer offset by half-widths so that each cell has inlets from two adjacent cells in the preceding layer and outlets to two cells in the next layer. Flow is only taken in the axial direction with radial effects being approximated by the radial coupling of cells in adjacent axial layers. For a reactor containing intraparticle resistances, each ring-shaped cell of fluid surrounds a "typical" spherical solid cell describing effects in the pellets, or a solid cell can be split between adjacent longitudinal layers; i.e., small functional variations over a particle length are assumed. Use of the finite stage model renders differential-difference equations (26) or difference equations (10) rather than differential equations. It can be used only when the fixed bed Reynold's number exceeds 100.

Two types of stochastic models were also presented. The first or "purely stochastic" model is developed by considering the stage size variable in a mixing cell model based upon matching stage sizes with the size distribution of void spaces in the bed. The "random perturbation" model is attained by using a deterministic model to compute concentration and temperature patterns while considering

random variations in the size and position of voids within the bed as sources of perturbations in these patterns.

Use of either of the stochastic models should yield a more accurate simulation than the deterministic models since packed beds exhibit stochastic rather than deterministic behaviour. These models are very difficult to implement and require more experimetal data (imformation on structure of bed void spaces) than the deterministic models however. The "random perturbation" model has only been applied to beds of dumped spheres with no reaction occuring. Thus, these stochastic models are impractical at present. Considering the bed as a single hypothetical phase is reasonable when the pellet and fluid temperatures are equivalent and the chemical reaction rate controls. In comparison to continuum models, the mixing cell model reduces time of computation, especially when the effects of axial dispersion and radial diffusion of heat and mass and/or thermal radiation are incorporated, and is more appealing since it is a heterogeneous, discrete system similar to the hetergeneous bed. Conversely the continuum approach presents a contradiction in that the model is discrete when considering particles but a continuum for the intersticial fluid. Furthermore, the mathematical system itself is a continuum but numerical solutions are often required which contain space increments less than the diameter of a particle. Physically, the assumption of negligible variation across the pellets when deriving the pellet equations may be grossly in error, since systems with rapid highly exothermic reactions may contain large gradients in the space of a particle diameter. The mixing cell

models also utilize this last assumption however. It should also be pointed out that mixing cell models have one other advantage over continuum models. In order to obtain tractable solutions to continuum models which incorporate intraparticle diffusion effects, the pseudosteady state approximation (5,7,46) usually has to be made. In this approximation the accumulation of energy and/or mass of the fluid in the pellet pores is considered negligible in comparison to the rate of reaction in the pellet. Mixing cell models can incorporate the completely transient pellet conservation equations, since the system of equations to be solved vary from algebraic equations in the steady state case to ordinary differential equations in the transient analysis.

In conclusion, the continuum approach is used overwhelmingly in fixed bed reactor modelling since the mixing cell model is very difficult to implement, especially when intraparticle resistances and nonlinear reactions are included. At present McGuire and Lapidus (26) have developed the most complete finite stage model by including film, pore and reaction resistances in the pellets. Even the steady state solution required a prohibitive amount of IBM 7090 time however. Mixing cell models are in order only when radiation or diffusion of mass or energy is an overiding transfer phenomenon.

2.2 Literature Fixed-Bed Models

Once a model is developed, a suitable solution algorithm, analytical or numerical, must be devised. Many models and their

algorithms have been published, but the specific assumptions and simplifications performed often are not explicitly stated. A review of these studies will help to determine the optimum balance between accuracy and practicality required and illustrate the need for the present investigation.

Table 1 lists some of the pertinent published work in the field of fixed bed reactor design and summarizes the various physical processes included in each study. Table 2 is a similar synopsis of single pellet studies which consider spherical pellets in a gas stream of constant composition utilizing the shrinking core model. Table 1 is divided into two sections with the first consisting of fixed bed design incorporating the homogeneous reaction in the solid phase and another on fixed bed designs incorporating the shrinking core meachanism for reaction in the solid phase. The references in each section and in Table 2 are arranged in chronological order and are identified according to their sequence in the bibliography. The model type refers to whether the system was simulated using the continuum (C), finite stage (FS), or stochastic (S), approach. The significant transfer phenomena included in the model under both categories of Table 1 are in addition to the axial convection of energy and mass, while those listed in Table 2 are inclusive since intersticial fluid phase phenomena do not apply. The various symbols utilized in Tables 1 and 2 to describe the transport phenomena are identified at the end of Table 2. The physical property variation is with respect to temperature and not concentration. The abbreviation CTX under the solution method heading indicates that the characteristic transformation was utilized. This transformation

TABLE 1

Published Fixed Bed Reactor Models

Reference	Model Type	Transfer Phenomena* Mass	Heat	Reaction Rate	Physical Property Variation	Solution Method
			#1: Homogeneous Solid Phase Reaction			
(42)	C	CR	CR	constant	constant	Graphical(CTX)
(1)	C	A	F,A	linear rev.adsorp.	constant	Numerical(CTX)
(10)	FS	AD,RD,CR	AD,RD,CR	irrev.1st order	Ahrrenius "k"	Numerical
(21)	C	F,CR	F,CR	irrev.1st order	Ahrrenius "k"	Numerical(CTX)
(15)	C	CR	CR	empirical 1st order	constant	Analytical
(18)	S	AD,RD	AD,RD	no reaction	constant	Numerical
(13)	C	CR	CR	fn(conc.,temp)	constant	Numerical
(23)	C	F-P-A	isothermal	linear rev.adsorp.	constant	Semi-Analytical
(26)	FS	AD,RD,F,P,CR	AD,RD,FP,CR	irrev.1st order	Ahrrenius "k", ρ_g.	Numerical
(43)	FS	AD,F,CR	AD,R,F,CR	irrev.1st order	Ahrrenius "k"	Numerical
(11)	C	F,A	isothermal	linear irrev.adsorp.	constant	Hybrid Comp.
(32)	C	CR	CR	"k" * (solid conc) * (fluid conc)	Ahrrenius "k"	Semi-Analytical (Legendre Transf.)
(15)	C	CR	CR,wall cooling	irrev. 1st order	Ahrrenius "k"	Anal.Comp.(CTX)

* See Nomenclature Key of Table 2.

TABLE 1 (Cont'd)

Published Fixed Bed Reactor Models

Reference	Model Type	Transfer Phenomena* Mass	Heat	Reaction Rate	Physical Property Variation	Solution Method
		#2: Shrinking Core Solid Phase Reaction				
(31)	C	F,P	F,CR	not limiting	vary in algorithm only	Numerical
(29)	C	F,P,CR	isothermal	irrev.1st order	constant	Numerical (CTX)
(38)	C	F,P	isothermal	not limiting	constant	Numerical (CTX)
(6)	C	F,P,CR	isothermal		constant	Semi-Analytical
(33)	C	F,P,CR	isothermal		constant	Semi-Analytical
Present Study	C	F,P,CR	F,CR	multiple reactions, 2nd order	vary in algorithm	Num.(CTX) and Anal.

* See Nomenclature Key, of Table 2.

TABLE 2

Single Pellet Studies Using Shrinking Core Model

Reference	Transfer Phenomena: Mass	Transfer Phenomena: Heat	Multiple Reactions	Reaction Rate(s)	Physical Property Variation	Solution Method
(39)	F,P,CR	F,P,CR	No	irrev.1st order	Ahrrenius "k"	Numerical
(46)	F,P,CR	isothermal	No	irrev.zero, 1st, and 2nd order	constant	Anal.and Num.
(22)	F,P	F,P,CR	No	not limiting	constant	Analytical
(49)	F,P,CR	F,R,P,CR	Yes	irrev.1st order	De,ρ_g,"k"	Anal.and Num.
(47)	F,P,CR	isothermal	Yes	irrev.zero or 1st order	constant	Analytical
(48)	F,P,CR	F,P,CR	Yes	irrev.zero or 1st order	De,ρ_g,"k"	Analytical

Nomenclature Key (Tables 1 and 2):

CR = chemical reaction or heat of reaction

F = mass or heat film transfer

AD = axial mass diffusion or heat conduction in bulk fluid phase

RD = radial mass diffusion or heat conduction in bulk fluid phase

RC = radial mass convection or heat convection in bulk fluid phase

R = radiation

A = adsorption or heat of adsorption

P = diffusion or conduction in pores

CTX = utilized characteristic transformation

will be described in the next chapter. Furthermore, the models will be assumed to represent unsteady state, unless stated otherwise.

The early work by van Deemter (42) and the more recent studies of Johnson et al (15) and Gonzalez and Spencer (13) are very simple single phase, one-dimensional models devised to analyze the adiabatic regeneration of coke-deposited catalysts by oxidation. They considered the chemical reaction to be the controlling step and utilized oversimplified rate expressions. The analytical solutions of Johnson and van Deemter predicted regeneration time, maximum temperature rise, and temperature and concentration profiles outside of the reaction zone satisfactorily, but failed to adequately describe the length of the reaction zone and temperature and concentration profiles in the reaction zone. Their results should be especially valid in low temperature regeneration since chemical reaction controls in this region, whereas pore diffusion controls at high temperatures (15,31,32).

Ozawa used a more realistic reaction rate in his low temperature coke regeneration model and obtained a semi-analytical solution by employing the Legendre transformation (32). He employed the quasisteady state approximation which assumes the accumulation of energy and mass in the intersticial fluid phase are negligible in comparison with the convective flow. Ozawa later generalized his solution technique (33) to obtain analytical or semi-analytical solutions to the quasilinear nonhomogeneous partial differential equations describing one-dimensional fixed bed systems provided that the nonhomogeneous term is separable in the dependent variables.

Bischoff (6) also presents a generalized technique applicable to the preceding system of equations. These two papers are listed in Section 2 of Table 1, but they apply equally to both sections. Through the use of the Legendre transformation, Ozawa derives his solution on a firmer mathematical basis than Bischoff who utilizes a "mathematical trick" based on hindsight. The "trick" involves guessing the solution form based on the results of solutions to similar problems. Bischoff's technique is easier to implement however. These techniques will be discussed further in Chapter IV where their applicability to unsteady state problems will be illustrated. Bischoff (6) and Ozawa (32,33) only applied their techniques to quasisteady state problems. Both of these methods can be applied to models incorporating either the shrinking core or the homogeneous solid phase reactions in which all three intraparticle resistances - film transfer, pore diffusion, and chemical reaction - are significant.

The analytical expressions of both Ozawa and Bischoff are implicit with regard to the dependent variables, however, and analytical inversion to develop the concentration profiles is usually impossible. A numerical inversion scheme is presented by Ozawa (32). In addition, both these techniques solve only the material balance equations for fixed bed systems. A method of incorporating the energy balance solution is developed for the particular homogeneous reaction system under study by Ozawa (32). Bischoff (6) presents methods for developing profiles of the bed-average amount of solid product and catalyst activity ratio

with respect to time. The catalyst activity ratio was defined as the bed-average effectiveness factor with time versus the initial bed-average effectiveness factor.

The utility of the method of characteristics in solving partial differential equations describing fixed bed operation was presented by Acrivos (1) in 1956. It was applied to a fixed bed adsorber in which adsorption, heat film transfer and heat of adsorption were significant. Various cases were studied including varying velocity, reversible adsorption, and multiple species of adsorbates. In addition to these cases, it was stated that the method of characteristics applies even when the flow rate varies, composition or temperature of the feed varies with time, density depends on composition and/or temperature, and the initial solid phase concentration is nonuniform. Thus, the method can always be used to reduce a set of quasilinear, totally hyperbolic partial differential equations to a set of nonlinear ordinary differential equations and will be used extensively in later chapters where a full explanation of the method will be presented.

The significance of pore diffusion in adsorption rate studies was studied by Masamune and Smith (23). Simple isothermal models with semi-analytical solutions were developed for each of the following mass transfer rates controlling: film transfer, pore diffusion, and linear reversible adsorption. Eteson and Zwiebel (11) utilize a simple isothermal model consisting of linear irreversible adsorption, film transfer, axial convection and constant physical properties to compare the efficiency of the hybrid computer

to that of the digital computer with regard to time and hardware. They concluded that the hybrid was better than most digitals of the time (1969) and indicated that it may be far superior for nonlinear problems. The IBM 360-40 was considered better, however, and the newest high storage, high speed digital machines would no doubt be competitive with the hybrid when solving the nonlinear problems. Another relatively simple model was presented recently to study hot spot control. Kardos and Stevens (15) use an irreversible first order highly exothermic reaction as the rate controlling step for heat and mass transfer and also consider removal of heat at the walls in developing a model to show that a control system for a packed bed reactor can be simulated on conventional analog equipment. They also employed the method of characteristics to simplify the system. Liu and Amundson (21) studied the stability of an adiabatic reactor involving film transfer and an irreversible exothermic first order reaction. The characteristic equations were solved with predictor-corrector and Runge-Kutta algorithms. Stability was found to depend upon existence of multiple stationary states for single particles.

All of the models discussed previously and those presented in the second section of Table 1 are one-dimensional and neglect axial and radial diffusion of heat and mass. These phenomena are included in the mixing cell models of Deans and Lapidus (10), McGuire and Lapidus (26), and Vanderveen et al (43). Each of these studies utilizes a single irreversible exothermic first order reaction in conjunction with an Ahrrenius temperature dependency for the reaction

rate constant. The remaining physical properties are considered constant.

As mentioned previously, McGuire and Lapidus (26) developed the most complex model in Table 1, but even the steady state solution was too expensive to obtain. Thus it was necessary to decrease the number of axial and radial cells which correspondingly reduced the accuracy of the model. The purpose of their study was to utilize the mixing cell model in analyzing reactor stability under perturbations in bed inlet conditions. Instability was defined as runaway temperature. The two-dimensional model of Deans and Lapidus included radial and axial gradients in concentration and temperautre, but intraparticle heat and mass transfer consisted of chemical reaction only. The more recent finite stage model of Vanderveen is intermediate in complexity to the two preceding models. It is a one-dimensional mixing cell model (axial variations in temperature and concentration) which accounts for radiation, diffusion and convection in the bulk fluid phase and film transfer and chemical reactions in the porous solid.

These studies (10,26,33) showed that the effects of diffusion and radiation in the bulk fluid phase tended to shift the reaction zone upstream, increase the time of transient behaviour, and decrease the possibility for multiple steady states. McGuire and Lapidus also found that the pseudosteady state approximation may yield misleading results in regard to stability when pellets are subjected to perturbations in the surrounding fluid temperature.

Lamb and Wilhelm's simple analysis (18) represented an initial

attempt to develop a stochastic model for fixed bed equipment. The model only considered axial and radial diffusion of heat and mass. Convection and reaction were not included, and the authors recommend use of the model only to estimate the variance of concentration and temperature at each point in the bed for this limited system.

While not listed in Table 1, the recent papers by Hlavacek (14), Paris and Stevens (34), and J. M. Smith (41) are excellent comprehensive articles in the general area of continuum modelling of fixed bed chemical reactors. Each gives insight into the need and utility of models, the significant physical phenomena which might be included in a realistic model, the interaction between these physical phenomena and chemical reaction, and the criteria which must be met in order to simplify models so that tractable solutions can be obtained.

Hlavacek (14) presents equations representing a cylindrical catalytic fixed bed reactor containing spherical catalyt pellets in which axial convection, axial and radial diffusion (conduction), external particle film transfer, pore diffusion (conduction) and chemical reaction at the catalyst surface contribute terms to the conservation of mass and energy. Chemical reaction consists of a single irreversible first order fluid reaction, $A \rightarrow B$. The single pellet equations, a two dimensional steady state model neglecting axial mixing of heat and mass, and a one-dimensional transient model neglecting radial concentration and temperature

variation are investigated. Justification of simplifications, recommended solution techniques, and criteria for stability are presented for each case. Paris and Stevens (34) examine continuum and discrete models, develop continuum equations for the phenomena included in Hlavacek's system plus the addition of radiation and radial convection of mass and heat, systematically investigate the effects of each of these phenomena seperately, and present justifications and limitations of the one dimensional model. This represents an excellent review article on fixed bed reactor modelling. J.M. Smith (41) discusses the need and utility of models in scaling up laboratory and pilot-plant reactors and makes several interesting observations:

1) The failure of a model to match experimental data may be due to inaccurate transport constants (especially intraparticle) rather than faulty models.

2) Published comparisons between models and pilot plant data are rare because data is rarely available.

3) A model is essential in designing commercial heterogeneous (fixed bed, slurry and fluidized bed) reactors and enables one to rapidly explore effects of critical parameters such as flow rate, initial temperature, particle size, and particle to bed diameter ratio.

Although these last three papers and others (10,15,18,21,26,43) in Table 1 deal with catalytic fluid reactions, their results can be applied to noncatalytic solid-fluid reactions because both cases involve adsorption on the porous solid and are therefore described by similar equations. In catalytic reactions, it is hypothesized

that the fluid reactants adsorb onto catalyst sites where the reactions occur and the product(s) then desorb. This is very similar to the steps in a solid-fluid reaction in which the fluid reactant is considered to be adsorbed by the solid reactant, the reaction occurs, and either the fluid products desorb or a solid stationary product is formed. Thus, additional mass conservation equations are necessary in fluid-solid reaction systems to describe the solid reactant concentrations. Comments on the bulk fluid phase equations and the transfer terms between this phase and the solids of either situation are especially applicable to each other.

K.E. Olson et al (31) and J. H. Olson (29) examined the high temperature regeneration of coke-deposited catalyst beds using the shrinking core model. The latter study considered all three intraparticle resistances to mass transfer in a transient, isothermal model and was solved numerically using the method of characteristics. Also this model was generalized and enabled consideration of irreversible adsorption problems. Olson et al (31) included intraparticle heat film transfer and heat of reaction in their study of an adiabatic reactor and assumed the rate of pore diffusion and mass film transfer were limiting in comparison to chemical reaction rate. Only the quasisteady state and stationary state were studied in this model however. The stationary state model consists of a moving coordinate in the combustion zone for the quasisteady state; that is, the dependent variables (concentration and temperature) in the combustion zone remain fixed with time with respect to this moving coordinate system. The movement of the combustion zone down the

bed is taken as constant and is a function of stoichiometry. This model gave accurate profiles only after long elapsed times, but resulted in a savings of computer time. The resulting equations for both the quasisteady and stationary states were solved using the Runge-Kutta-Gill method and the change of properties such as density, heat capacity, mass and heat transfer coefficients, diffusivity, heat of reaction, and thermal conductivity with temperature was performed at each point in the numerical algorithm. The variation of physical properties was not rigorously accounted for in the derivation of the differential equations however. Nevertheless, this was the only study which contained the temperature variation of properties other than reaction rate constant as illustrated in the second-to-last column in Table 1. The present study incorporates the variation of density and diffusivity in deriving the differential equations and includes variation of properties with temperature in the numerical algorithm. Other studies (1,34) discuss qualitatively the physical effects and mathematical complexities generated by allowing physical properties to vary.

A continuum model of an isothermal fixed bed reactor characterized by a rapid, irreversible solid-fluid reaction influenced by film and pore diffusion of the fluid reactants in the solid is developed by Scott (38) in order to analyze the oxidation of hydrogen in a helium stream by copper dioxide (copper oxide + water = copper + adsorbed water). Using the shrinking core mechanism in conjunction with the pseudosteady state approximation, a pair of quasilinear first order partial differential equations are derived. The method of

characteristics is applied and the resulting pair of ordinary differential equations are solved numerically using a simple Euler formula. Fixed bed experiments were used to verify the kinetic model and consequently allowed determination of the mass transfer parameters. The model verification was obtained by comparing the S-shaped breakthrough curves generated by the computer and those obtained from the experimental data. Breakthrough curves are simply a plot of exit concentration versus time and a study of the effects of flow rate, inlet concentration and temperature, and bed diameter on these curves was facilitated by the model. From this study a generalized chart useful in the design of any fixed bed system which follows the aforementioned reaction mechanism is developed. The chart consisted of a plot of breakthrough time versus a number characterizing external mass transport with an internal transport property number as another independent parameter. Breakthrough time is defined as the time when the exit concentration reached ten percent of the inlet concentration. This study also gives further proof that the use of spherical pellets in models renders accurate simulations for systems utilizing nonspherical pellets.

Among the single pellet studies of exothermic diffusion controlled solid-fluid reactions listed in Table 2, Luss and Amundson (22) present an analysis of the maximum temperature rise in a pellet and across the gas film surrounding the pellet using the shrinking core model. They include the heat capacity of the unreacted core in their model which is usually neglected in previous studies. Results indicate that theoretically, temperature rises

large enough to cause sintering of catalyst particles could occur. The potential temperature rise predicted by neglecting the heat capacity of the unreacted core proves to be too conservative.

The remaining works in Table 2 represent excellent state-of-the-art articles for intraparticle and external film rate phenomena in conjunction with the shrinking core mechanism in fluid-solid reactions. The early work of Shen and Smith (39) analyzes the interaction of diffusion and reaction by utilizing a single first order reversible or irreversible reaction with an Ahrrenius reaction rate constant. An isothermal study is performed using a reversible reaction to develop conversion-time relationships using the pseudo-steady state approximation. The conversion of solid reactant is shown to be a function of time and two parameters which measure film and pore diffusion resistances. This was accomplished by solving the resulting ordinary differential equations analytically and then comparing the solution to experimental data. Similar relationships are developed numerically for the nonisothermal case where three additional transport parameters are required. The pseudosteady state approximation is applied to both the heat and mass balances, and stability for exothermic reactions is shown to be impossible in certain temperature regions.

In his classic papers (46,49) on noncatalytic heterogeneous solid-fluid reaction models, Wen presents a workable organization and arrangement sorely needed in this field. The classification of solid-fluid reactions commonly encountered was accomplished by two methods in the first paper (46). The following scheme represents

classification based on the phases in which the various species appear:

Solid reactant → fluid products	(I)
Solid reactants → fluid and solid products	(II)
Fluid and solid reactants → fluid products	(III)
Fluid and solid reactants → solid products	(IV)
Fluid and solid reactants → fluid and solid products	(V)

Classification according to the manner by which the reaction progresses, that is unreacted shrinking core, homogeneous reaction, or a combination of these two extremes, was discussed earlier. Examples of the many industrially important applications of these heterogeneous noncatalytic systems are given, and it is stated that relatively few studies are available on these systems. Reasons given for the lack of study and organization in this area are the intricate interactions among the rates of chemical reaction and rates of energy and mass transfer and the widely scattered applications of these models, such as in the leaching of ores, drying of porous particles, melting and freezing, crystallization, ion-exchange processes, and solid-fluid reacting systems.

Several other important rules and concepts are presented in the first paper (46). It has been shown that the order of solid-gas reactions varies from zero to two based on adsorption isotherms and on numerous experimental studies. The incorporation of varying particle size in the shrinking core model is illustrated in this paper and others (39,47,48,49). Geometrical instability and two types of thermal instability for exothermic reactions are described

in this paper and by Wen and Wang (49). Thermal instabilities can be caused by the effect of the solid reaction product in impeding the loss of heat or by the multiple intersection of the heat loss and heat generation curves when plotted versus pellet temperature. Geometrical instability occurs when the rate of reaction per unit area increases as the reaction interface penetration deepens and great uneveness of the reaction surface results. This latter instability can occur under both isothermal and nonisothermal conditions. Thermal instability can cause sudden transitions in rate controlling steps even when surrounding conditions remain constant (39,46,49).

The effectiveness factor for noncatalytic solid-fluid reactions is introduced (39,46,47,48,49). Its utility in describing geometrical instability and the transition in rate controlling steps concisely are illustrated when plotting it versus conversion of the solid reactant. During such transitions it is shown that use of the pseudosteady state may be misleading. The effectiveness factor and the concept of selectivity are utilized in analyzing multiple reactions in these systems (47,48,49). Three categroies of multiple reactions are analyzed - independent, parallel, and consecutive reactions. In each category the reaction rate is considered to be irreversible and zero or first order since only a single fluid reactant is involved in each reaction. The pseudosteady state is used in each study involving multiple reactions to assure tractable solutions.

In the nonisothermal studies of Wen and Wang (49) and Wen and

Wei (48), the diffusivity, gas density and reaction rate constant vary with temperature, and it is shown how the pseudosteady state approximation may be innacurate for the pellet energy balance. Criteria for obtaining high selectivities are presented in these studies (47,48,49), since selectivity is usually more important than rate of reaction in multiple reactions. Stability analyses are also performed.

Wen and Wang (49) mention that a single rate determining step is only a limiting case and that a solid-fluid process is usually simultaneously influenced by more than one step. The cases of intraparticle mass transfer controlling, chemical reaction controlling, and heat transfer controlling along with the three cases in which pairs of the previous phenomena are considered significant and the remaining phenomenon negligible are analyzed separately. Expressions for the effectiveness factor and the conversion-time relationships are derived for each case. Also for the case of all three of these phenomena being significant simultaneously, the influence of surrounding gas temperature, heat transfer around and within particles, gas film diffusion, and heat of reaction and activation energy on the effectiveness factor and thereby stability, is presented by way of graphs of effectiveness versus solid conversion with pertinent descriptive constants as parameters. It is also shown that radiation decreased the possibility of instability which agrees with the findings of Vanderveen et al (43) discussed earlier.

Criteria for validity of the pseudosteady state approximation

in both the energy and material balances are derived theoretically by Wen (46) for a single reaction system. For the material balance, it is shown to be valid for solid-gas systems except with very high pressures and extremely low solid reactant concentration. Its use in solid-liquid systems is not recommended. The approximation is also shown to be valid for the energy balance when solid heat capacity and intraparticle temperature variations are small in solid-gas systems. It may lead to errors during transistions in the rate controlling steps in solid-gas systems and for all solid-liquid systems however. Another important point stressed in this article is the lack of experimental studies for multiple reactions in noncatalytic solid-fluid heterogeneous systems.

Conclusions

None of the studies in Tables 1 and 2 consider multiple solid reactants involved in a mixed reaction system except the present study. By mixed reaction, the reactions do not fit the definition of an independent, parallel or consecutive system of reactions and must be described as a combination (mix) of the latter two. Furthermore, of the papers dealing explicitly with the shrinking core model or, for that matter, all of the continuum models, none includes heat effects when all three intraparticle resistances to mass transfer are simultaneously significant. The mixing cell studies incorporate this combination, but they exclude multiple reactions and nonlinear reactions. In addition, the complex mixing cell models which included most of the intraparticle effects (26)

required an extraordinary amount of computer time for their solution.

Thus, none of the fixed bed models, with the exception of the present study, treat multiple reactions or nonlinear reactions. Variation of physical properties besides the reaction rate constant with temperature is included only in some of the single pellet studies (48,49) and by Olson (31) and the present study in Table 1.

In conclusion, a void exists in fixed bed simulations. No tractable solution has been reported for the transient, variable property (with temperature) analysis of fluid-solid reactions with multiple solid reactants in which the shrinking core mechanism where all three intraparticle mass transfer resistances and heat effects are significant.

2.3 Removal of Sulfur Dioxide from Flue Gas

2.3.1 Sulfur Removal Processes

Sulfur dioxide has been recognized for a number of years as a major air pollutant (4,24,37,40,50) and is termed by some the worst industrial air pollutant (27). The magnitude of the problem is expressed by the fact that 34 million tons of sulfur dioxide were emitted into the U.S. in 1970 (24,50), and estimates are that three-fourths of this total was produced by electrical power plants burning fossil fuels. Due to the large increase in demand of electricity, the amount of sulfur dioxide exposed to the atmosphere is expected to quadruple by the end of the century (50).

Standards on maximum allowable SO_2 levels to be enforced in 1975 under the 1970 Clean Air Act and proposed new taxes on sulfur

emissions have generated increased interests in sulfur removal (50). The Environmental Protection Agency has recommended upper limits of 80 micrograms per cubic meter annual arithmetic average concentration and a 365 micrograms per cubic meter 24-hour concentration. Several alternatives currently under study to remove sulfur from gaseous effluents include the transition to natural gas or to low sulfur coal and fuel oil, desulfurization of coal and fuel oil before consumption by utilities, and flue gas desulfurization processes. Each have their relative merits and demerits, but it is the consensus that a successful process to remove sulfur dioxide from flue gas must be developed within the next several years.

At least fifty waste gas sulfur recovery approaches are being developed (37) at the present time. The basic flue gas desulfurization processes consist of wet scrubbing, adsorption, reaction with metals or metal oxides, reduction with gases or with carbon, and catalytic oxidation (4,37,40) to SO_3. The main criteria for each of these processes is that they reduce the ambient SO_2 concentration in a manner which is both commercially practical and economical. The goal set by most investigators to ensure reduction to a safe (and legal) level is 90 percent sulfur removal from the flue gas (45). Furthermore, emphasis has been applied towards recovery of a marketable sulfur compound since this would defray the cost of cleaning the flue gas. The most preferred final by-product mentioned is elemental sulfur (4,45) when no local market for sulfuric acid exists. Simultaneously, this would also ensure that one pollution problem is not being solved by substituting another; i.e.,

an air pollution problem is solved, but a solid waste disposal or water pollution problem is caused by the by-product. Thus processes which possess a regenerable reagent and a marketable by-product are very favorable.

Sladek et al (40) investigate flue gas sulfur removal by reaction with metal oxides enabling the use of thermal, rather than chemical, regeneration. The authors indicate that thermal regeneration should lead to operating cost advantages. Thermal regeneration consists of decomposing the sorbed sulfate to the metal oxide and sulfur trioxide at high temperatures. The solid-gas reaction is termed sorption and the solid reactants (metal oxides) are termed sorbents. These systems of nomenclature will be used interchangeably in the remainder of this study. The authors examine a moving bed process proposed earlier by Newell (27) which is shown in Figure 2 in conjunction with typical inlet conditions and optimal outlet conditions established by the authors. Flue gases usually contain nitrogen, water vapor, carbon dioxide, oxygen and sulfur dioxide with concentration of the latter species usually less than 3.5 and 0.3 volume percent respectively and are available at temperatures varying between 100 to 450°C (17,40). The maximum SO_2 content in the sorber effluent is set at 0.015 volume per cent and an upper limit of 750°C is chosen for the maximum temperature during the sorption cycle to prevent damage to the solid.

Reaction paths of various metal-oxygen-sulfur systems are developed through the use of published data and thermodynamic calculations. Thermodynamic requirements on the sorbent were

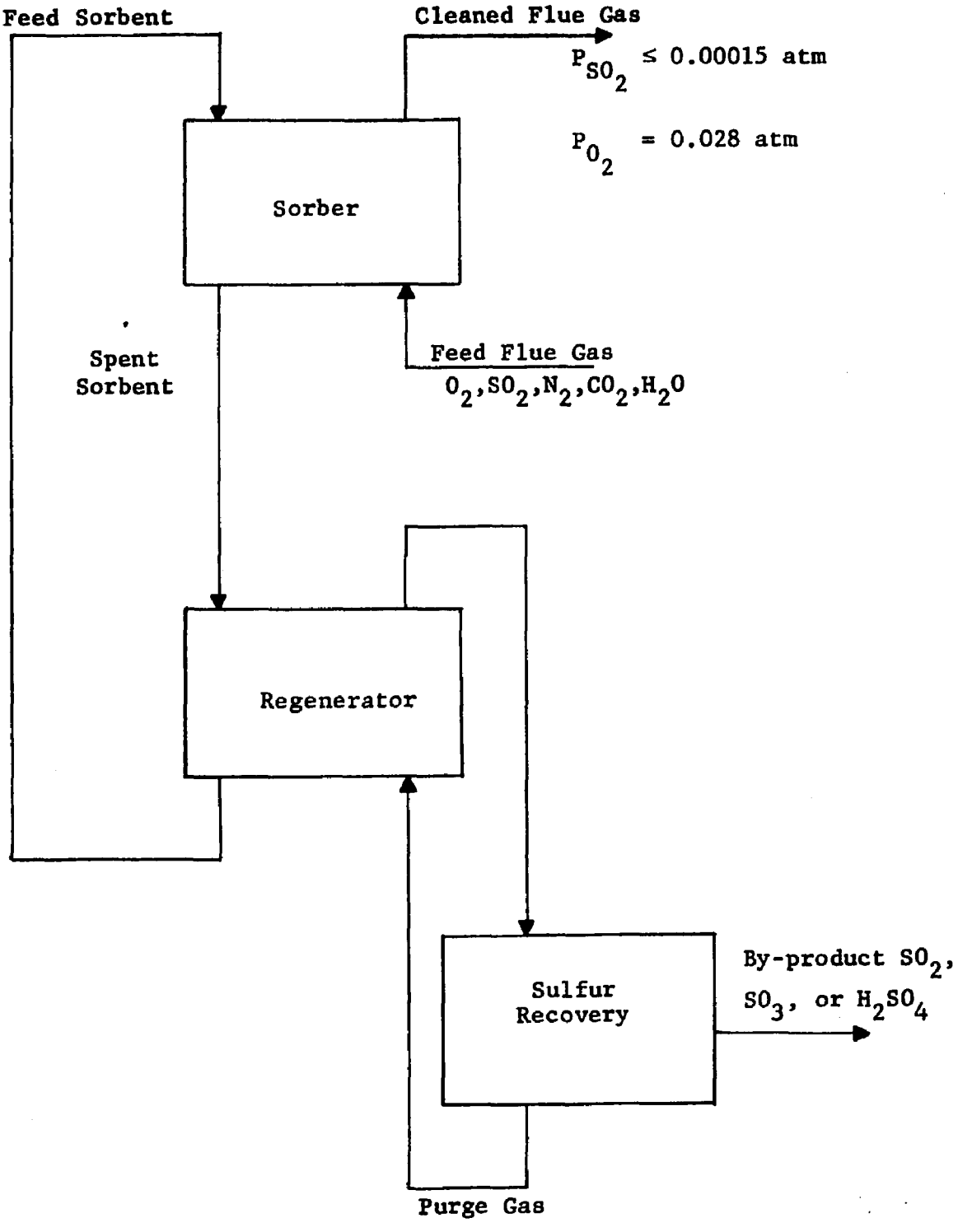

FIGURE 2. Typical Moving Bed SO_2 Removal Process

generated by the process criteria mentioned. Based on these reaction paths and thermodynamic requirements, the oxides of aluminum, bismuth, cerium, cobalt, chromium, copper, iron, hafnium, nickel, tin, thorium, titanium, vanadium, uranium, zinc and zirconium are shown to be favorable candidates. Possible by-products after thermal regeneration are sulfuric acid and high concentration (25%) SO_2 or SO_3 gas. Also, many possible reaction paths were investigated for both sorption and regeneration, but it was concluded that formation and decomposition of sulfates are the most likely reactions.

Bienstock et al (4) have compiled published information on the physical properties and chemistry of SO_2. Reactions with potential application to the problem of air pollution are emphasized. State-of-the-art discussions are presented for each of the flue gas sulfur recovery approaches mentioned earlier, and several of the most promising untried (at the time) processes are recommended. Among the highly feasible processes is the high temperature sorption of SO_2 by cupric oxide ($CuO + \frac{1}{2} O_2 + SO_2 = CuSO_4$) and thermal regeneration with dry air at 736°C ($CuSO_4 \triangleq CuOSO_3 \triangleq CuO + SO_3$).

Published data on sorption processes for flue gas sulfur recovery are rare. Godfrey, et al (12) analyze a moving bed sorption-regeneration cycle using alkalized alumina ($Na\,Al_2$), Norman and Wood (28) present sorption data and kinetic expressions using manganese oxide and alkalized alumina, and Bares et al (3) list fixed bed data on the reaction between solid sodium carbonate and sulfur dioxide.

2.3.2 Copper Sorbent

As mentioned in the first chapter, fixed bed sorption over copper pellets was chosen as the system to be studied. It was chosen for several reasons. Oxides of copper have great theoretical potential in comparison to other metal oxides and approaches (4,40) and have been proven commercially practical (45). Also, this system presents the opportunity to fill the void which currently exists in fixed bed simulations; i.e., the transient analysis of multiple solid reactants in fluid-solid reactions described by the shrinking core model where all three intraparticle mass transfer resistances and heat effects are significant.

The various reaction paths for the Cu-S-O system entail the following reactions (40):

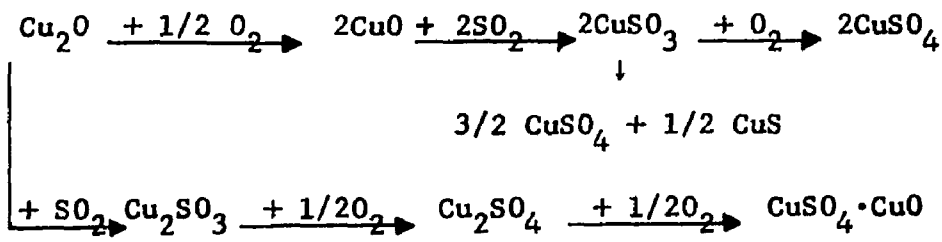

Parsons et al (35) have experimentally determined the temperature dependency and order of the reaction rate for the sulfation reaction

$$CuO + SO_2 + 1/2\ O_2 \rightarrow CuSO_4$$

using very small particles in order to minimize diffusion effects. A linear dependence on SO_2 concentration, an activation energy of 27 K cal/g.mole, verification of the shrinking core model with both diffusion and surface chemical reaction significant, and a

frequency factor of $4.27.10^{9}$ min^{-1} atm^{-1} were exhibited by the copper oxide system in the temperature range of 325 - 404°C. The authors note that an Ahrrenius plot (ln k vs. 1/T) for copper oxide exhibited a deviation at high temperatures. As mentioned previously, this may be caused by transition in rate controlling mechanisms. Thus a flexible model based on as many significant rate phenomena as possible would be very useful in analyzing such a system.

Their study also contains expressions for the heat of reaction for the sulfation reaction, heat of formation, and the heat capacity as functions of temperature for the various metal oxides and sulfates. Methods for preparing the pellets are discussed and pellet properties, such as density, surface area per unit weight, and dimensions are tabulated.

CHAPTER III

MODEL DEVELOPMENT

In the development of models the approach utilized will be to create the most general and complex simulation and then simplify the resulting system of equations. This will be accomplished by showing that under certain conditions some of the transfer phenomena can be safely ignored since an upper limit can be assigned to the terms describing their effects. In certain cases the equations may still be unsolvable and additional expedient simplifications may be accepted in order to obtain tractable solutions.

3.1 General Fixed Bed Model

3.1.1 System Description

Consider a cylindrical vessel randomly packed with uniform porous spheres. Each sphere is impregnated with a single solid reactant which is evenly dispersed throughout the pellet. The fluid flowing in the intersticial void space between pellets will be referred to as the bulk gas or external phase, while the immobile fluid in the pellet pores will be termed the pellet gas or internal phase. The continuum approach will be used and functional variations over an axial increment equivalent to a pellet sphere diameter will be considered negligible. Justification for the use of spherical pellets in the simulation, even though the bed may contain other shapes is cited in Appendix B-2.

Assume that the external phase is in fully developed turbulent flow. This criterion is satisfied for modified Reynolds numbers

exceeding 100 (10) where the modified Reynolds number, N_{Re}, is given as

$$N_{Re} = 2G\,R/\mu$$

where G = superficial mass velocity, g/sq.cm-sec.

R = pellet radius, cm.

μ = external viscosity, g/cm-sec.

This condition is verified in Appendix A-9 where the modified Reynolds number varies between 100 and 200. Transport of energy and mass in the external field is due to forced convection and diffusion (conduction of heat) in the axial direction.

The bulk gas stream contains fluid reactants which undergo irreversible exothermic reactions with the solid reactant. The overall reaction rate is determined by mass transfer of the reacting fluid species from the bulk fluid to the reaction site within the solid porous pellet, the reaction occuring on the interior surfaces of the solid, and energy transfer from the reaction site to the bulk fluid. Internal pellet phase mass transfer will include both diffusion through the external film surrounding each pellet and pore diffusion. Similarly, energy transfer between the reaction site and the fluid phase consists of conduction within the pellet and film transfer at the outer surface of the pellet.

The fluid consists of five components, O_2, SO_2, N_2, CO_2 and H_2O, which will be identified with subscripts 1 through 5 respectively throughout the remainder of this study. The stoichiometry to be used is that given by Sladek (40) and Bienstock (4) in Section 2.3.2 describing the irreversible exothermic reactions of cuprous oxide

with oxygen and sulfur dioxide as shown below:

Reaction I(oxidation):

$$Cu_2O + 1/2O_2 \rightarrow 2CuO$$

Reaction II (sulfation):

$$CuO + SO_2 + 1/2O_2 \rightarrow CuSO_4$$

which can be stated in general form as

$$\sum_{j=1}^{8} \gamma_{ij} A_j = 0 \qquad i = I, II$$

where

$\gamma_{i,j}$ = stoichiometric coefficient for the j^{th} component in Reaction i which is positive for products and negative for reactants

A_j = molar quantities of component j.

The component subscripts 6 through 8 represent Cu_2O, $CuSO_4$ and CuO respectively.

According to Wen and Wang (49) and Parsons et al (35), the foregoing fluid-solid reactions can be described by the shrinking core mechanism. A cross-sectional view of a partially reacted spherical particle would reveal three distinct layers - an outer layer of $CuSO_4$, an intermediate layer of CuO, and an unreacted inner core of pure Cu_2O. If Reaction I is much faster than Reaction II, the situation illustrated below results.

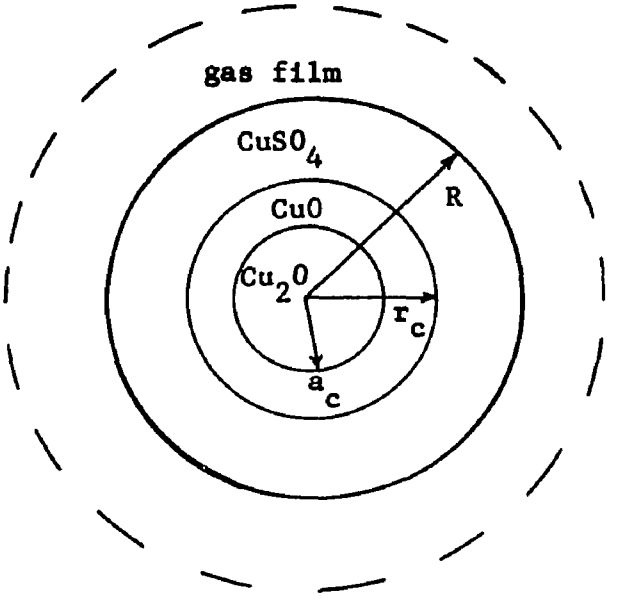

A sphere of radius R is surrounded by a gas film offering resistance to mass transfer. In the outer portion of the sphere, r_c to R, both reactions have occurred and in another section, a_c to r_c, only Reaction I has occurred. An inner core of unreacted pellets exists from the center of a pellet to radius a_c. Both the inner solid phase interface, a_c, and the outer solid phase interface radius, r_c, are moving inward with respect to time, while the pellet outside radius, R, is constant.

Gas phase concentration gradients exist in the external gas film due to diffusional resistance, and gradients also exist within the reacted solid phase of the pellet due to pore diffusion. Similarly a temperature profile may exist within a particle, and typical profiles for a partially reacted particle are given in Figure 3. For exothermic reactions the temperature at the center of the pellet

FIGURE 3

Pellet Concentration and Temperature Profiles

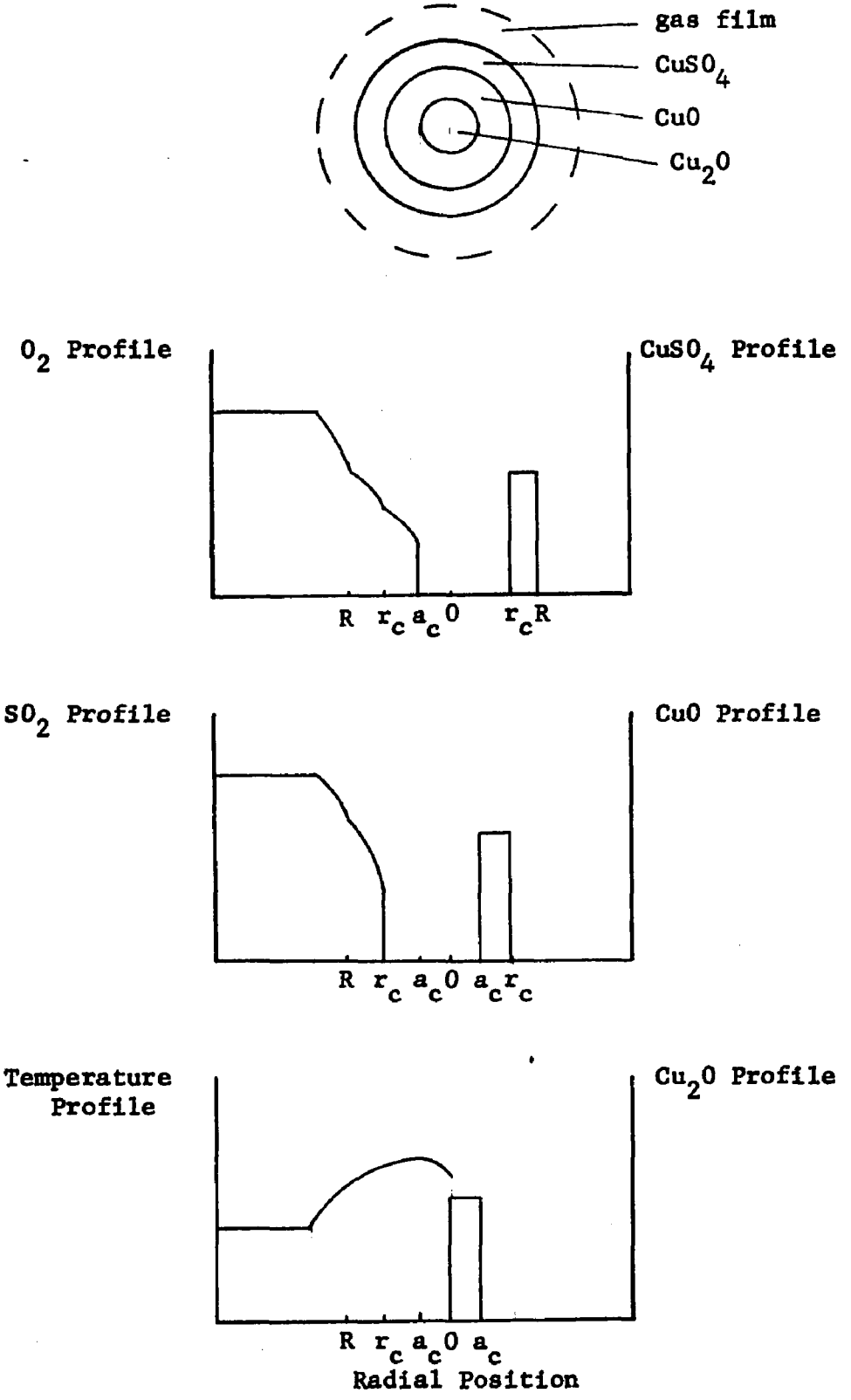

represents a minimum, and then increases with time. Once the maximum temperature of the pellet begins to decrease, the center temperature represents the pellet maximum and decreases with time. Thus the temperature profile in Figure 3 represents the pellet before the maximum temperature is attained and the heat of reaction for the oxidation reaction greater than or equal to that of the sulfation reaction. The latter assumption is verified in Appendix B-7.

Before deriving the conservation equations, all the assumptions implicitly stated in the preceding disucssion are summarized:

(1) Pressure drop across the length of the reactor is negligible so that momentum balances are unnecessary.

(2) Radial convection of energy and mass are negligible.

(3) Radial diffusion of mass and radial conduction of heat are negligible.

(4) Axial dispersion of heat and mass are negligible.

(5) Thermal equilibrium exists between the solid and gas in the pellet pores.

(6) Radial symmetry exists within each spherical pellet.

(7) Radiation and conduction of heat between adjacent pellets is ignored.

As mentioned previously axial pressure drop in similar full scale commercial reactors is less than 200mm of water (45). Radial convection is absent since the reactor operates adiabatically and no fluid is removed through the reactor walls.

Based on both theoretical and experimental evidence, Paris and Stevens (34) indicate that radial mass diffusion may be neglected for

modified Reynolds numbers exceeding 50. This criterion is satisfied in the present study, and radial temperature gradients are absent in adiabatic operation.

Additional arguments for neglecting radial terms even for the nonadiabatic case are presented (34). For streams with equivalent mean velocities, conditions for piston flow are simulated closer in a packed bed than an empty bed of the same dimensions because the pellets force fluid elements to split and intermingle constantly. Therefore temperature and concentration profiles are relatively flat in fixed beds. Even if radial gradients exist, the one-space dimensional form of the conservation equations can be used rigorously when only the mean concentration and temperature over a cross section of the bed are required. The mean values are of interest in most stability, hot spot control, and design studies. In this situation, nonadiabatic conditions are accounted for by simply adding a wall exchange term, $h(T_{gas}-T_{wall})$, to the energy balance. Experience indicates that radial temperature gradients are small except in a narrow annulus near the wall (34). The mean temperature therefore approximates the maximum temperature which is the temperature along the axis of the bed. Furthermore, tractable solutions for the transient bulk gas phase energy and material balances with radial mass and energy diffusion have not yet been developed. Thus the loss in accuracy in neglecting radial terms is amply compensated for by the great simplifications allowed in the numerical or analytical solution by reducing the number of independent variables from three to two.

Similar reasoning is presented (30,34) for neglecting axial diffusion of energy and mass. The turbulent convection effects in the packed bed predominate over transport by diffusion. It has even been proposed that packed beds be used to prevent axial dispersion in reactors. Also the mathematical complexities presented by the second order derivatives of the diffusion terms are again not worthwhile considering the accuracy attained by the models neglecting axial dispersion.

The radial symmetry assumption for the pellets is valid as long as functional variations over a pellet length are small. The weaknesses and advantages of this assumption were discussed in Chapter II.

Interparticle radiation and conduction could be accounted for by utilizing an empirical effective solid phase thermal conductivity in conjunction with an additional energy balance on the solid (30). The complexity introduced versus the signifigance of the effects usually encountered when including these phenomena (30,43), indicate that they can be neglected in this study.

3.1.2 External Material Balances

Consider the conservation of oxygen and sulfur dioxide in a differential cylindrical element with diameter equal to that of the bed, D_B, and axial thickness of ΔZ. Accounting for convection into and out of the element, accumulation, and loss of mass to the internal phase, the following expression describes flow of fluid components in the external or bulk gas phase,

$$\left.\frac{GAx_i}{M}\right|_{Z} - \left.\frac{GAx_i}{M}\right|_{Z+\Delta Z}$$

$$- \frac{4\pi R^2}{\frac{4}{3}\pi R^3}(1-\epsilon)A\Delta Z k_i'(x_i - X_{iR}) = \frac{\partial}{\partial t}(A\Delta Z \epsilon\, y_i);\ i = 1,2 \qquad (3\text{-}1)$$

where x_i = external mole fraction of component i

X_i = internal mole fraction of component i

y_i = external molar concentration of specy i, g mole/cc

M = gas mixture molecular weight, g/g mole

ϵ = bed porosity or void fraction

A = cross sectional area of the bed, sq.cm($\pi D_B^2/4$)

R = pellet radius, cm

G = superficial mass velocity, g/sq.cm-sec

Z = axial bed length measured from bed entrance, cm

k_i' = mass film transfer coefficient for component i, g mole/sq.cm-sec.

t = time, sec.

Units on quantities are merely examples, and any consistent set of units can be utilized. The subscript R represents conditions at the outer surface of the pellets.

Variation of the mass velocity, G, and the mixture molecular weight, M, can be considered negligible since the combined concentration of oxygen and sulfur dioxide is less than 4 per cent. Dividing both sides of Equation (3-1) by $A\epsilon\Delta Z$, evaluating the limit of each expression as ΔZ approaches zero, and rearranging terms

renders,

$$\frac{\partial y_i}{\partial t} + \frac{G}{\epsilon M}\frac{\partial x_i}{\partial Z} = \frac{-3(1-\epsilon)k_i'}{R\,\epsilon}(x_i - X_{iR});\ i=1,2 \qquad (3\text{-}2)$$

Boundary and initial conditions applying to Equations (3-2) are,

$$y_i(Z,t=0) = 0;\ i=1,2 \qquad (3\text{-}3)$$

$$x_i(Z=0,t) = x_{i0};\ i=1,2 \qquad (3\text{-}4)$$

where

X_{i0} = inlet mole fraction of specie i, which may vary with time

Utilizing the ideal gas law, the conversion between mole fraction and molar concentration is,

$$y_i = \frac{\rho_g x_i}{M} = \frac{P x_i}{R'T} \qquad (3\text{-}5)$$

where P represents pressure in atmospheres and R' is the universal gas constant. It is necessary to use both methods for expressing composition in developing the nonisothermal conservation equations since the convection of mass is proportional to the mole fraction gradient, rate of mass accumulation to the time variation of concentration, transfer across the gas-solid interface to mole fraction differences, and pore diffusion to mole fraction gradients.

3.1.3 External Energy Balance

Neglecting kinetic, potential, nuclear, electromagnetic, and radiative energies, a general energy balance can be expressed as,

(accumulation of internal energy) = (net gain of enthalpy by convection) + (net gain of energy thru conduction) + (net gain of energy through generation or "source" terms)

where net gain = input-output

The "source" term might consist of energy transferred between the external and internal phases by film transfer of heat due to finite temperature differences in the two phases and/or by transfer of sensible heat due to mass transfer between the two phases.

Applying the general energy balance to the differential element used in the preceeding section gives the following,

$$\frac{\partial}{\partial t}(\epsilon A\Delta Z\ \rho_g\ U_g) = \frac{GA}{M}\ \Sigma_i(x_i\ h_i)\Big|_Z$$

$$- \frac{GA}{M}\ \Sigma_i(x_i\ h_i)\Big|_{Z+\Delta Z} + (-A\epsilon\ k_g\ \frac{\partial T_g}{\partial Z})\Big|_Z$$

$$- (-A\epsilon\ k_g\ \frac{\partial T_g}{\partial Z})\Big|_{Z+\Delta Z} + \frac{3(1-\epsilon)A\Delta Z}{R}\Big[h(T_{S,R}-T_g)$$

$$- \Sigma_i\ k_i'(x_i-X_{iR})h_i(T_{S,R})\Big] \qquad (3\text{-}6)$$

where U_g = intensive internal energy of the gas mixture, cal/g

ρ_g = gas density, g/cc

h_i = partial molal enthalpy of specy i, cal/g mole

T_g = bulk gas phase temperature, °C

T_S = solid phase temperature, °C

h = film heat transfer coefficient, cal/sq.cm-sec-°C

k_g = gas mixture thermal conductivity, cal/cm-sec-°C.

The subscript R denotes conditions at the pellet surface. The molal enthalpies are evaluated at the external temperature, T_g, except in the interphase mass transfer term where a film temperature is used. This temperature is between the external and internal temperatures, T_g and $T_{S,R}$, and is consistent with the conditions used to predict the film transfer coefficients (see Appendix A-9).

Neglecting axial dispersion, dividing both sides of Equation (3-4) by $A\epsilon\ \Delta Z$, and evaluating the limit of each expression as ΔZ approaches zero yields,

$$- \frac{G}{M\epsilon} \frac{\partial}{\partial Z} \sum_i (x_i\ h_i) + \frac{3(1-\epsilon)}{R\epsilon} \left[h(T_{SR}-T_g) - \sum_i k_i' (x_i - X_{iR}) h_i(T_{SR}) \right] = \frac{\partial}{\partial t} (\rho_g U_g) \qquad (3\text{-}7)$$

For an ideal gas, enthalpy is a function of temperature only and the following relation between heat capacity and temperature applies,

$$\frac{\partial h_i}{\partial m} = \frac{dh_i}{dT} \frac{\partial T}{\partial m} = c_i \frac{\partial T}{\partial m} \qquad (3\text{-}8)$$

where c_i represents the molar heat capacity of the i^{th} component in cal/g mole-°C and m is an unspecified variable. The bulk gas heat capacity, C_g, and the molar heat capacities are related by,

$$C_g = \frac{1}{\rho_g} \sum_i (y_i\ c_i) = \frac{1}{M} (x_i\ c_i) \qquad (3\text{-}9)$$

where C_g = gas mixture heat capacity at constant pressure, cal/g-°C. Also, if the variation of the heat capacity across the fluid film surrounding a pellet is neglected, one obtains,

$$h_i(T_g)-h_i(T_{SR}) = c_i(T_g-T_{SR}) \qquad (3\text{-}10)$$

from Equation(3-8).

By performing the following steps,

1) expand the left-most term in Equation (3-7) by differentiating within the summation.

2) utilize Equation (3-8) in the expansion, then Equation (3-9) where the former was used.

3) substitute Equation (3-2) where appropriate in the expansion.

4) neglect the accumulation of energy due to the accumulation of mass term.

5) rearrange terms so that interphase mass transfer terms are within a single summation.

6) utilize Equation (3-10) in the preceding step.

7) assume that the interphase mass fluxes are related by stoichiometry; that is,

$$\sum_i k_i'(x_i-X_{iR}) \approx 2k_1'(x_1-X_{1R})$$

it can be shown that Equation (2-7) reduces to,

$$-\frac{GC_g}{\epsilon}\frac{\partial T_g}{\partial Z} + \frac{3(1-\epsilon)}{R\epsilon}\left[h - 2c_1k_1'(x_1-X_{1R})\right](T_{SR}-T_g)$$

$$= \frac{\partial}{\partial t}(\rho_g U_g) \qquad (3\text{-}11)$$

Steps 4) and 7) are approximations. The latter step neglects diffusion of the inert components which would only be significant when the initial front of flue gas passes through the bed. The former is necessary to obtain tractable solutions.

Using typical values (T_g = 350°C) for the pertinent parameters as given in Appendices A and B and the maximum oxygen mole fraction differential possible, the ratio of the interphase heat transfer due to mass transfer to that due to film heat convection is

$$\frac{2k_1(x_1-X_{1R})c_1}{h} \leq 0.05$$

Thus, the interphase heat transfer due to mass transfer can be neglected, and Equation (3-11) reduces to,

$$\frac{\partial}{\partial t}(\rho_g U_g) + \frac{GC_g}{\epsilon}\frac{\partial T_g}{\partial Z} = \frac{3(1-\epsilon)h}{\epsilon R}(T_{S,R}-T_g) \qquad (3\text{-}12)$$

Neglecting potential and kinetic energy effects, the internal energy and enthalpy are related by the following expression,

$$H_g = U_g + J\,P/\rho_g \qquad (3\text{-}13)$$

where H_g = intensive enthalpy of the gas mixture, cal/g

J = an energy conversion factor, cal/g-cm

Also, note that Equation (3-8) remains valid when H_g replaces h_i and C_g replaces c_i.

By utilizing Equations (3-13) and (3-8) in conjunction with constant pressure in the bulk gas phase, Equation (3-12) could be simplified to,

$$\frac{\partial T_g}{\partial t} + \frac{G}{\rho_g \epsilon}\frac{\partial T_g}{\partial Z} = \frac{3(1-\epsilon)h}{\epsilon R C_g \rho_g}(T_{S,R}-T_g) \qquad (3\text{-}14)$$

if the gas density and heat capacity are considered constant.

The following boundary and initial conditions apply to both Equations (3-12) and (3-14),

$$T_g(Z,t=0) = T_{gi} \qquad (3\text{-}15)$$

$$T_g(Z=0,t) = T_{g0}, \quad t > 0 \tag{3-16}$$

where T_{gi} = initial flue gas temperature which is a constant

T_{g0} = inlet flue gas temperature which may vary with time.

3.1.4 Surface Kinetics

For solid-fluid reactions, Wen (46) discusses the merits of describing the reaction rate on the porous surface based on the Langmuir adsorption isotherm versus simple n^{th} order rate expressions. For design purposes, it was concluded that the n^{th} order equations are satisfactory provided extrapolation beyond the experimental range in which the rate expression was determined is not involved.

Thus define the overall reaction rate per unit of pellet surface area as

$$R_I = k''_I \, y_{s6}^{a_1} \, y_{s1}^{a_2}$$

$$= \frac{d(Vy_{s6})/dt}{\gamma_{16}(4\pi a_c^2)} = \frac{d(Vy_{s1})/dt}{\gamma_{11}(4\pi a_c^2)}$$

$$R_{II} = k''_{II} \, y_{s8}^{a_3} \, y_{s1}^{a_4} \, y_{s2}^{a_5}$$

$$= \frac{d(Vy_{s8})/dt}{\gamma_{28}(4\pi r_c^2)} = \frac{d(Vy_{s1})/dt}{\gamma_{21}(4\pi r_c^2)} = \frac{d(Vy_{s2})/dt}{\gamma_{22}(4\pi r_c^2)}$$

where a_i $(i = 1,2...5)$ = constants

R_j = overall reaction rate for reaction j based on pellet surface area, g moles/sq.cm-sec.

y_{si} = internal or solid phase molar concentration; g mole i/cc of fluid, for i = 1,...5; or g mole i/cc of pellet, for i = 6,7,8

k''_j = reaction rate constant for reaction j with units depending on the value of the a_i's

V = volume, cc

The rate expressions represent irreversible reactions, since most reactions with solid surfaces cannot be truly reversible (46). Also, Parsons et al (35) have demonstrated experimentally that the copper reaction system under study is irreversible and that Reaction II has a linear dependence on SO_2. Both theoretical and experimental evidence (46) indicate that the order of gas-solid reactions varies between zero and two. Thus allow

$$a_2 = a_4 = a_5 = 1$$

for this study.

In most applications the solid phase concentrations at the reaction interface are constant, but it may vary with radial position in certain processes. Due to the simplifications allowed, however, solid phase reactant will be considered to be evenly distributed. Thus regardless of the values of a_1 and a_3, the solid phase concentrations can be incorporated into the rate constants without loss of generality.

Utilizing the preceding information, rate expressions for the consumption per unit area of oxygen in Reaction I, $R_{I,1}$, and the consumption of sulfur dioxide in Reaction II, $R_{II,2}$, can be obtained as follows,

$$R_{I,1} = k_I y_{s1} = \text{g mole } O_2/\text{sq.cm.-sec}$$

$$R_{II,2} = k_{II} y_{s1} y_{s2} = \text{g mole } SO_2/\text{sq.cm-sec}$$

where

$$k_I = |\gamma_{11}| k_I'' y_{s6}^{a_1} = \text{cm/sec}$$

$$k_{II} = |\gamma_{22}| k_{II}'' y_{s8}^{a_3} = \text{cm}^4/\text{sec-g mole of } O_2$$

3.1.5 Internal Material Balances

Considering a one-dimensional flow, the molar flux of a fluid component, N_i through a plane perpendicular to the flow direction due to molecular diffusion is given by (49)

$$N_i = -\frac{\rho_g}{M} D_i \nabla x_i + x_i \sum_j N_j$$

where D_i is the molecular diffusivity of component i in sq.cm/sec. For equimolar counter diffusion or for very dilute concentrations of component i, Fick's Law is valid.

$$N_i = -\frac{\rho_g}{M} D_{ei} \nabla x_i \qquad (3\text{-}17)$$

The flue gas stream will be considered dilute with respect to O_2 and SO_2.

Applying the conservation of mass to a differential element consisting of the shell between two concentric spheres of radius r and r + Δr respectively, the flow of fluid component i through the porous solid is described by

$$-4\pi r^2 \frac{\rho_g}{M} D_{ei} \frac{\partial X_i}{\partial r}\Big|_r + \left(4\pi r^2 \frac{\rho_g}{M} D_{ei} \frac{\partial X_i}{\partial r}\right)\Big|_{r+\Delta r}$$

$$= \frac{\partial}{\partial t}\left(4\pi r^2 \Delta r \epsilon_S \frac{\rho_g}{M} X_i\right) \qquad (3\text{-}18)$$

where D_{ei} = effective pore diffusivity of component i, sq.cm/sec.

ϵ_S = porosity of the pellets

Surface migration and mass flow due to pressure gradients within the pores have been neglected in the preceding equation. A complete discussion of these phenomena and the concept of effective diffusivities within porous solids is given in Appendix B-6.

Dividing both sides of Equation (3-18) by $4\pi r^2 4r$ and utilizing the definition of the partial derivative renders,

$$\frac{1}{r^2} \frac{\partial}{\partial r} \left(r^2 \rho_g De_1 \frac{\partial X_i}{\partial r}\right) = \epsilon_S \frac{\partial}{\partial t} (\rho_g X_i) \qquad (3\text{-}19)$$

The effective diffusivity in the molecular diffusion regime varies with temperature to the 3/2 or second power; whereas in Knudsen diffusion, the variation is proportional to the square root of temperature. The effective diffusivity may be considered proportional to the first power in temperature, since the actual diffusion mechanism will probably be a combination of both types. The fluid density under the ideal gas assumption is inversely proportional to temperature, hence the product of the fluid density and effective diffusivity is insensitive to temperature. Thus neglecting variations due to composition, this product may be considered constant, and the general internal fluid balance becomes,

$$\frac{1}{r^2} \frac{\partial}{\partial r} \left(r^2 \frac{\partial X_i}{\partial r}\right) = \frac{\epsilon_S}{\rho_g D_{ei}} \frac{\partial}{\partial t} (\rho_g X_i); \; i=1,2 \qquad (3\text{-}20)$$

Denoting the mole fraction of component i in the oxidation or intermediate zone of the pellet ($a_c < r < r_c$) as X_{i*} and that of the components in the outer or sulfation layer ($r_c < r < R$) as X_i, Equation (3-20) represents the flow of reactants in the outer layer while Equation (3-21) represents the flow of oxygen in the intermediate pellet zone,

$$\frac{1}{r^2}\ \frac{\partial}{\partial r}\left(r^2\ \frac{\partial X_*}{\partial r}\right) = \frac{\epsilon_S}{\rho_g D_{e1}}\ \frac{\partial}{\partial t}\ (\rho_g X_*) \tag{3-21}$$

using X_* to represent oxygen fluid concentration, since O_2 is the only component of interest in this zone.

The initial condition for these internal material balances is as follows,

$$X_i(Z,r,t = 0) = 0;\ i=1,2,* \tag{3-22}$$

while the pertinent boundary conditions are:

at the pellet surface:

$$\left(\frac{\rho_g D_{ei}}{M}\ \frac{\partial X_i}{\partial r}\right)\Big|_R = k_i'[x_i - X_{iR}];\ i=1,2 \tag{3-23}$$

at the inner solid interface ($r = a_c$):

$$\left(\frac{\rho_g D_{e1}}{M}\ \frac{\partial X_1}{\partial r}\right)\Big|_{a_c} = k_I\ y_{s*}|_{a_c} \tag{3-24}$$

at the outer solid interface ($r = r_c$):

$$X_1(Z,r_c,t) = X_*(Z,r_c,t) \tag{3-25}$$

$$\left(\frac{\rho_g D_{e2}}{M}\ \frac{\partial X_2}{\partial r}\right)\Big|_{r_c} = k_{II}\ y_{s1}\ y_{s2}\Big|_{r_c} \tag{3-26}$$

$$\left(\frac{\rho_g D_{e1}}{M} \frac{\partial X_1}{\partial r} \right)\Big|_{r_c} = \gamma\, k_{II}\, y_{s1}\, y_{s2}\Big|_{r_c}$$

$$+ \left(\frac{\rho_g D_{e1}}{M} \frac{\partial X_*}{\partial r} \right)\Big|_{r_c} \qquad (3\text{-}27)$$

where $\gamma = \gamma_{21}/\gamma_{22}$

These boundary conditions state that the molar flux through the film equals that diffusing through the porous solid at the pellet surface (Equation (3-23)); the mass diffusing into a solid interface from the pellet surface equals the mass consumed by reaction plus the mass diffusing away on the other side of the interface (Equations (3-24, 26, and 27)); and the fluid concentration profile within a pellet is continuous (Equation 3-25).

Employing the pseudosteady state approximation which was defined in Section 2.1 Equations (3-20, 21) reduce to

$$\frac{1}{r^2} \frac{\partial}{\partial r} \left(r^2 \frac{\partial X_i}{\partial r} \right) = 0 \; ; \; i = 1,2,* \qquad (3\text{-}28)$$

which is Laplace's equation. The approximation should be valid for the present system, since pressure is not high while solid reactant concentration is not extremely low (46). The approximation is also verified by Bischoff (5) and Blakemore (7) for similar conditions.

The general solution for Laplace's equation is,

$$X_i = - \frac{A_i}{r} + B_i \; ; \; i = 1,2,* \qquad (3\text{-}29)$$

where A_i and B_i are constant (with respect to r) and depend on the boundary conditions. Note that the solution is undefined at the center of a pellet. This means that special precautions may have to

be made later whenever the solid interfaces approach the pellet center (complete solid conversion).

Solving Equations (3-23,34,35,36, 37,39) simultaneously yields,

$$X_1(Z,r,t) = \frac{x_1\left[\frac{1}{a_c} - \frac{1}{r} + \frac{D_{e1,ac}}{k_I a_c^2} + \frac{\gamma k_{II} r_c^2 y_{s2,rc}}{D_{e1,rc}}\left(\frac{1}{a_c} - \frac{1}{r_c} + \frac{D_{e1,ac}}{k_I a_c^2}\right)\left(\frac{1}{r_c} - \frac{1}{r}\right)\right]}{\left[\frac{1}{a_c} - \frac{1}{R} + \frac{D_{e1,ac}}{k_I a_c^2} + \frac{\rho_{g,R} D_{e1,R}}{MR^2 k_1'} + \left(\frac{1}{r_c} - \frac{1}{R} + \frac{\rho_{g,R} D_{e1,R}}{R^2 k_1' M}\right)\left(\frac{1}{a_c} - \frac{1}{r_c} + \frac{D_{e1,ac}}{k_I a_c^2}\right)\frac{\gamma k_{II} r_c^2 y_{s2,rc}}{D_{e1,rc}}\right]} \qquad (3\text{-}30)$$

$$X_2(Z,r,t) = \frac{\left[1 + \left(\frac{1}{r_c} - \frac{1}{r}\right)\frac{k_{II} r_c^2 y_{s1,rc}}{D_{e2,rc}}\right]}{\left[1 + \frac{k_{II} r_c^2 y_{s1,rc}}{D_{e2,rc}}\left(\frac{1}{r_c} - \frac{1}{R} + \frac{\rho_{g,R} D_{e2,R}}{R^2 k_2' M}\right)\right]} \qquad (3\text{-}31)$$

where the subscripts r_c, a_c, and R preceded by a comma infer that the parameter or variable in question is evaluated at the conditions existing at the pellet radius indicated.

These last two expressions are coupled and implicit through the molar concentration terms, y_{s1} and y_{s2}, evaluated at the outer reaction interface r_c. The mole fractions, x_i, and the molar concentrations, y_{si}, are related by Equation (3-5),

$$y_{si,rc} = \left.\frac{\rho_g X_i}{M}\right|_{r_c} \quad ; \; i = 1,2 \tag{3-32}$$

Using Equation (3-32), explicit expressions can be obtained for X_1 and X_2 by solving Equations (3-30,31) simultaneously. This operation will be performed later.

3.1.6 Solid Phase Material Balances

Considering stoichiometry at the solid phase interfaces, r_c and a_c, the rates of consumption of the solid reactant (Cu_2O) and intermediate product (CuO) can be related to the rate of shrinkage of the unreacted core and the outer reaction interface radii respectively.

The rate of sulfate production at the outer interface in terms of the sulfation reaction is,

$$\frac{d\underline{N}_7}{dt} = \alpha(4\pi r^2 k_{II} y_{s1} y_{s2})\Big|_{r_c}$$

where $\underline{N}_i$ = weight of component i per pellet, g

α = weight of sulfate per mole of SO_2 consumed, g $CuSO_4$/g mole SO_2

$= |\gamma_{27} M_7 / \gamma_{22}|$

M_i = molecular weight of component i, g/g mole

This rate is also equivalent to the product of the sulfate density and the rate of sulfate volume change with respect to time,

$$\frac{dN_7}{dt} = \rho_s W_7 \frac{\partial(\frac{4}{3}\pi R^3 - \frac{4}{3}\pi r_c^3)}{\partial t}$$

$$= -\rho_s W_7 \, 4\pi r_c^2 \frac{\partial r_c}{\partial t}$$

where W_i represents the weight fraction of component i. Equating the two preceding equations and rearranging yields,

$$\frac{\partial r_c}{\partial t} = \frac{-\alpha k_{II}}{\rho_s W_7} (y_{s1} y_{s2})\Big|_{r_c} \qquad (3\text{-}33)$$

Similar reasoning at the inner interface, a_c, for the Cu_2O consumption renders the following expression for the shrinkage of the inner unreacted core,

$$\frac{\partial a_c}{\partial t} = - \frac{\beta k_I}{\rho_s W_6} y_{s1}\Big|_{a_c} \qquad (3\text{-}34)$$

where $\beta = \gamma_{16} M_6 / \gamma_{11}$ = g Cu_2O/g mole O_2

The initial conditions for these balances are,

$$r_c(Z, t = 0) = R \qquad (3\text{-}35a)$$

$$a_c(Z, t = 0) = R \qquad (3\text{-}35b)$$

Thus Equations (3-33) and (3-34) describe the movement of the solid reaction interfaces within the pellets for a given cross section of the bed. The relation between the solid conversion and the sulfate radius r_c can be defined by,

$$X' = \begin{matrix}\text{solid reactant} \\ \text{conversion}\end{matrix} \cdot \frac{\frac{4}{3}\pi(R^3 - r_c^3)}{\frac{4}{3}\pi R^3} = 1 - \left(\frac{r_c}{R}\right)^3 \qquad (3\text{-}36a)$$

thereby rendering the following relationship between the rate of solid reactant conversion and movement of the sulfate radius

$$\frac{\partial X'}{\partial t} = 3\left(\frac{r_c}{R}\right)^2 \frac{\partial}{\partial t}\left(\frac{r_c}{R}\right) \qquad (3\text{-}36b)$$

3.1.7 General Pellet Energy Balance

Applying the general energy balance of Section 3.1.3 to the differential element described in Section 3.1.5 while assuming that thermal equilibrium exists between the solid and fluid phase within the pellet, one obtains,

$$\frac{\partial}{\partial t}\left[4\pi r^2 \Delta r(\rho_s U_s + \rho_g \epsilon_s U_g)\right]$$

$$= \left[4\pi r^2 \sum_i^5 \rho_g D_{ei}\left(\frac{\partial X_i}{\partial r}\right) h_i\right]_{r+\Delta r} - \left[4\pi r^2 \sum_i^5 \rho_g D_{ei}\left(\frac{\partial X_i}{\partial r}\right) h_i\right]_r$$

$$+ \left[4\pi r^2 k_s \frac{\partial T_s}{\partial r}\right]_{r+\Delta r} - \left[4\pi r^2 k_s \frac{\partial T_s}{\partial r}\right]_r$$

where k_s = effective thermal conductivity of the porous pellet (including the fluid phase), cal/cm-sec-°C

U_s = intensive internal energy of the solid, cal/g

The individual contributions of the various solid reactants and products (Cu_2O, CuO, $CuSO_4$) to U_s have been included in the pellet heat capacity, C_s (see Appendix B-5). Similar techniques were used

to estimate the effective conductivity and pellet density, thus C_s, k_s, and ρ_s are not dependent on the solid phase composition.

Dividing both sides of the preceding equation by $4\pi r^2 \Delta r$, evaluating the limit of each term as Δr becomes infinitesmal, and utilizing Equation (3-14) yields,

$$\frac{\partial}{\partial t}\left\{\rho_s\left[H_s - \frac{JP}{\rho_s}(1-\epsilon_s)\right] + \rho_g \epsilon_s \left[H_g - \frac{JP}{\rho_g}\right]\right\}$$

$$= \frac{1}{r^2}\frac{\partial}{\partial r}\left[r^2 \sum_i^5 \rho_g D_{ei}\left(\frac{\partial X_i}{\partial r}\right) h_i + r^2 k_s \frac{\partial T_s}{\partial r}\right] \qquad (3\text{-}37)$$

where H_s = intensive enthalpy of the solid, cal/g

For the pellet gas phase, the intensive enthalpy and partial molal enthalpies can be related as follows,

$$H_g = \frac{1}{\rho_g}\sum_i^5 y_{si} h_i = \frac{1}{M}\sum_i^5 X_i h_i \qquad (3\text{-}38)$$

Incorporating Equations (3-8,38) and isobaric conditions, Equation (3-37) can be simplified to,

$$\rho_s C_s \frac{\partial T_s}{\partial t} + \epsilon_s \frac{\partial}{\partial t}\sum_i^5 (y_{si} h_i) = \frac{\partial T_s}{\partial r}\sum_i^5 \rho_g D_{ei}\left(\frac{\partial X_i}{\partial r}\right) c_i$$

$$+ \frac{1}{r^2}\sum_i^5 h_i \frac{\partial}{\partial r}\left(r^2 \rho_g D_{ei}\frac{\partial X_i}{\partial r}\right) + \frac{1}{r^2}\frac{\partial}{\partial r}\left(r^2 k_s \frac{\partial T_s}{\partial r}\right)$$

The preceding equation can be simplified further by using Equation (3-20) in the second term from the right, followed by expansion of the internal energy accumulation team in conjunction with (3-8) and finally cancelling like terms rendering,

$$\rho_s C_s \frac{\partial T_s}{\partial t} + \epsilon_s \frac{\partial T_s}{\partial t} \sum_i^5 y_{si} c_i$$

$$= \frac{\partial T_s}{\partial r} \sum_i^5 \rho_g D_{ei} \frac{\partial X_i}{\partial r} c_i + \frac{1}{r^2} \frac{\partial}{\partial r} \left(r^2 k_s \frac{\partial T_s}{\partial r} \right)$$

Using Equation (3-9) in this equation yields,

$$(\rho_s C_s + \epsilon_s \rho_g C_g) \frac{\partial T_s}{\partial t} = \frac{\partial T_s}{\partial r} \sum_i^5 \rho_g D_{ei} \frac{\partial X_i}{\partial r} c_i + \frac{1}{r^2} \frac{\partial}{\partial r} \left(r^2 k_s \frac{\partial T_s}{\partial r} \right) \quad (3\text{-}39)$$

The heat capacity of the gas in the pores may be neglected, since the ratio $\frac{\epsilon \rho_g C_g}{\rho_s C_s}$ is less than 0.001 using values given in the appendices. Furthermore, the molar fluxes within the pores can be related by stoichiometry, since the reaction rate was considered much faster than the accumulation in the internal phase in Section 3.1.5. Thus,

$$\sum_i^5 \rho_g D_{ei} \frac{\partial X_i}{\partial r} c_i \approx 2 \rho_g D_{e1} \frac{\partial X_1}{\partial r} c_1 = 2 c_1 \frac{R^2 k_1' (x_1 - X_{1r})}{r^2} \quad (3\text{-}40)$$

neglecting internal accumulation. Again this approximation neglects the flow of inerts in the pellet pores which may not be rigorous as the flue gas initially passes through the bed.

Equation (3-39) can now be reduced to,

$$r^2 \rho_s C_s \frac{\partial T_s}{\partial t} = 2 r^2 \rho_g D_{e1} \frac{\partial X_1}{\partial r} c_1 \frac{\partial T_s}{\partial r} + 2 k_s r \frac{\partial T_s}{\partial r} + k_s r^2 \frac{\partial T_s}{\partial r}$$

Using Equation (3-40) and the values for the parameters in the appendices, the ratio of the energy transfer by mass diffusion to

that by conduction, $\frac{R^2 k_1'(x_1 - X_1)}{2k_s r}$, is less than 0.1 for most applications. The preceding equation can therefore be simplified to,

$$\rho_s C_s \frac{\partial T_s}{\partial t} = \frac{1}{r^2} \frac{\partial}{\partial r}\left(r^2 k_s \frac{\partial T_s}{\partial r}\right) \tag{3-41}$$

Denoting the temperature in the outer pellet layer ($r_c < r < R$), the intermediate layer ($a_c < r < r_c$), and the inner core as T_{s1}, T_{s2}, and T_{s3} respectively, the pellet energy balances and initial and boundary conditions follow.

$$\frac{1}{r^2} \frac{\partial}{\partial r}\left(r^2 k_s \frac{\partial T_{si}}{\partial r}\right) = \rho_s C_s \frac{\partial T_{si}}{\partial t} \; ; \; i=1,2,3 \tag{3-42}$$

$$T_{si}(Z,r,t=0) = T_g(Z,0); \; i=1,2,3 \tag{3-43}$$

$$k_s \left.\frac{\partial T_{s1}}{\partial r}\right|_R = h\left[T_g(Z,t) - T_{s1}(Z,R,t)\right] \tag{3-44}$$

$$k_s \left.\frac{\partial T_{s1}}{\partial r}\right|_{r_c} = \left[k_{II} y_{s1} y_{s2} \Delta H_{II} + k_s \frac{\partial T_{s2}}{\partial r}\right]_{r_c} \tag{3-45}$$

$$T_{s1}(Z,r_c,t) = T_{s2}(Z,r_c,t) \tag{3-46}$$

$$k_s \left.\frac{\partial T_{s2}}{\partial r}\right|_{a_c} = \left[k_I y_{s2} \Delta H_I + k_s \frac{\partial T_{s3}}{\partial r}\right]_{a_c} \tag{3-47}$$

$$T_{s2}(Z,a_c,t) = T_{s3}(Z,a_c,t) \tag{3-48}$$

$$\left.\frac{\partial T_{s3}}{\partial r}\right|_{r=0} = 0 \tag{3-49}$$

where ΔH_I = heat of reaction for Reaction I, cal/g mole O_2

ΔH_{II} = heat of reaction for Reaction II, cal/g mole-SO_2

and $k_j = k_j^o \exp(-\Delta E_j/RT)$

which are the Arrhenius expressions for temperature dependency of reaction rates with k_j^o representing frequency factors and ΔE_j representing activation energies.

Equations (3-42) must be solved in order to obtain expressions for $T_s(Z,a_c,t)$, $T_s(Z,r_c,t)$ and $T_s(Z,R,t)$. A tractable simultaneous solution of these three equations with the coupled boundary conditions is much more feasible if the pseudosteady state approximation is performed. Physically, this implies that the accumulation of energy is negligible in comparison to the energy being generated by reaction. It is usually valid for small pellet heat capacity and small pellet radial temperature gradients. To introduce further simplification, assume that the temperature variation of the effective thermal conductivity is negligible.

Equations (3-42) become,

$$\frac{\partial}{\partial r}\left(r^2 \frac{\partial T_{si}}{\partial r}\right) = 0; \quad i = 1,2,3 \tag{3-50}$$

with general solutions,

$$T_{si}(Z,r,t) = \frac{-A_i}{r} + B_i \; ; \quad i = 1,2,3 \tag{3-51}$$

where A_i and B_i depend on Equations (3-43) through (3-49) and are independent of r.

Solving Equations (3-51) and (3-43) through (3-49) simultaneously leads to,

$$T(Z,R,t) = T_g(Z,t) + \frac{(k_I y_{s1})\Big|_{a_c}(-\Delta H_1)a_c^2 + (k_{II} y_{s1} y_{s2})\Big|_{rc}(-\Delta H_2)r_c^2}{R^2 h}$$

$$= T_g + \frac{F + G}{R^2 h} \tag{3-52}$$

$$T(Z,r_c,t) = T_g + \left(\frac{1}{r_c} - \frac{1}{R} - \frac{k_s}{R^2 h} \right) \frac{F + G}{k_s} \tag{3-53}$$

$$T(Z,a_c,t) = T_g + \left(\frac{1}{a_c} - \frac{1}{R} + \frac{k_s}{R^2 h}\right) \frac{F}{k_s} + \left(\frac{1}{r_c} - \frac{1}{R} + \frac{k_s}{R^2 h}\right) \frac{G}{k_s} \tag{3-54}$$

where $F = (k_I y_{s1})\Big|_{a_c}(-\Delta H_1)a_c^2$

$G = (k_{II} y_{s1} y_{s2})\Big|_{rc}(-\Delta H_2)r_c^2$

Equations (3-53,54) represent an implicit set of algebraic relations for $T_s(r_c)$ and $T_s(a_c)$.

When the accumulation of energy in the unreacted core is included and the variation of temperature in this region with respect to radius is neglected, the following set of equations result,

$$T_s(Z,R,t) = T_g + \frac{F' + G}{R^2 h} \tag{3-55}$$

$$T_s(Z,r_c,t) = T_g + \left(\frac{1}{a_c} - \frac{1}{R} \frac{k_s}{R^2 h}\right) \frac{F' + G}{k_s} \tag{3-56}$$

$$T_s(Z,a_c,t) = T_g + \left(\frac{1}{a_c} - \frac{1}{R} + \frac{k_s}{R^2 h}\right)\frac{F'}{k_s}$$

$$+ \left(\frac{1}{r_c} - \frac{1}{R} + \frac{k_s}{R^2 h}\right)\frac{G}{k_s} \qquad (3\text{-}57)$$

where $$F' = F + \frac{a_c^3 \rho_s C_s}{k_s} \frac{dT_s(Z,a_c,t)}{dt}$$

Thus the three preceding equations represent an implicit set of nonhomogeneous first order ordinary differential equations with initial condition given by Equation (3-43).

In either case, any prospect for a tractable solution of the implicit equations for $T_s(a_c)$ and $T_s(r_c)$ seems rather remote. If the activation energies are very small, however, the exponential Arrhenius terms revert to constants at elevated temperatures. This assumption simplifies Equations (3-53,54) and (3-56,57) into explicit expressions for $T_s(r_c)$ and $T_s(a_c)$ which are useful as expressions for estimating the maximum temperature differences in the pellet. This assumption may not be entirely rigorous, however, since the activation energy for the sulfation reaction is estimated at 27 K cal/mole (35). Such a value is not low enough to make the temperature effect in the reaction rate constant negligible.

3.1.8 Film-Controlled Pellet Energy Balance

Hlavacek (14), Paris et al (34) and Olson (30) indicate that, in many cases, the pellet interior is practically isothermal, and the major resistance to energy transfer occurs at the pellet surface where the film resistance predominates. Thus there should be a

finite temperature difference across the "film" surrounding each pellet, but only a negligible difference between the pellet surface temperature and the interior reaction site temperature. This assumption would lead to a great deal of simplification in the pellet energy balance and would allow the inclusion of the accumulation of energy within the pellet.

The development in the previous section ignored energy accumulation. This could lead to large errors, especially when the heat capacity of the solid is not negligible (22). Furthermore, to make practical use of the pellet energy balance presented in the preceding section, it was necessary to assume that the activation energies of both the oxidation and sulfation reactions were negligible. This was shown to be a poor approximation for the sulfation reaction, however.

Neglecting the resistance to energy transfer in the pellet interior reduces the maximum pellet temperature attainable (for exothermic reactions), since the heat liberated by reaction can escape from the pellet to the bulk fluid phase much faster when only an external resistance must be encountered. An estimate of the relative importance of the internal and external heat transfer resistances is given by the Biot number, N_{Bi}. This dimensionless number is the ratio of the internal pellet heat transfer resistance divided by the external resistance,

$$N_{Bi} = \frac{hR}{k_s}$$

Using Appendices A and B, $N_{Bi} \approx 10$, which infers that internal

resistance is much more significant than external resistance.

Thus, two unsatisfactory alternatives exist -

a) utilize a pellet energy balance incorporating the internal resistance k_s, but neglect accumulation of energy and significant activation energies.

b) utilize a pellet energy balance including energy accumulation and large activation energy (reaction rate constants vary with temperature), but neglect heat conduction within the pellets ($k_s \rightarrow \infty$) even though this effect is known to be significant.

The second approach will be utilized since energy accumulation should not be ignored. Also, the pellet heat transfer resistances can be lumped at the outer pellet surface, thereby artifically allowing higher temperatures to be attained at the reaction site. This will in turn have a greater effect on the reaction rate, since the reaction rate constants increase with temperature. Variation of the rate constants with temperature can be included without appreciably affecting the ease of solution which is not the case in the first alternative.

The lumped surface resistance, h', which combines interior and external resistances, can be roughly approximated by

$$\frac{1}{h'} = \frac{1}{h} + \frac{R}{k_s}$$

since the two resistances in question occur in series.

Under these circumstances, the pertinent terms for the pellet energy balance over a differential element described in Section 3.1.2 are:

into pellet by mass transfer:

$$A\Delta Z(1-\epsilon)\ \frac{4\pi R^2}{\frac{4}{3}\pi R^3}\left[\sum_{i=1}^{5} k_i'\,(x_i - X_{i,R})h_i(T_s)\right]$$

leaving pellet by convection film transfer:

$$A\Delta Z\ (1-\epsilon)\ \frac{3}{R}\left[h(T_s - T_g)\right]$$

accumulation:

$$A\Delta Z(1-\epsilon)\ \frac{\partial}{\partial t}\left[\rho_s U_s + \epsilon_s \rho_g U_g\right]$$

generation:

$$A\Delta Z(1-\epsilon)\ \frac{3}{R}\left[k_2'(x_2 - X_{2,R})(-\Delta H_{II})\right.$$

$$\left. + \left(k_1'(x_1 - X_{1,R}) - \gamma k_2'(x_2 - X_{2,R})\right)(-\Delta H_I)\right]$$

In the generation term, the pseudosteady state approximation for intrapellet mass transfer and stoichiometry controlling are assumed as was done previously in Section 3.1.3.

Combining these terms, dividing by $A\Delta Z(1-\epsilon)$, neglecting the heat capacity of the gas in comparison to that of the solid, and then utilizing Equations (3-8) and (3-14) along with isobaric conditions, the pellet energy balance becomes,

$$\rho_s\, C_s\, \frac{\partial T_s}{\partial t} + \frac{3}{R}\left[k_1'(x_1 - X_{1,R})(-\Delta H_1) + k_2'(x_2 - X_{2,R})(\gamma\Delta H_1 - \Delta H_2)\right]$$

$$= \frac{3}{R}\left[\sum_i k_i'(x_i - X_{i,R})h_i\{T_s\} - h(T_s - T_g)\right]$$

Using typical values taken from the appendices, the ratio of the energy transfer due to mass transfer across the fluid film to the energy generated by reaction is negligible, and the preceding relation reduces to,

$$\rho_s C_s \frac{\partial T_s}{\partial t} = \frac{-3}{R}\left[h(T_s-T_g) + k_1'(x_1-X_{1,R})\Delta H_1 + k_2'(x_2-X_{2,R})(\Delta H_{II}-\gamma\Delta H_I)\right] \quad (3\text{-}58)$$

with initial condition represented by Equation (3-42).

Unless stated otherwise, the pellet energy balance with film transfer controlling will be used throughout the remainder of the study.

3.2 Characteristic Transformations

3.2.1 Constant Property Equation System

In fixed bed reactor models, the fluid density and heat capacity, heat and mass transfer coefficients, and the stream velocity are usually considered constant (14,34). Even though one or more of these assumptions may not be rigorously satisfied, they are utilized because of the considerable degree of simplification allowed by their use and because of the degree of accuracy attained in most practical applications with their use. Ideally, they should be used only when changes in temperature and pressure are relatively small. Their use can be enhanced by use of average values or by actually allowing these parameters to vary in the numerical solution algorithms even

though the equation system was derived based on constant properties.

In this section, simplifications in the equations developed in Section 3.1 resulting from the utilization of constant gas density will be presented. The resulting differential equations may not seem simpler in form (they may even become more complex), but their solution is much simpler if constant density is assumed.

Utilizing Equation (3-5) in conjunction with constant gas density, the external mass balances represented by Equation (3-2) become,

$$\frac{\partial y_i}{\partial t} + \frac{G}{\epsilon \rho_g} \frac{\partial y_i}{\partial Z} = \frac{-3(1-\epsilon)K_i}{R\epsilon} \left[y_i - y_{si,R} \left(\frac{T_s}{T_g} \right) \right] ; i=1,2 \qquad (3\text{-}59)$$

where K_i = modified film mass transfer coefficient for compound i

$= k_i' R' T_g / P = k_i' M / \rho_g$ = cm/sec

The external energy balance with constant density was derived previously and is given by Equation (3-14). Movement of the reaction interfaces within the pellets are still described by Equations (3-33) and (3-34).

Again using Equation (3-5) and constant gas density, the internal mass balances for the film-controlling pellet temperature case reduces to:

pellet oxygen profile:

$$y_{s1}(Z,r,t) = \frac{y_1 \left[\frac{1}{a_c} - \frac{1}{r}\frac{D_{e1}}{k_I a_c^2} + \frac{\gamma k_{II} r_c^2 y_{s2,rc}}{D_{e1}} \left(\frac{1}{a_c} - \frac{1}{r_c}\frac{D_{e1}}{k_I a_c^2} \right)\left(\frac{1}{r_c} - \frac{1}{r} \right) \right]}{\left[\frac{1}{a_c} - \frac{1}{R} + \frac{D_{e1}}{k_I a_c^2} + \frac{D_{e1}}{R^2 K_1} + \left(\frac{1}{r_c} - \frac{1}{R} + \frac{D_{e1}}{R^2 K_1} \right)\left(\frac{1}{a_c} - \frac{1}{r_c} + \frac{D_{e1}}{k_I a_c^2} \right) \frac{\gamma k_{II} r_c^2 y_{s2,rc}}{D_{e1}} \right]} \tag{3-60}$$

pellet sulfur dioxide profile:

$$y_{s2}(Z,r,t) = \frac{y_2 \left[1 + \left(\frac{1}{r_c} - \frac{1}{r} \right) \frac{k_{II} r_c^2 y_{s1,rc}}{D_{e2}} \right]}{\left[1 + \frac{k_{II} r_c^2 y_{s1,rc}}{D_{e2}} \left(\frac{1}{r_c} - \frac{1}{R} + \frac{D_{e2}}{R^2 K_2} \right) \right]} \tag{3-61}$$

Note that the relation between the modified mass transfer coefficient, K_i, and the mass transfer coefficient, k_i', has also been utilized.

The pellet energy balance is defined by Equation (3-62) when Equations (3-5) and (3-58) are combined.

$$\rho_s C_s \frac{\partial T_s}{\partial t} = \frac{-3}{R}\left[h(T_s-T_g) + K_1(y_1-y_{s1,R}T_s/T_g)\Delta H_I \right.$$

$$\left. + K_2(y_2-y_{s2,R}T_s/T_g)(\Delta H_{II}-\gamma\Delta H_I)\right] \qquad (3\text{-}62)$$

3.2.2 Characteristics

For both variable and constant gas density, the material and energy balances describing the reactor represent a system of quasi-linear partial differential equations of the first order for functions of two independent variables. Courant and Friederichs (9) present a complete mathematical treatment for the solution of these systems based on the concept of characteristics,provided the equations are hyperbolic. Criteria for existence, uniqueness and convergence of the solutions for these systems are also presented.

Characteristics are curves in the domain space of the differential equations system; that is, a relationship between the independent variables of the system. If a linear combination of the differential equations can be found such that the derivatives of the dependent variables combine to derivatives in the same direction (the directional derivatives of each has the same direction) then this direction is termed characteristic. Thus along a characteristic, the system reduces to ordinary rather than partial differential equations.

For n differential equations, n linear combinations of these equations are sought in which the directional derivatives of the dependent variables are in the same direction for each combination. If each of these n characteristic directions are real and distinct, the system is totally hyperbolic. The differential equations are classified as parabolic when exactly one real characteristic direction exists and elliptic when complex or imaginary characteristics arise. For hyperbolic systems, a systematic procedure called the method of characteristics is presented to obtain the characteristic directions and the resulting ordinary differential equation system.

If $u_j(Z,t)$ represents the j^{th} dependent variable in a system of n dependent variables, the linear combination $a \frac{\partial u_j}{\partial Z} + b \frac{\partial u_j}{\partial t}$ is the directional derivative of u_j along the curve or direction $dZ/dt = a/b$. Consider the following system of quasilinear partial differential equations,

$$L_i = \sum_{j=1}^{n} \left(a_{ij} \frac{\partial u_j}{\partial Z} + b_{ij} \frac{\partial u_j}{\partial t} \right) + c_i ; \; i=1,n$$

where a_{ij}, b_{ij} and c_{ij} depend on Z,t and u_j's. From linear algebra, Courant and Friederichs (9) show that the condition represented by Equation (3-63) must be satisfied for a linear combination of the equations to possess directional derivatives along the curves (Z_σ, t_σ) in which $\frac{Z_\sigma}{t_\sigma} = \frac{dZ}{dt} = \delta_i$. The δ_i are the characteristic directions and σ is the curve parameter.

$$\left| a_{ij} \, t_\sigma - b_{ij} \, Z_\sigma \right| = 0 \qquad (3\text{-}63)$$

A similar determinant equation exists for determining the characteristic ordinary differential equations for the dependent variables.

Associating variables as follows,

$$u_1 = y_1,\ u_2 = y_2,\ u_3 = a_c,\ u_4 = r_c,$$

$$u_5 = T_g,\ u_6 = T_s$$

the expansion of determinant Equation (3-63) for the constant density system represented by Equations (3-13), (3-33), (3-34), (3-59), and (3-62) results in,

$$\left(\frac{G}{\rho_g \epsilon}\, t_\sigma - Z_\sigma\right)^3 Z_\sigma^3 = 0$$

Thus the characteristic directions are given by,

$$dZ = 0$$

$$dZ/dt = G/\rho_g \epsilon$$

Normalizing the independent variables, the characteristics are,

$$\lambda = Z/L \tag{3-64}$$

$$\theta = \frac{Gt}{\rho_g \epsilon L} - \lambda = \xi - \lambda \tag{3-65}$$

where $\xi = \frac{Gt}{\rho_g \epsilon L}$. Thus the characteristic directions are real but not distinct.

The θ- characteristics of Equation (3-65) represent the trajectory in the t-Z plane, of inert elements in the fluid as they move through the bed with velocity $G/\rho_g \epsilon$. For an inert which enters the bed at t = 0, its movement is traced by,

$$Z = Gt/\rho_g \epsilon$$

and providing that the reactants are not totally consumed, the above

curve represents the interface between the unreacted, fresh part of the bed and the portion of the bed in which sulfation and oxidation have occurred. The elapsed time t_E, for an inert particle to pass through the bed to a point Z_E is given by

$$t_E = \frac{Z_E \rho_g \epsilon}{G}$$

Another useful physical interpretation of the θ- characteristic is that a disturbance in the composition or temperature of the feed will be propogated along this trajectory.

The characteristics in the t-Z plane for this system of equations are the straight lines traversing the domain shown below.

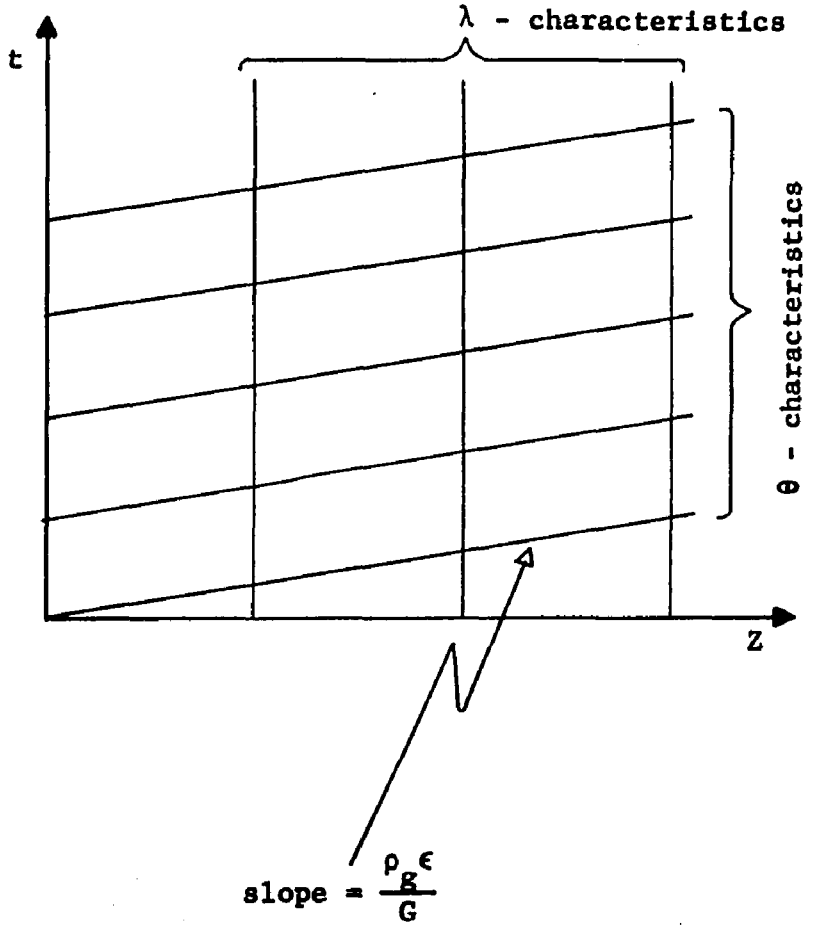

3.2.3 Transformations of Independent Variables

Consider the general equation,

$$\frac{\partial u}{\partial \lambda} + \frac{\partial u}{\partial \xi} = F(u,v) \tag{3-66}$$

where $u(\lambda,\xi)$ is a dependent variable in the (λ,ξ) domain. If u is also a function of λ and θ, $u(\lambda,\theta)$, where λ, ξ, and θ are defined by Equations (3-64) and (3-65), the rules of partial differentiation allow the following relations to be developed:

$$\frac{\partial \theta}{\partial \lambda} = -1 \tag{3-67}$$

$$\frac{\partial \theta}{\partial \xi} = 1 \tag{3-68}$$

and

$$\frac{\partial u(\lambda,\xi)}{\partial \lambda} = \frac{\partial u}{\partial \lambda} + \frac{\partial u}{\partial \theta}\frac{\partial \theta}{\partial \lambda} = \frac{\partial u}{\partial \lambda} - \frac{\partial u}{\partial \theta} \tag{3-69}$$

$$\frac{\partial u(\lambda,\xi)}{\partial \xi} = \frac{\partial u}{\partial \theta}\frac{\partial \theta}{\partial \xi} = \frac{\partial u(\lambda,\theta)}{\partial \theta} \tag{3-70}$$

Substituting Equations (3-69) and (3-70) into Equation (3-66) yields,

$$\frac{\partial u(\lambda,\theta)}{\partial \lambda} = F \tag{3-71}$$

Thus transforming from the original independent variables to the characteristics can be used to eliminate the $\frac{\partial}{\partial t}$ terms from equations such as (3-59) and (3-13).

3.3 Normalized System Equations-Model 1

By nondimensionalizing the conservation equations with respect to both their independent and dependent variables, the solutions

obtained will be as independent of the properties of a particular system as possible. Therefore use the following group of relations in normalizing the system equations

$$\omega = r_c/R \qquad \Psi = y_1/y_{10}$$
$$\phi = a_c/R \qquad S = y_2/y_{20} \qquad (3\text{-}72)$$
$$\mu = T_s/T_0 \qquad \Psi = T_g/T_0$$

and Equations (3-64), (3-65), (3-70) and (3-71).

The normalized equations will be even more general if the following group of dimensionless numbers is also defined.

$$N_{D1} = \frac{Rk_I}{D_{e1}} = \text{modified Damkohler number for Reaction I}$$

$$N_{D21} = \frac{Rk_{II}y_{10}}{D_{e2}} = \text{modified Damkohler number for Reaction II, component 1 } (O_2)$$

$$N_{D22} = \frac{R\gamma k_{II}y_{20}}{D_{e1}} = \text{modified Damkohler number for Reaction II, component 2 } (SO_2)$$

$$N_{sh_j} = \frac{RK_j}{D_{ej}} = \text{Sherwood number for component j.}$$

The subscript 0 implies inlet conditions.

Before applying these definitions to the differential equations, analyze the algebraic internal material balances, Equations (3-60) and (3-61), with regard to Equation (3-72) and the dimensionless numbers. Evaluating the internal material balance for sulfur dioxide (Equation (3-61)) at $r = r_c$, then substituting the resulting expression for $y_{s2}(r_c)$ into Equation (3-60) evaluated at

$r = r_c$, and finally using Equation (3-72) and the dimensionless groups, the following quadratic expression is obtained for the oxygen pellet concentration at the sulfation reaction site.

$$YRC = \frac{-B \pm \sqrt{B^2-4AC}}{2A} \tag{3-73}$$

where

$$YRC = \frac{y_{s1}(Z,r_c,t)}{y_{10}}$$

and

$$A = \left[\phi-\phi^2\left(1- \frac{1}{N_{sh1}}\right) + \frac{1}{N_{D1}}\right]\left[\omega + \omega^2\left(\frac{1}{N_{sh2}} - 1\right)\right] \tag{3-74}$$

$$B = \frac{1}{N_{D21}}\left[\phi - \phi^2\left(1 - \frac{1}{N_{sh1}}\right) + \frac{1}{N_{D1}}\right]$$

$$+ \left[\phi\left(1 - \frac{\phi}{\omega}\right) + \frac{1}{N_{D1}}\right]\left[\frac{N_{D22}}{N_{D21}}\left\{\omega + \omega^2\left(\frac{1}{N_{sh1}} - 1\right)\right\}\right.$$

$$\left. - Y\left\{\omega + \omega^2\left(\frac{1}{N_{sh2}} - 1\right)\right\}\right] \tag{3-75}$$

$$C = \frac{-Y}{N_{D21}}\left[\phi\left(1 - \frac{\phi}{\omega}\right) + \frac{1}{N_{D1}}\right] \tag{3-76}$$

Explicit expressions for the other important terms involving Equations (3-60) and (3-61) can now be normalized and are presented below.

$$SRC = \frac{y_{s2}(Z,r_c,t)}{y_{20}} = \frac{S}{1 + N_{D21}YRC\left[\omega+\omega^2\left(\frac{1}{N_{sh2}} - 1\right)\right]} \tag{3-77}$$

$$YAC = \frac{y_{s1}(Z,a_c,t)}{y_{10}} = \frac{Y}{N_{D1}\left[\left\{\phi-\phi^2\left(1-\frac{1}{N_{sh1}}\right)+\frac{1}{N_{D1}}\right\}+N_{D22}SRC\left\{\omega+\omega^2\left(\frac{1}{N_{sh1}}-1\right)\right\}\cdot\left\{\phi\left(1-\frac{\phi}{\omega}\right)+\frac{1}{N_{D1}}\right\}\right]} \quad (3\text{-}78)$$

$$\left[Y-\frac{y_{s1}(Z,R,t)}{y_{10}}\cdot\frac{\mu}{\Psi}\right]=$$

$$Y\cdot\frac{\left[\phi-\phi^2\left(1-\frac{1}{N_{sh1}}\right)+\frac{1}{N_{D1}}\right]+N_{D22}SRC\left[\omega+\omega^2\left(\frac{1}{N_{sh1}}-1\right)\right]\left[\phi\left(1-\frac{\phi}{\omega}\right)+\frac{1}{N_{D1}}\right]-\left[\left(\phi-\phi^2+\frac{1}{N_{D1}}\right)+N_{D22}SRC\left\{\phi\left(1-\frac{\phi}{\omega}\right)+\frac{1}{N_{D1}}\right\}\left(\omega-\omega^2\right)\right]\frac{\mu}{\Psi}}{\left[\phi-\phi^2\left(1-\frac{1}{N_{sh1}}\right)+\frac{1}{N_{D1}}\right]+N_{D22}\,SRC\left[\omega+\omega^2\left(\frac{1}{N_{sh1}}-1\right)\right]\left[\phi\left(1-\frac{\phi}{\omega}\right)+\frac{1}{N_{D1}}\right]}$$

$$= (\Delta Y) \quad (3\text{-}79)$$

$$\left[S - \frac{y_{s2}(Z,R,t)}{y_{20}}\right] \cdot \frac{\mu}{\Psi} = S \cdot \frac{1 + N_{D21}YRC\left[\omega + \omega^2\left(\frac{1}{N_{sh2}}\right)\right] - \left[1 - N_{D21}YRC(\omega-\omega^2)\right]\frac{\mu}{\Psi}}{1 + N_{D21}\,YRC\left[\omega + \omega^2\left(\frac{1}{N_{sh2}} - 1\right)\right]} = (\Delta S) \qquad (3\text{-}80)$$

Utulizing Equations (3-73), (3-77), (3-78), (3-79) and (3-80) along with the normalized dependent and independent variables and the dimensionless numbers, the remaining normalized, dimensionless conservation equations, (3-34), (3-59), (3-14), and (3-62), become respectively:

external temperature balance:

$$\frac{\partial \Psi}{\partial \xi} + \frac{\partial \Psi}{\partial \lambda} = \frac{-3(1-\epsilon)Lh}{GRC_g} \cdot (\Psi - \mu) \tag{3-81}$$

external oxygen balance:

$$\frac{\partial Y}{\partial \xi} + \frac{\partial Y}{\partial \lambda} = \frac{-3(1-\epsilon)\rho_g K_1 L}{GR} \cdot (\Delta Y) \tag{3-82}$$

external sulfur dioxide balance:

$$\frac{\partial S}{\partial \xi} + \frac{\partial S}{\partial \lambda} = \frac{-3(1-\epsilon)\rho_g K_2 L}{GR} \cdot (\Delta S) \tag{3-83}$$

oxidation reaction interface movement:

$$\frac{\partial \phi}{\partial \xi} = \frac{-\epsilon \rho_g \beta k_1 y_{10} L}{GR\ \rho_s W_6} \cdot YAC \tag{3-84}$$

sulfation reaction interface movement:

$$\frac{\partial \omega}{\partial \xi} = \frac{-\epsilon \rho_g \alpha k_{II} y_{10} y_{20} L}{GR\ \rho_s W_7} \cdot \frac{S(YRC)}{1 + N_{D21}(YRC)\left[\omega + \omega^2\left(\frac{1}{N_{sh2}} - 1\right)\right]} \tag{3-85}$$

pellet temperature balance:

$$\frac{\partial \mu}{\partial \xi} = \frac{-3\epsilon \rho_g L_h}{GR\rho_s C_s}\left[(\mu - \Psi) + \frac{K_1 \Delta H_I y_{10}\ (\Delta Y)}{hT_0} + \frac{K_2(\Delta H_{II} - \gamma \Delta H_I) y_{20}\ (\Delta S)}{hT_0}\right] \tag{3-86}$$

The normalized, dimensionless boundary and initial conditions for the preceding differential equations become:

at the bed inlet,

$$\Psi(0,\xi) = Y(0,\xi) = S(0,\xi) = 1.0$$

and at the instant flue gas is admitted to the bed,

$$\phi(\lambda,0) = \omega(\lambda,0) = 1.0$$

$$\mu(\lambda,0) = T_i/T_0$$

where T_i represents the initial bed temperature and T_0 the inlet flue gas temperature.

Transforming from the usual space-time (λ,ξ) independent variables to the characteristic domain (λ,θ) as explained in Section 3.2.3, Equations (3-81) through (3-86) become,

$$\frac{\partial\Psi}{\partial\lambda} = \frac{-3(1-\epsilon)Lh}{GRC_g} \cdot (\Psi-\mu) = -A_1(\Psi-\mu) \qquad (3\text{-}87)$$

$$\frac{\partial Y}{\partial\lambda} = \frac{3(1-\epsilon)\rho_g K_1 L}{GR} \cdot (\Delta Y) = -A_2\ (\Delta Y) \qquad (3\text{-}88)$$

$$\frac{\partial S}{\partial\lambda} = \frac{-3(1-\epsilon)\rho_g K_2 L}{GR} \cdot (\Delta S) = -A_3(\Delta S) \qquad (3\text{-}89)$$

$$\frac{\partial\phi}{\partial\theta} = \frac{-\epsilon\rho_g \beta k_I y_{10} L}{GR\rho_s W_6} \cdot YAC = -A_4 YAC \qquad (3\text{-}90)$$

$$\frac{\partial\omega}{\partial\theta} = \frac{-\epsilon\rho_g \alpha k_{II} y_{10} y_{20} L}{GR\rho_s W_7} \cdot (YRC)(SRC)$$

$$= -A_5(YRC)(SRC) \qquad (3\text{-}91)$$

$$\frac{\partial \mu}{\partial \theta} = \frac{-3\epsilon\rho_g Lh}{GR\rho_s C_s}\left[(\mu-\Psi) + A_7(\Delta Y) + A_8(\Delta S)\right]$$

$$= -A_6\left[(\mu-\Psi) + A_7(\Delta Y) + A_8(\Delta S)\right] \qquad (3\text{-}92)$$

where the dimensionless constants A_i are defined as

$$A_1 = \frac{3(1-\epsilon)Lh}{GRC_g} \qquad A_2 = \frac{3(1-\epsilon)\rho_g K_1 L}{GR}$$

$$A_3 = \frac{3(1-\epsilon)\rho_g K_2 L}{GR} \qquad A_4 = \frac{\epsilon\rho_g \beta k_I y_{10} L}{GR\rho_s W_6}$$

$$A_5 = \frac{\epsilon\rho_g \alpha k_{II} y_{10} y_{20} L}{GR\rho_s W_7} \qquad A_6 = \frac{3\epsilon\rho_g Lh}{GR\rho_s C_s}$$

$$A_7 = \frac{K_1 \Delta H_I y_{10}}{hT_0} \qquad A_8 = \frac{K_2(\Delta H_{II} - \gamma\Delta H_I) y_{20}}{hT_0}$$

The boundary conditions for this system of differential equations are as follows:

at the bed inlet:

$$\Psi(0,\theta) = Y(0,\theta) = S(0,\theta) = 1.0 \qquad (3\text{-}93)$$

and at the instant the initial wave of flue gas components reaches each point down the bed length:

$$\phi(\lambda,0) = \omega(\lambda,0) = 1.0$$
$$\mu(\lambda,0) = T_i/T_0 \qquad (3\text{-}94)$$

Equations (3-87) through (3-92) will be termed Model 1. As mentioned previously, pore diffusion and chemical reaction are the

significant resistances existing within the pellets for this model. These equations cannot be solved analytically, and a numerical solution algorithm will be developed in Chapter IV.

In the next section, Model 2 will be introduced. It is similar to Model 1 except that Model 2 utilizes thermal equilibrium between the pellet and external gas phases and pore diffusion as the controlling resistance within the porous pellets. Furthermore, only the sulfation reaction will be considered. In other words, it will be assumed that the pellets initially consist of CuO dispersed throughout the pellets rather than Cu_2O. This could be accomplished in thermal regeneration by reducing the maximum temperature level during regeneration (4), thereby only partially reducing the $CuSO_4$ to the oxide state. This could also be accomplished after complete thermal regeneration to Cu_2O by oxidation with air to CuO.

It will be shown in Chapter V that Model 2 possesses an analytical solution. Thus Model 2 can be utilized to check the accuracy of the numerical algorithm developed to solve the equations of Model 1, since the numerical and analytical solutions of Model 2 can be compared.

3.4 Pore Diffusion Controlling - Model 2

Parsons et al (35) determined experimentally that a shift in the sulfate reaction mechanism may occur at high temperatures. If the surface reaction rate constant possesses an exponential temperature dependency, a shift from a mechanism consisting of diffusion and surface kinetics to one controlled by diffusion can be expected at

elevated temperatures. At high temperatures, the reaction rates of the sulfur dioxide at the solid interface, due to the exponential increase with temperature, could become infinitely great in comparison with the diffusion of this component across the film resistance surrounding the pellets and the diffusion through the pellet pore structure.

At such a temperature level the sulfur dioxide concentration at the sulfation interface r_c approaches zero, since the reaction rate constant becomes infinite and the reaction is irreversible. This condition makes the solution of the pseudosteady state internal mass balance, Equation (3-28), much simpler, and the resulting system conservation equations are much less complex than those of Model 1.

Furthermore, thermal equilibrium between the external gas phase and the pellets should be more likely for diffusion controlling, since the reaction and heat generation rates possess a weaker temperature dependence than chemical reaction controlling. This will make the system equations even simpler while still rendering reasonable temperature and concentration profiles.

Thus Model 2 contains pore diffusion and film mass transfer, whereas Model 1 includes pore diffusion, film heat and mass transfer, and surface reaction as significant intraparticle rate processes. Also, only the sulfation reaction, Reaction II, is included, since the initial state of the bed when flue gas is introduced is considered to be cupric oxide, CuO, rather than cuprous oxide, Cu_2O.

To develop the sulfur dioxide profile within the pellet pores, the pertinent conservation relation, Equation (3-28), and its

boundary conditions for pore diffusion controlling need to be solved. The boundary condition for Equation (3-28) at the pellet surface remains the same, Equation (3-23), but the condition at the reaction interface r_c becomes,

$$X_2(Z,r_c,t) = 0 \tag{3-95}$$

Solving Equations (3-28), (3-23) and (3-95) for SO_2(i=2) simultaneously and utilizing constant gas density leads to the following expression for the sulfur dioxide profile within the pellets.

$$y_{s2}(Z,r,t) = y_2(Z,t) \frac{\left(\frac{1}{r_c} - \frac{1}{r}\right)}{\left(\frac{1}{r_c} - \frac{1}{R} + \frac{D_{e2}}{K_2 R^2}\right)} \tag{3-96}$$

Similar reasoning for the oxygen internal mass balance renders the expression below for the pellet oxygen profile.

$$y_{s1}(Z,r,t) = \frac{y_1\left(\frac{1}{r_c} - \frac{1}{r}\right)}{\left(\frac{1}{r_c} - \frac{1}{R} + \frac{D_{e1}}{K_1 R^2}\right)} \tag{3-97}$$

The movement of the sulfation reaction interface r_c within the pellet is developed similarly to Equation (3-33). Relating the change in pellet sulfate volume to the rate of change in the weight of sulfate for each pellet yields,

$$\frac{dN_7}{dt} = -\rho_s W_7 (4\pi r_c^2) \frac{\partial r_c}{\partial t}$$

and relating the production of sulfate by reaction to the rate of change in the weight of sulfate for each pellet yields

$$\frac{dN_7}{dt} = \alpha\left(4\pi r^2 D_{e2} \frac{\partial y_{s2}}{\partial r}\right)\Big|_{r_c}$$

$$= \alpha\left(4\pi r_c^2\right) \frac{D_{e2} y_2 / r_c^2}{\left(\frac{1}{r_c} - \frac{1}{R} + \frac{D_{e2}}{K_2 R^2}\right)}$$

Equating these two expressions and rearranging terms leads to the following expression for solid reaction interface movement in the diffusion controlled case.

$$\frac{\partial r_c}{\partial t} = \frac{-\alpha D_{e2}}{\rho_s W_7} \frac{y_2 / r_c^2}{\left(\frac{1}{r_c} - \frac{1}{R} + \frac{D_{e2}}{K_2 R^2}\right)} \tag{3-98}$$

Evaluating Equations (3-96) and (3-97) at r = R and substituting the resulting expressions into the oxygen and sulfur dioxide external balances, Equations (3-59), the external mass balances for diffusion controlling and gas-solid thermal equilibrium become,

$$\frac{\partial y_i}{\partial t} + \frac{G}{\epsilon \rho_g} \frac{\partial y_i}{\partial Z} = \frac{-3(1-\epsilon) D_{ei}}{R^3 \epsilon} \frac{y_i}{\left(\frac{1}{r_c} - \frac{1}{R} + \frac{D_{ei}}{K_i R^2}\right)} \tag{3-99}$$

The energy balance for solid-gas thermal equilibrium and sulfation reaction under diffusion control can be obtained by: 1) combining the pellet and external phase energy balances of Model 1, Equations (3-13) and (3-62), in such a manner that the gas-solid heat transfer terms cancel; 2) allowing $T_s = T_g = T$; and 3) setting

$\Delta H_I = 0$. Performing these operations yields,

$$\left[\epsilon\rho_g C_g + (1-\epsilon)\rho_s C_s\right] \frac{\partial T}{\partial t} + GC_g \frac{\partial T}{\partial Z}$$

$$= \frac{-3(1-\epsilon)K_2}{R} (y_2 - y_{s2,R})\Delta H_{II}$$

Neglecting the heat capacity of the gas in comparison to the solid phase heat capacity, and utilizing Equation (3-96) for $y_{s2,r}$, the preceding equation reduces to,

$$(1-\epsilon)\rho_s C_s \frac{\partial T}{\partial t} + GC_g \frac{\partial T}{\partial Z} = \frac{-3(1-\epsilon)D_{e2}\Delta H_{II}}{R^3} \frac{y_2}{\left(\frac{1}{r_c} - \frac{1}{R} + \frac{D_{e2}}{K_2 R^2}\right)} \tag{3-100}$$

The system of conservation equations for Model 2, Equations (3-98), (3-99) and (3-100), can be normalized and transformed by utilizing characteristics in a manner identical to that used on the Model 1 system in the last section. Thus upon rearranging terms and using Equations (3-64), (3-65), (3-70), (3-71) and (3-72), the diffusion controlling equations become:

external oxygen balance:

$$\frac{\partial Y}{\partial \lambda} = -A_1' \frac{Y\omega}{\left[1 + \omega\left(\frac{1}{N_{sh1}} - 1\right)\right]} \tag{3-101}$$

external sulfur dioxide balance:

$$\frac{\partial S}{\partial \lambda} = -A_2' \frac{S\omega}{\left[1 + \omega\left(\frac{1}{N_{sh2}} - 1\right)\right]} \tag{3-102}$$

pellet unreacted core radius:

$$\frac{\partial \omega}{\partial \theta} = -A_3' \frac{S}{\left[\omega + \omega^2\left(\frac{1}{N_{sh2}} - 1\right)\right]} \tag{3-103}$$

reactor temperature:

$$(1-\epsilon)\rho_s C_s \frac{\partial \Psi}{\partial \theta} + \rho_g \epsilon C_g \frac{\partial \Psi}{\partial \lambda}$$

$$= \frac{-3(1-\epsilon)\epsilon\rho_g D_{e2} y_{20} L \Delta H_{II}}{GR^2 T_0} \cdot \frac{S\omega}{\left[1 + \omega\left(\frac{1}{N_{sh2}} - 1\right)\right]} \tag{3-104}$$

where $\Psi = T/T_0$

$$A_1' = \frac{3(1-\epsilon)\rho_g D_{e1} L}{GR^2}$$

$$A_2' = \frac{3(1-\epsilon)\rho_g D_{e2} L}{GR^2}$$

$$A_3' = \frac{\epsilon\rho_g \alpha D_{e2} y_{20} L}{GR^2 \rho_g W_7}$$

The boundary and initial conditions are identical to those for Model 1.

$$\Psi(0,\theta) = Y(0,\theta) = S(0,\theta) = 1.0 \tag{3.93}$$

$$\Psi(\lambda,0) = T_i/T_0,\ \omega(\lambda,0) = 1.0 \tag{3.94}$$

In Section 3.1.7, the ratio between the bulk gas phase and pellet phase heat capacities, $\frac{\epsilon\rho_g C_g}{(1-\epsilon)\rho_s C_s}$, was shown to be less than 0.0001. Therefore as a rough approximation, the reactor temperature

profiles become simply,

$$\frac{\partial \Psi}{\partial \theta} = -A_4' \frac{S\omega}{\left[1 + \omega\left(\frac{1}{N_{sh2}} - 1\right)\right]} \qquad (3\text{-}105)$$

where $$A_4' = \frac{3\epsilon\rho_g D_{e2} y_{20} L\Delta H_{II}}{GR^2 \rho_s C_s T_0}$$

The pertinent boundary condition for the reactor energy balance is Equation (3-94).

In the remainder of this study, analysis of Model 2 will consist of differential equations (3-101), (3-102), (3-103) and (3-105).

3.5 Reactor Temperature Control - Nonadiabatic Model

Kardos and Stevens (15) study control of run-away temperature in fixed bed chemical reactors by dividing the reactor into sections with each section having a different rate of external cooling. These run-away temperatures may occur in systems containing exothermic reactions. In the sections near the bed entrance, a low external cooling rate allows the reaction to get started. The next sections, where the bed temperature and reaction rate reach a maximum possess high cooling rates. A low cooling rate in the last section is utilized to enable the reaction to go to completion.

To implement such temperature control schemes, the external phase temperature balance for Model I Equation (3-13), becomes

$$\frac{\partial T_g}{\partial t} + \frac{G}{\rho_g \epsilon} \frac{\partial T_g}{\partial Z} = \frac{-3(1-\epsilon)h}{\epsilon R \rho_g C_g} (T_g - T_s) - \frac{4h_w}{\epsilon \rho_g C_g D_B} (T_g - T_w)$$

where $T_w(Z,t)$ = reactor wall temperature, °C

h_w = heat transfer coefficient for transfer between reactor fluid and the wall, cal/sq cm-°C-sec

D_B = reactor diameter, cm

Normalizing and transforming to the characteristic independent variables, the bulk gas phase energy balance with external cooling can be written as

$$\frac{\partial \Psi}{\partial \lambda} = \frac{-3(1-\epsilon)Lh}{GRC_g}(\Psi-\mu) - \frac{4Lh_w}{GC_gD_B}(\Psi-\Psi_w)$$

$$= -A_1(\Psi-\mu) - A_9(\Psi-\Psi_w) \qquad (3\text{-}107)$$

where $\Psi_w = T_w/T_0$.

$A_9 = 4Lh_w/GC_gD_B$

This equation is subject to boundary condition (3-93).

Thus nonadiabatic operation of the fixed bed reactor is described by replacing Equation (3-87) by (3-107) in the Model 1 equation system. The set of Equations (3-88) through (3-92) and Equation (3-107) and boundary conditions given by Equation (3-93) will be referred to as Model 3.

3.6 Summary

Three distinct models have been developed in this chapter. The assumptions common to all three models are:

1) the fluid stream is in plug flow with negligible pressure loss between the entrance and exit of the bed.

2) the fluid stream is in fully developed turbulent flow.

3) radial gradients of temperature and concentration in the bed are negligible.

4) axial dispersion of heat and mass are negligible.

5) the solid phase of the bed consists of spherical porous pellets of uniform size.

6) radial symmetry exists within each spherical pellet, and the solid reactant is dispersed evenly throughout the pore structure.

7) radiation and conduction of heat between adjacent pellets is ignored.

8) thermal equilibrium exists between the solid and fluid in the pellet pores.

9) the pellet pores contain no temperature or pressure gradients

10) the irreversible solid-gas reactions occur via the shrinking core mechanism; that is, the chemical reaction rates are fast relative to the pore diffusion rates.

11) the accumulation of mass within the pellet pores is negligible in comparison to the reaction rates at the shrinking core interfaces (pseudosteady state approximation).

12) oxidation of the initial solid reactant occurs faster than sulfation of the intermediate solid reactant.

13) the mass velocity, G, and the molecular weight of the gas stream are constant.

14) sensible energy transfer due to mass transfer is negligible .

15) fluxes of O_2 and SO_2 through the "film" resistance surrounding each pellet are significant and can be related by stoichiometry.

The distinguishing features between each model are:

	Model 1	Model 2	Model 3
Nonisothermal nature of bed operation:	adiabatic	adiabatic	nonadiabatic
Pellet-bulk gas phase temperature equilibrium?	no	yes	no
Intraparticle mass transfer:	pore diff. and chem. reaction	pore diff. control-ling	pore diff. and chem. reaction

In addition, the heat capacity of the bulk gas phase is neglected in Model 2. Justifications for the various assumptions were presented previously.

After applying the characteristic transformation and normalizing, the final form of each model is given by Equations (3-87) through (3-94) for Model 1; (3-101), (3-102), (3-103), (3-105), (3-93) and (3-94) for Model 2; and (3-88) through (3-94) and (3-107) for Model 3.

techniques for the numerical solution of ordinary differential equations, because along the characteristic curves the partial differential system reduces to ordinary differentials. Within this solution approach, there are two categories of solution methods (8). One involves "open" type formulas characterized by the Runge-Kutta technique, while the other category consists of "closed" type formulas characterized by the predictor-corrector technique. In open formulas, the solution for the variable u, which is a function of an independent variable x, at the point $u(x+\Delta x)$ is expressed in terms of the function and its derivative, $\frac{du}{dx} = f(x)$, evaluated at point x and points backward, $x-\Delta x$, $x-2\Delta x$, etc. which are already known. Whereas closed formulas express the solution for $u(x+\Delta x)$ in terms of backward points and at $x+\Delta x$ by estimating the value of the function at this point and iterating until a correct value is found.

In the second approach, the system equations (3-81) through (3-86) are investigated. These equations are approximated by the use of finite differences producing a system of algebraic equations to be solved. Von Rosenburg (44) recommends various finite difference schemes based on the class (parabolic, elliptic or hyperbolic) of the partial differential equation. For quasilinear systems of the hyperbolic type, the centered-difference scheme is recommended. In this scheme, the partial derivative terms are approximated through use of truncated Taylor's series at the midpoint or center of two consecutive discrete independent variable locations. Thus, for the simple system u(x), the centered-difference approximation

at the point $x - \frac{\Delta x}{2}$ is,

$$\left.\frac{du}{dx}\right|_{-\Delta x/2} = \frac{u\{x\} - u\{x-\Delta x\}}{\Delta x}$$

and terms such as u^2 are evaluated by simple averaging,

$$u^2|_{-\Delta x/2} = \frac{1}{2}\left(u^2\{x-\Delta x\} + u^2\{x\}\right)$$

Each of the aforementioned techniques was explored and implemented. Of these, only the predictor-corrector method discussed in the first approach proved satisfactory. The unsuccessful Runge-Kutta and finite-difference schemes were beset with numerical instability problems.

4.1.2 Discrete Variable Notation

Consider the evaluation of the system variables only at a finite number of points spaced equally in each direction. The domain of interest of the bed is represented by the value of the discrete independent variables at each of these points described by the subscripts i,j where

$$\lambda_i = i(\Delta\lambda) \quad i = 0,1,\ldots.\frac{1.0}{\Delta\lambda}$$

$$\theta_j = j(\Delta\theta) \quad j = 0,1,\ldots\ldots$$

with $\Delta\theta$ not necessarily equal to $\Delta\lambda$. A grid network describing the bed is

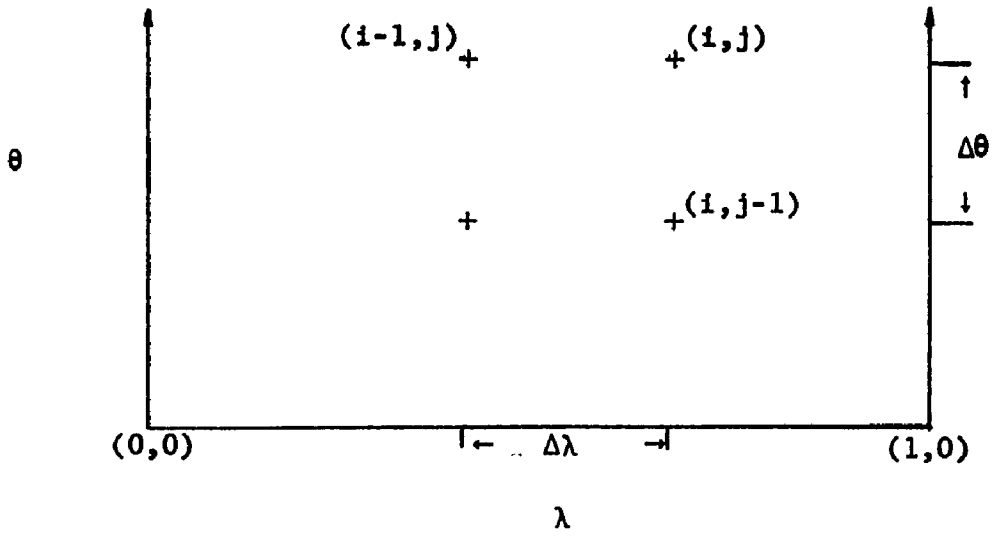

The notation for the dependent variables at a specific discrete point (i,j) is expressed in the following manner,

$$u(\lambda_i, \theta_j) = u_{i,j}$$

for $u = \Psi, Y, S, \phi, \omega, \mu$.

4.1.3 Predictor Corrector Algorithm

The characteristic differential equations of Model 1 were solved using a second-order predictor-corrector integration scheme. The various integration formulas which apply for the system

$$\frac{du}{dl} = f(u,l) \qquad (4\text{-}1)$$

can be presented in simplified form as

Starter

$$u_{m+1} = u_m + h\, f\left[l_m + \frac{h}{2},\ u_m + \frac{h}{2} f(l_m, u_m)\right] \qquad (4\text{-}2)$$

Predictor

$$u_{m+1}^{(o)} = u_{m-1} + 2h\ f(l_m, u_m) \tag{4-3}$$

Corrector

$$u_{m+1}^{(k)} = u_m + \frac{h}{2}\left[f(l_m, u_m) + f(l_{m+1}, u_{m+1}^{(k-1)})\right] \tag{4-4}$$

where $h = \Delta l$.

$l_m = mh$

and the superscript k represents the k^{th} iteration.

The starter is the modified Euler formula (25), and it is used near boundaries when values of u are known at only one level back fron m+1. Once the integration has been started, the predictor formula is utilized to estimate the value of u at the new point, and the corrector is then used iteratively to improve upon this value. The predictor is a multistep integration formula incorporating Newton's backward formula (8), while the corrector is a second-order Euler formula utilizing an average slope between the point of interest, m+1, and the next point, m.

To facilitate implementation of this integration scheme to Equations (3-87) through (3-92), use the following functional notation

$$F_1\{\Psi,\mu\} = -A_1(\Psi-\mu) \tag{4-5}$$

$$F_2\{\Psi,Y,S,\phi,\omega,\mu\} = -A_2\Delta Y \tag{4-6}$$

$$F_3\{\Psi,Y,S,\phi,\omega,\mu\} = -A_3\Delta S \tag{4-7}$$

$$F_4\{\Psi,Y,S,\phi,\omega,\mu\} = -A_4(YAC) \tag{4-8}$$

$$F_5\{\Psi,Y,S,\phi,\omega,\mu\} = -A_5(YRC)\cdot(SRC) \tag{4-9}$$

$$F_6\{\Psi,Y,S,\phi,\omega,\mu\} = -A_6\left[(\mu-\Psi) + A_7\Delta Y + A_8\Delta S\right] \tag{4-10}$$

where A_i, ΔY, ΔS, YRC, SRC, and YAC are defined in Chapter III. Furthermore, define

$$F_{K,i,j} = F_K(\Psi_{i,j}, Y_{i,j}, S_{i,j}, \phi_{i,j}, \omega_{i,j}, \mu_{i,j});$$

$$K = 1,2\ldots6 \tag{4-11}$$

$$u_{i-1/2,j} = \frac{u_{i-1,j} + u_{i,j}}{2} \quad ; \quad u = \phi,\omega,\mu \tag{4-12}$$

$$u_{i,j-1/2} = \frac{u_{i,j} + u_{i,j-1}}{2} \quad ; \quad u = \Psi,Y,S \tag{4-13}$$

$$u_{\underline{i-1/2},j} = u_{i-1,j} + \frac{\Delta\lambda}{2} F_{Ki-1,j} \begin{cases} u = \Psi,Y,S \\ \vdots\ \vdots\ \vdots \\ K = 1,2,3 \end{cases} \tag{4-14}$$

$$u_{i,\underline{j-1/2}} = u_{i,j-1} + \frac{\Delta\theta}{2} F_{Ki,j-1} \begin{cases} u = \phi,\omega,\mu \\ \vdots\ \vdots\ \vdots \\ K = 4,5,6 \end{cases} \tag{4-15}$$

Utilizing Equations (4-2) through (4-15), the second-order starter, predictor and corrector formulas for Equations (3-87) through (3-92) become,

starter equations:

$$\Psi_{i,j} = \Psi_{i-1,j} + \Delta\lambda\, F_1\left\{\Psi_{i-1,j} + \frac{\Delta\lambda}{2} F_1\left\{\Psi_{i-1,j},\mu_{i-1,j}\right\},\right.$$

$$\left.\frac{\mu_{i-1,j} + \mu_{i,j}}{2}\right\} = \Psi_{i-1,j} + \Delta\lambda\left\{\Psi_{\underline{i-1/2},j},\mu_{i-1/2,j}\right\}$$

(4-16a)

$$Y_{i,j} = Y_{i-1,j} + \Delta\lambda\, F_2 \left\{ \begin{matrix} \Psi_{\underline{i-1/2},j},\ Y_{\underline{i-1/2},j},\ S_{\underline{i-1/2},j}, \\ \phi_{i-1/2,j},\ \omega_{i-1/2,j},\ \mu_{i-1/2,j} \end{matrix} \right\} \tag{4-16b}$$

$$S_{i,j} = S_{i-1,j} + \Delta\lambda\, F_3 \left\{ \begin{matrix} \Psi_{\underline{i-1/2},j},\ Y_{\underline{i-1/2},j},\ S_{\underline{i-1/2},j}, \\ \phi_{i-1/2,j},\ \omega_{i-1/2,j},\ \mu_{i-1/2,j} \end{matrix} \right\} \tag{4-16c}$$

$$\phi_{i,j} = \phi_{i,j-1} + \Delta\theta\, F_4 \left\{ \begin{matrix} \Psi_{i,j-1/2},\ Y_{i,j-1/2},\ S_{i,j-1/2}, \\ \phi_{i,\underline{j-1/2}},\ \omega_{i,\underline{j-1/2}},\ \mu_{i,\underline{j-1/2}} \end{matrix} \right\} \tag{4-17a}$$

$$\omega_{i,j} = \omega_{i,j-1} + \Delta\theta\, F_5 \left\{ \begin{matrix} \Psi_{i,j-1/2},\ Y_{i,j-1/2},\ S_{i,j-1/2}, \\ \phi_{i,\underline{j-1/2}},\ \omega_{i,\underline{j-1/2}},\ \mu_{i,\underline{j-1/2}} \end{matrix} \right\} \tag{4-17b}$$

$$\mu_{i,j} = \mu_{i,j-1} + \Delta\theta\, F_6 \left\{ \begin{matrix} \Psi_{i,j-1/2},\ S_{i,j-1/2},\ Y_{i,j-1/2}, \\ \phi_{i,\underline{j-1/2}},\ \omega_{i,\underline{j-1/2}},\ \mu_{i,\underline{j-1/2}} \end{matrix} \right\} \tag{4-17c}$$

predictor equations:

$$\Psi^{(o)}_{i,j} = \Psi_{i-2,j} + 2\Delta\lambda\, F_{1,i-1,j} \tag{4-18a}$$

$$Y^{(o)}_{i,j} = Y_{i-2,j} + 2\Delta\lambda\, F_{2,i-1,j} \tag{4-18b}$$

$$S^{(o)}_{i,j} = S_{i-2,j} + 2\Delta\lambda\, F_{3,i-1,j} \tag{4-18c}$$

$$\phi^{(o)}_{i,j} = \phi_{i,j-2} + 2\Delta\theta\, F_{4,i,j-1} \tag{4-19a}$$

$$\omega_{i,j}^{(o)} = \omega_{i,j-2} + 2\Delta\theta\ F_{5,i,j-1} \tag{4-19b}$$

$$\mu_{i,j}^{(o)} = \mu_{i,j-2} + 2\Delta\theta\ F_{6,i,j-1} \tag{4-19c}$$

corrector equations:

$$\Psi_{i,j}^{(k)} = \Psi_{i-1,j} + \frac{\Delta\lambda}{2}\left[F_{1,i-1,j} + F_1\left\{\Psi_{i,j}^{(k-1)}, \mu_{i,j}^{(k-1)}\right\}\right] \tag{4-20a}$$

$$Y_{i,j}^{(k)} = Y_{i-1,j} + \frac{\Delta\lambda}{2}\left[F_{2,i-1,j} + F_2\left\{\begin{matrix}\Psi_{i,j}^{(k)}, Y_{i,j}^{(k-1)}, S_{i,j}^{(k-1)}, \\ \phi_{i,j}^{(k-1)}, \omega_{i,j}^{(k-1)}, \mu_{i,j}^{(k-1)}\end{matrix}\right\}\right] \tag{4-20b}$$

$$S_{i,j}^{(k)} = S_{i-1,j} + \frac{\Delta\lambda}{2}\left[F_{3,i-1,j} + F_3\left\{\begin{matrix}\Psi_{i,j}^{(k)}, Y_{i,j}^{(k)}, S_{i,j}^{(k-1)}, \\ \phi_{i,j}^{(k-1)}, \omega_{i,j}^{(k-1)}, \mu_{i,j}^{(k-1)}\end{matrix}\right\}\right] \tag{4-20c}$$

$$\phi_{i,j}^{(k)} = \phi_{i,j-1} + \frac{\Delta\theta}{2}\left[F_{4,i,j-1} + F_4\left\{\begin{matrix}\Psi_{i,j}^{(k)}, Y_{i,j}^{(k)}, S_{i,j}^{(k)}, \\ \phi_{i,j}^{(k-1)}, \omega_{i,j}^{(k-1)}, \mu_{i,j}^{(k-1)}\end{matrix}\right\}\right] \tag{4-21a}$$

$$\omega_{i,j}^{(k)} = \omega_{i,j-1} + \frac{\Delta\theta}{2}\left[F_{5,i,j-1} + F_5\left\{\begin{matrix}\Psi_{i,j}^{(k)}, Y_{i,j}^{(k)}, S_{i,j}^{(k)}, \\ \phi_{i,j}^{(k)}, \omega_{i,j}^{(k-1)}, \mu_{i,j}^{(k-1)}\end{matrix}\right\}\right] \tag{4-21b}$$

$$\mu_{i,j}^{(k)} = \mu_{i,j-1} + \frac{\Delta\theta}{2}\left[F_{6,i,j-1} + F_6\left\{\begin{matrix}\Psi_{i,j}^{(k)}, Y_{i,j}^{(k)}, S_{i,j}^{(k)}, \\ \phi_{i,j}^{(k)}, \omega_{i,j}^{(k)}, \mu_{i,j}^{(k-1)}\end{matrix}\right\}\right] \tag{4-21c}$$

Before presenting the solution algorithm, consider the λ,θ grid network shown below

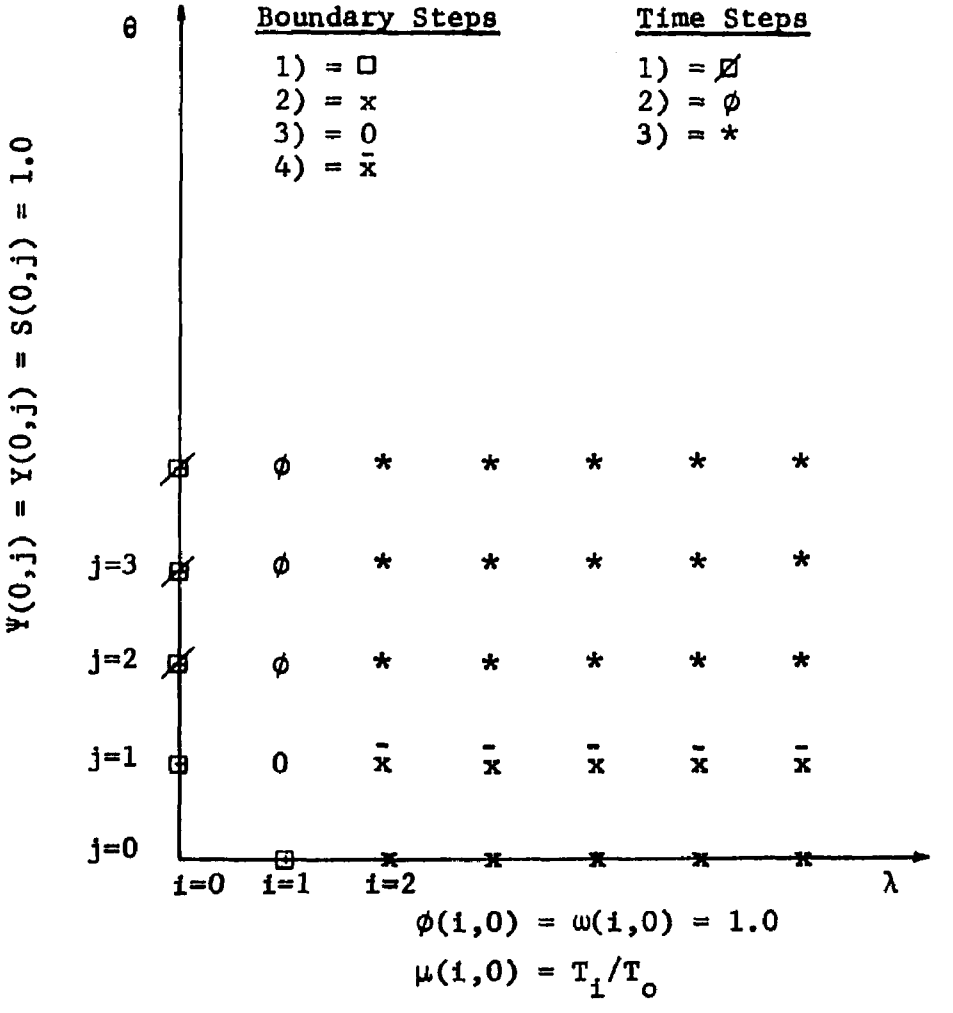

The boundary and initial conditions are shown along their respective axes to give a better perspective as to which variables are known along each λ, θ axis. Thus values for the oxidation reaction radius, sulfation reaction radius and pellet temperature (ϕ, ω, μ respectively) are known along the upper horizontal line, j = 0, while the bulk gas temperature, O_2 concentration and SO_2

concentration (Ψ, Y and S respectively) are given along the vertical θ axis, $i = 0$. At the point $j = 0$, $i = 0$ all six independent variables are known. The symbols on the grid represent points at which the steps in the following algorithm will apply. The steps are divided into two basic categories. The first set contains the "boundary" steps which will be utilized only at the beginning of the integration primarily to incorporate the inlet conditions and to start integration in the θ-direction. The second category includes the "time" steps which will be repeated at each new θ level (increment in j). Notice from Equation (3-65) that increasing θ, corresponds directly to increasing time for a fixed bed position λ.

The solution algorithm for the prediction of the concentration and temperature profiles in the bed based on the Model 1 characteristic differential equations is as follows:

Boundary Steps

1) Determine $\Psi(1,0)$, $Y(1,0)$ and $S(1,0)$ through use of the pertinent starter equation, Equation (4-16), and then obtain $\phi(0,1)$, $\omega(0,1)$, and $\mu(0,1)$ by starter Equation (4-17). In using Equation (4-16), the values for $\phi(1,0)$, $\omega(1,0)$ and $\mu(1,0)$ are given by boundary condition (3-94) (see, for example, the expanded form of Equation (4-16a) for $i = 1$, $j = 0$). Similarly the values of $\Psi(0,1)$, $Y(0,1)$ and $S(0,1)$ are known by boundary condition (3-93) for Equation (4-17).

2) Calculate $\Psi(i,0)$, $Y(i,0)$ and $S(i,0)$ at each i, for $i = 1,2,3....1/\Delta\lambda$, by predictor-corrector integration along the bed length at $\theta = j = 0$. At each i, first use

predictor Equation (4-18). then use corrector Equation (4-20) interatively until Ψ, Y and S are <u>each</u> changing by less than a specified tolerance, σ. Start this procedure at i = 2 and then repeat it as i is incremented by one until i = $1/\Delta\lambda$ is reached.

The convergence criteria used throughout the solution technique will be as follows:

Convergence of variable u(i,j) will be accepted when

$$\left| \frac{u_{(i,j)}^{(k)} - u_{(i,j)}^{(k-1)}}{u_{(i,j)}^{(k-1)}} \right| < \sigma \qquad (4\text{-}22)$$

where $\sigma = 10^{-5}$ for example.

3) Determine Ψ, Y, S, φ, ω, μ at the point i = 1, j = 1 by applying starter Equation (4-16), then starter Equation (4-17). To insure accuracy, correct the values obtained by utilizing Equations (4-20) then (4-21) iteratively until <u>each</u> of the six dependent variables is changing by less than the specified tolerance. Before using Equation (4-16), however, values for φ(1,1), ω(1,1) and μ(1,1) must be approximated. The approximation utilized, is to set them equal to their respective values at i = 1, j = 0.

4) Determine Ψ(i,1), Y(i,1), S(i,1), φ(i,1), ω(i,1) and μ(i,1) at each i for i = 2,3,...$1/\Delta\lambda$. Starting at i = 2 and increasing i until the value $1/\Delta\lambda$ is reached, apply the following steps at each new point (i,1):

a) Use predictor Equation (4-18) to obtain

$$\Psi_{(i,1)}^{(o)}, \; Y_{(i,1)}^{(o)} \text{ and } S_{(i,1)}^{(o)} .$$

b) Use starter Equation (4-17) to obtain

$$\phi_{(i,1)}^{(o)}, \; \omega_{(i,1)}^{(o)} \text{ and } \mu_{(i,1)}^{(o)} .$$

c) Set the counter, k, to 1.

d) Use corrector Equation (4-20) to obtain

$$\Psi^{(k)}_{(i,1)},\ Y^{(k)}_{(i,1)} \text{ and } S^{(k)}_{(i,1)}.$$

e) Use corrector Equation (4-21) to obtain

$$\phi^{(k)}_{(i,1)},\ \omega^{(k)}_{(i,1)} \text{ and } \mu^{(k)}_{(i,1)}.$$

f) Use the convergence test, Equation (4-22), on all six of the dependent variables. If each of them is changing by less than the specified tolerance, increment i and proceed to step a). Otherwise, increment the counter, k, by one and proceed to step d).

Time Steps

After completion of the boundary steps, repeat the following three steps at each new level of θ as j is increased (j=2,3,...).

1) Calculate $\phi(0,j)$, $\omega(0,j)$ and $\mu(0,j)$ by using predictor Equation (4-19), followed by the iterative application of corrector Equation (4-21) until each of these three variables is changing by less than the specified tolerance.

2) Compute values for Ψ, Y, S, ϕ, ω, and μ at the point (1,j) by applying predictor Equation (4-19), followed by use of starter Equation (4-16). Next, improve on these initial values by utilizing corrector Equations (4-20) and (4-21) iteratively, and in that order, until each of the six variables has satisfied the convergence criteria.

3) Determine $\Psi(i,j)$, $Y(i,j)$, $S(i,j)$, $\phi(i,j)$, $\omega(i,j)$, and $\mu(i,j)$ for $i = 2,3,\ldots 1/\Delta\lambda$. Again starting at i = 2 and incrementing by one until $i = 1/\Delta\lambda$, apply predictor Equation (4-18), then predictor Equation (4-19) followed by the use of corrector Equations (4-20) and (4-21) iteratively and in that order until each of the six

dependent variables has converged at each value of i.

It should be noted that whenever Equations (4-16) through (4-21) are utilized in the above algorithm, each of them are always implemented in the a, b, c sequence. When applying Equation (4-16), for example, first (4-16a) is utilized, followed by (4-16b) and lastly (4-16c). The computations in the algorithm can be terminated when the breakthrough concentration is attained or after a specified elapsed time has occurred.

Several subjects pertaining to this solution algorithm deserve further comment. By use of Equation (4-14) in Equation (4-16), the pellet temperature, oxidation reaction radius and sulfation reaction radius (μ, Ψ and ω) have been considered to vary linearly between the points $i\Delta\lambda$ and $(i-1)\Delta\lambda$ along the axis of the bed. Referring back to Equations (3-84), (3-85) and (3-86), the variation of these three dependent variables with axial distance is incorporated by the variation of Ψ, Y, and S with distance. This is a relatively weak dependence, however, as will be illustrated in the results section. Thus the major variations in μ, ϕ and ω occur with time, or the θ-characteristic in this case, and the assumption of linear profiles between axial grid points is acceptable when integrating Ψ, Y and S axially through use of the starter Equation (4-16). Furthermore, if any significant error were introduced by this assumption, it would be rectified by the subsequent correction of the values for Ψ, Y and S at this point by use of corrector formula (4-20). The corrector does not depend on values at the point (i-1/2,j) or any other points between normal

grid points. Values predicted by the starter formula are always readjusted by the iterative use of corrector formulas except in boundary step 1). Similar comments can be made on the use of Equation (4-15) in starter Equation (4-17) with regard to the linear profiles of Ψ,Y and S between grid points along the θ-characteristic.

The algorithm was devised in as general a manner as possible, so that it can be used to solve any system of first order coupled nonlinear partial differential equations of the following form,

$$\frac{\partial u_i}{\partial z_1} = F_i\{\underline{u}, \underline{u'}, z_1, z_2\} \qquad i = 1,\ldots n \tag{4-23}$$

$$\frac{\partial u'_j}{\partial z_2} = F'_j\{\underline{u}, \underline{u'}, z_1, z_2\} \qquad j = 1,\ldots m \tag{4-24}$$

with boundary conditions given by,

$$\begin{aligned} u_i\{z_1 = 0,\ z_2\} &= \text{arbitrary function of } z_2 \\ u'_i\{z_1,\ z_2 = 0\} &= \text{arbitrary function of } z_1 \end{aligned} \tag{4-25}$$

where the F'_i and F_j represent arbitrary functions of the dependent variables $\underline{u} = \{u_1, u_2 \ldots u_n\}$ and $\underline{u'} = \{u'_1, \ldots u'_m\}$ and the independent variables z_1 and z_2. Thus the nonadiabatic case, Model 3, and the diffusion controlling case, Model 2, can also be solved using this algorithm. The algorithm may be applicable to a large class of partial differential equations, since systems of n^{th} order quasi-linear partial differential equations can always be reduced to a

system of first order partial differential equations by transformation of the dependent variables.

The algorithm is also very efficient in that relatively little storage of profile information is required. Referring to the last grid network shown, it can be seen that at most only three θ-levels plus convergence and error estimation criteria for the dependent variables need storage allocations in order to predict their values along the length of the reactor at the next θ-level. Three θ-levels are required, because a two-step predictor-corrector technique has been applied. Thus for $\Delta\lambda = 0.05$, a maximum of only 390 dependent variable storage locations are required when implementing this algorithm on a digital computer for the Model 1 characteristic equations.

Whenever corrector Equations (4-20) and (4-21) are used in succession, the number of dependent variables evaluated at the current or k^{th} iteration increases and those evaluated at the preceding or (k-1) correction iteration decrease correspondingly as the sequence of formulas (4-20a), (4-20b),...(4-21b), (4-21c) are being implemented in succession. This should lead to faster convergence for the variables at the end of the sequence.

The predictor-corrector solution algorithm presented in this section has been translated into an equivalent digital computer program written in Fortran IV language for either the IBM 360-65 at the Computer Research Center or the XDS Sigma 5 in the Chemical Engineering Building at Louisiana State University. A copy of the Fortran IV program is listed in Appendix C.

4.2 Analytical Solution Technique - Model 2

4.2.1 Description

Ozawa (33) studies the solution of the following set of partial differential equations,

$$\frac{\partial u}{\partial z_1} = \frac{\partial v}{\partial z_2} = f(u,v) \tag{4-26}$$

subject to the boundary conditions

$$u(z_1 = 0,\ z_2) = u_o(z_2);\ z_2 > 0 \tag{4-27}$$

$$v(z_1,\ z_2 = 0) = v_o(z_1);\ z_1 > 0 \tag{4-28}$$

where dependent variables u and v are each functions of independent variables z_1 and z_2, u_o and v_o represent known functions of z_2 and z_1 respectively and f is a known function of both u and v. This equation set arises often when describing transient, reacting systems in fixed beds with one-dimensional geometry.

Noting that $\partial u/\partial z_1 - \partial v/\partial z_2 = 0$, Ozawa introduces a potential function, Q, such that

$$u = \partial Q/\partial z_2;\ v = \partial Q/\partial z_1$$

$$\frac{\partial^2 Q}{\partial z_1 \partial z_2} = f(\partial Q/\partial z_1, \partial Q/\partial z_2)$$

If f is separable, that is,

$$f(u,v) = g(u)\ h(v)$$

and if either of the functions g or h is linear, analytical or semianalytical solutions for Equations (4-26) can be obtained by utilizing the Legendre transformation. The Legendre transform, I, of Q is defined as (2),

$$I = vz_1 + uz_2 - Q$$

Utilizing the relationships between the potential function, Legendre transform and the original equation set, Ozawa establishes the following system of equations assuming that g(u) = u,

$$\frac{du}{u} = \frac{dv}{v - v_o + \frac{\partial v_o / \partial z_1}{h(v_o)}} \tag{4-29}$$

$$dz_1 = \frac{dv}{h(v)\left[v - v_o + \frac{\partial v_o / \partial z_1}{h(v_o)}\right]} \tag{4-30}$$

$$z_2 = \frac{\partial}{\partial u}\left[\int z_1 \cdot dv + \chi(u)\right] \tag{4-31}$$

where $\chi(u)$ is a function determined through the boundary condition (4-28). Thus from Equations (4-29), (4-30) and (4-31) with boundary conditions (4-27) and (4-28), Ozawa provides a procedure to obtain analytical expressions of the form

$$z_1 = F_1(u,v) \tag{4-32}$$

$$z_2 = F_2(u,v) \tag{4-33}$$

where F_1 and F_2 are functions of u and v obtained by this integration procedure.

The resulting solution, Equations (4-32) and (4-33), of the original system equations are implicit with respect to the dependent variables and usually may not be inverted analytically to obtain explicit expressions for u and v in terms of z_1 and z_2.

The major disadvantage of Ozawa's procedure is the difficulty

encountered in obtaining an expression for $F_2(u,v)$ from Equation (4-31). Bischoff (6) derives an analytical solution technique for Equations (4-26), (4-17), and (4-28) which is much easier to implement than Ozawa's by assuming a solution

$$u(z_1,z_2) = \frac{v(z_1,z_2) - v_o}{v(0,z_2) - v_o} \cdot u_o \tag{4-35}$$

based on intuition. Equation (4-35) is merely a special case of Ozawa's Equation (4-29) where v_o is restricted to a constant value rather than an arbitrary function of z_1. This is normally not a very restrictive condition, since it amounts to requiring that either the inlet or the initial concentration of one of the reacting species be a constant. This criterion is satisfied in most fixed bed applications.

Under this restriction, Bischoff obtains the following implicit solutions,

$$z_1 = \int_{v(0,z_2)}^{v(z_1,z_2)} \frac{dv}{(v-v_o)h(v)} \tag{4-37}$$

$$\int_0^{z_2} u_o dz_2 = \int_{v_o}^{v(0,z_2)} \frac{dv}{h(v)} \tag{4-38}$$

which apply to the differential equation system,

$$\frac{\partial u}{\partial z_1} = \frac{\partial v}{\partial z_2} = u \cdot h(v) \tag{4-39}$$

$$u(0,z_2) = u_o(z_2) \tag{4-40}$$

$$u(z_1,0) = v_o = \text{constant} \tag{4-41}$$

If u_o is also a constant, the relationship between Equations (4-32), (4-33), (4-37) and (4-38) can be expressed by

$$z_1 = F_1(u,v) = \int_{v(0,z_2)}^{v(z_1,z_2)} \frac{dv}{(v \cdot v_o)h(v)} \qquad (4\text{-}42)$$

$$z_2 = F_2(u,v) = \int_{v_o}^{v(0,z_2)} \frac{dv}{u_o h(v)} \qquad (4\text{-}43)$$

where $v(0,z_2)$ is related to u and v by Equation (4-35).

4.2.2 Analytical Solution for Model 2

The bulk gas phase SO_2 balance and pellet reaction interface (solid reactant material balance) equation for Model 2, mass diffusion controlling, are coupled to each other through the bulk gas phase SO_2 concentration, S, and the sulfation reaction interface radius, ω. However, these two equations are not functions of the O_2 concentration, Y, or the reactor temperature, Ψ.

The expressions for the variation of the SO_2 and solid reaction radius, Equations (3-101) and (3-102) for Model 2 are

$$\frac{\partial \omega}{\partial \theta} = \frac{-\epsilon \rho_g \alpha D_{e2} y_{20} L}{GR^2 \rho_s W_7} \cdot \frac{S}{\omega + \omega^2(\frac{1}{N_{sh2}} - 1)} \qquad (3\text{-}101)$$

$$\frac{\partial S}{\partial \lambda} = \frac{-3(1-\epsilon)\rho_g D_{e2} L}{GR^2} \cdot \frac{S\omega}{1 + \omega(\frac{1}{N_{sh2}} - 1)} \qquad (3\text{-}102)$$

with boundary conditions

$$\omega(\lambda,0) = S(0,\theta) = 1.0 \qquad (3\text{-}93)$$

By using the proper transformation, Equations (3-101), (3-102) and

(3-93) can be changed to match the form of Equations (4-39), (4-40) and (4-41). The transformed equations can then be solved analytically.

Define the variables $\Phi(\lambda,\theta)$ and $\chi(\lambda,\theta)$ as

$$\Phi = \frac{\omega^3}{3} \tag{4-44}$$

$$\chi = \frac{\alpha y_{20} \epsilon}{3(1-\epsilon)\rho_s W_7} \cdot S \tag{4-45}$$

Utilizing Φ and χ, Equations (3-101) and (3-102) become

$$\frac{\partial \chi}{\partial \lambda} = \frac{\partial \Phi}{\partial \theta} = \frac{-3(1-\epsilon)\rho_g D_{e2} L}{GR^2} \cdot \frac{\chi(3\Phi)^{1/3}}{1 + (3\Phi)^{1/3}(\frac{1}{N_{sh2}} - 1)} \tag{4-46}$$

with boundary conditions

$$\Phi(\lambda,0) = 1/3 = \Phi_o \tag{4-47}$$

$$\chi(0,\theta) = \frac{\alpha y_{20} \epsilon}{3(1-\epsilon)\rho_s W_7} = \chi_o \tag{4-48}$$

Associating variables between Equations (4-46), (4-47) and (4-48) and Equations (4-39), (4-40), and (4-41) as follows,

$$\lambda = z_1$$

$$\theta = z_2$$

$$\chi = u$$

$$\Phi = v$$

the solution can be obtained from Equations (4-35), (4-42) and (4-43).

Associating variables properly and rearranging terms, Equation

(4-35) yields

$$\Phi\{0,\theta\} = \frac{(\Phi - 1/3)\chi_o}{\chi} + 1/3$$

$$= \frac{1}{3}\left(\frac{\omega^3 - 1}{S} + 1 \right) \qquad (4\text{-}49)$$

Associating variables, integrating Equations (4-42) and (4-43), then utilizing Equation (4-49), and lastly retransforming to the original variables ω and S through Equations (4-44) and (4-45), the analytical expressions relating ω, S, λ and θ become,

$$\lambda = -C_1 \left[\sqrt{3} \arctan\left(\frac{2\omega' + 1}{-\sqrt{3}} \right) - \sqrt{3} \arctan\left(\frac{2\omega + 1}{-\sqrt{3}} \right) + \ln \left| \frac{\omega - 1}{\sqrt{1 + \omega + \omega^2}} \right| - \ln \left| \frac{\omega' - 1}{\sqrt{1 + \omega' + (\omega')^2}} \right| + \left(\frac{1}{N_{sh2}} - 1 \right) \ln|S| \right] \quad (4\text{-}50)$$

$$\theta = -C_2 \left[\left(\frac{\omega^3 - 1}{S} + 1 \right)^{2/3} - 1 + \frac{2\left(\frac{1}{N_{sh2}} - 1 \right)\left(\omega^3 - 1 \right)}{3\,S} \right] \quad (4\text{-}51)$$

where

$$\omega' = \left(\frac{\omega^3 - 1}{S} + 1 \right)^{1/3}$$

$$C_1 = \frac{GR^2}{3(1-\epsilon)\rho_g D_{e2} L}$$

$$C_2 = \frac{GR^2 \rho_s W_7}{2\epsilon \rho_g \alpha D_{e2} y_{20} L}$$

The last two equations are implicit in S and ω and cannot be analytically inverted to obtain explicit expressions for each of these variables in terms of θ and λ. Thus, numerical inversion techniques involving one or two-dimensional search techniques are required to develop the bed profiles for S and ω.

A two-dimensional search algorithm, such as pattern, gradient partan, steepest descent, Powell's nonderivative methods, etc., could be devised for Equations (4-50) and (4-51). The equations could be combined in the following manner, for example

1) Square both sides of each equation.
2) Combine the resulting expressions by simple addition.
3) Set this relation to zero by subtracting $\lambda^2 + \theta^2$ from each side.

One of the two-dimensional search routines could be implemented on the cost function resulting from the last step above, say $\underline{F}(\omega,S,\lambda,\theta)$, by

1) choosing particular values, λ^* and θ^*, for λ and θ.
2) obtaining the corresponding values S_o and ω_o for S and ω from the numerical solution of the original partial differential equation system, Equations (3-93), (3-101) and (3-102) (or simply guess the starting values S^o, ω^o).
3) evaluating $\underline{F}$ at λ^* and ω^*
4) starting the search for the location of $\underline{F}(S,\omega,\lambda^*,\omega^*) = 0$ at (S_o, ω_o).

Due to the complexity of Equation (4-50), these two dimensional searches will be very time consuming and the true roots of $\underline{F}(S,\omega,\lambda^*,\omega^*) = 0$ may be impossible to evaluate with any degree of accuracy.

A one-dimensional search routine would be much simpler to implement and would reduce the search time correspondingly. The following procedure for implementing a one-dimensional search algorithm to obtain the axial concentration profiles from Equations (4-50) and (4-51) could be used (32). Given a set of values of ω and θ, Equation (4-51) can be solved for S by using the Golden Section search method. The value of S obtained can be substituted into Equation (4-50), and a value for λ can be determined. The Golden Section technique can be utilized since the value for S is bounded by an upper limit of 1.0 and a lower limit of 0.0. Equation (4-51) would be chosen for the one-dimensional search because it is much simpler than Equation (4-50) which contains complex algebraic expressions within arctangent and natural logarithm functions. In evaluating the arctangent function by computer or otherwise, care must be taken since,

$$\arctan(x/(-y)) \neq \arctan(-x/y)$$

An algorithm to estimate the error involved in the numerical solution of partial differential equations (3-101) and (3-102) by comparison with the analytical solution, Equations (4-50) and (4-51), is given by:

1) Starting at the point ($i=n_1, j=2$) on the grid network shown in Section 4.1.3, perform the following steps,

   a) Evaluate Equations (4-50) and (4-51) using values for $\omega_{i,j}$ and $S_{i,j}$ obtained from the numerical solution of the differential equations. Thus the expected values for $\lambda_{i,j}$ and $\theta_{i,j}$ are available.

b) Compute the values for the independent variables used in the numerical solution at the point (i,j) by,

$$\lambda^*_{i,j} = i\Delta\lambda$$

$$\theta^*_{i,j} = j\Delta\theta$$

c) Determine the fractional errors between the numerical values, λ^* and θ^*, and the analytical values, λ and θ, at the point (i,j) by ,

$$\text{absolute fractional error in } \lambda = \left| \frac{\lambda-\lambda^*}{\lambda^*} \right|$$

$$\text{absolute fractional error in } \theta = \left| \frac{\theta-\theta^*}{\theta^*} \right|$$

2) Increment j by one and return to step 1-a) until $j = \theta_{max}/\Delta\theta$, then proceed to the following step

3) Increment i by n_2, set $j = 2$ and return to step 1-a). This step is repeated until $i = (1 + \Delta\lambda)/\Delta\lambda$

4) Evaluate the mean and variance of the errors in θ and λ.

where values for the constants n_1 and n_2 are chosen so that profiles in time at points at 1/3, 2/3 and the outlet of the bed are evaluated for accuracy.

The preceding algorithm has been programmed in Fortran IV language for use on the IBM 360-65 and the XDS Sigma 5 located in the Computer Science Center and the Chemical Engineering Building, respectively, at Louisiana State University. A copy of the computer program is listed in Appendix D.

Whichever method is used to develop profiles for S and ω for Model 2, a simple relation exists between the oxygen concentration

Y and the sulfur dioxide concentration S. Combining Equations (3-102) and (3-103), integrating and rearranging terms leads to,

$$Y = S^{(D_{e1}/D_{e2})} \tag{4-52}$$

if boundary condition (3-93) is utilized and if the Sherwood numbers are equal. The last assumption is a very good one for the system under study since

$$\frac{(N_{sh1} - 1)}{(N_{sh2} - 1)} = \frac{.9980}{.9983} = .9986$$

using values from Appendices A and B for the pertinent parameters.

Similar analytical expressions for the bed temperature, Ψ, cannot be obtained from either Equation (3-104) or (3-105) in conjunction with the analytical expressions for ω, S and Y. An approximate relationship for Ψ, accurate within numerical integration by quadratures, can be obtained through Equation (3-105) which neglects the heat capacity of the external gas phase.

From Equation (3-105), the following expression is valid at a given $\lambda = \lambda^*$,

$$\Psi(\lambda^*,\theta) = 1.0 - \frac{3(1-\epsilon)\epsilon\rho_g D_{e2} y_{20} L\Delta H_{II}}{GR^2 T_o} \int_o^{\theta} \frac{S\omega\, d\theta}{1+\omega(N_{sh2}-1)}$$

utilizing boundary condition (3-93). The integral can be evaluated numerically (44) using Guassian quadratures or simpler algorithms such as the trapezoidal rule. Values for $S(\lambda^*,\theta)$ and $\omega(\lambda^*,\theta)$ in the integration procedure can be evaluated using any of the numerical inversion algorithms for Equations (4-51) and (4-52) presented

earlier. This would be a very time-consuming procedure however, and is not recommended.

CHAPTER V

RESULTS

Mathematical models describing transient, nonisothermal operation of a fixed bed chemical reactor involving reactions between gaseous reactants in the feed stream and solid reactants distributed throughout the porous inert solid support were developed in Chapter III. Numerical and analytical solution techniques applicable to these models were introduced in Chapter IV. In this chapter, the accuracy of the numerical solution algorithm and an analysis of the transient operation of the reactor will be performed.

5.1 Operating Parameters for Flue Gas Sulfur Removal via Fixed Beds of Metal Oxides

Before presenting the concentration and temperature profiles for the various models, analysis of the differential equations may be helpful. The solution to these equations depends upon the constants $A_1 \rightarrow A_9$ and $A_1' \rightarrow A_4'$ as defined in Chapter III. These constants in turn depend upon the physical properties of the flue gas and the pellets, the reactor and pellet dimensions, and the inlet and initial conditions of the system.

Expressions for the physical properties of the flue gas and the porous pellets (consisting of copper oxide distributed on an inert alumina carrier) are developed in the appendices, and those appearing in the dimensionless constants are presented in Table 3. Values for these properties at 675°K (402°C) are also given, since 675°K and 1 atm will represent standard or reference operating

TABLE 3

Physical Properties with Temperature Effects

Property	Expression*	Value at 675°K, 1 atm	Units
ρ_g	$0.351T^{-1}$	$5.2 \cdot 10^{-4}$	g/cc
C_g	$0.228+8.33 \cdot 10^{-5}T + 3.04 \cdot 10^{-9}T^2$	0.286	cal/g-°K
C_s	$0.207+8.14 \cdot 10^{-5}T - 3130T^{-2}$	0.256	cal/g-°K
D_{e1}	$3.69 \cdot 10^{-4}T^{0.562}$	0.0144	sq.cm/sec
D_{e2}	$3.71 \cdot 10^{-4}T^{0.509}$	0.0102	sq.cm/sec
h	$8.85 \cdot 10^{-5}T^{0.445}$	$1.61 \cdot 10^{-3}$	cal/sq.cm-sec-°K
ΔH_I	2.61T-67500	-65740	cal/mole O_2
ΔH_{II}	7.41T-138640	-133600	cal/mole SO_2
k_I	$9.15 \cdot 10^6 \, e^{(\frac{-1350}{T})}$	$1.24 \cdot 10^6$	cm/sec
k_{II}	$8.92 \cdot 10^{14} \, e^{(\frac{-13500}{T})}$	$1.84 \cdot 10^6$	cm^4/mole-sec
K_1	$2.16 \cdot 10^{-3}T^{1.31}$	10.99	cm/sec
K_2	$8.39 \cdot 10^{-4}T^{1.41}$	8.19	cm/sec

* where T = °K

conditions for the purpose of demonstrating the numerical and analytical solutions. A comparison of the temperature and concentration profiles obtained by utilizing "average" constant values for the physical properties (at 675°K, 1 atm) versus those obtained by allowing the properties to vary with temperature will be performed.

Standard values for the remaining physical properties and operating conditions can be defined as:

gas mass velocity, G = 0.0359 g/sq-cm-sec
(linear velocity = 61 cm/sec)

bed void fraction, $\epsilon = 0.4$

pellet radius, R = 1/4 in. = .635 cm

pellet density, $\rho_s = 1.6$ g/cc

initial weight fraction cuprous oxide in pellet, $W_6 = 0.1$

inlet oxygen mole fraction, $X_{10} = 0.0304$

inlet sulfur dioxide mole fraction, $X_{20} = 0.0011$

reactor length, L = 61 cm

initial pellet temperature, $T_i = 615°K = 342°C = 650°F$

inlet gas temperature, $T_o = 615°K$

The effect of temperature on the dimensionless constants is given below using the preceding standard conditions and expressions:

$$A_1 \cong \frac{3}{2} T^{1/2} \qquad A_4 \cong 3.4 \cdot 10^6 T^{-1} \exp\left(\frac{-1350}{T}\right)$$

$$A_2 \cong \frac{7}{2} T^{1/3} \qquad A_5 \cong 3.4 \cdot 10^6 T^{-1} \exp\left(\frac{-13500}{T}\right)$$

$$A_3 \cong \frac{3}{2} T^{2/5} \qquad A_6 \cong 4 \cdot 10^{-2} T^{-1/2}$$

$$A_6 A_7 \cong 5 \cdot 10^{-5} T^{1/3} \qquad A_6 A_8 \cong 5 \cdot 10^{-8} T^{2/5}$$

$$N_{Shj} \cong 4\ T^{3/4} \quad ; \qquad j = 1,2$$

$$N_{D1} \cong \frac{3}{2}\ T^{-1/2} \exp\left(\frac{-1350}{T}\right)$$

$$N_{D2j} \cong 10^{12}\ T^{-1/2}\ \exp\left(\frac{-13500}{T}\right) \quad ; \quad j = 1,2$$

$$A_1' \cong \frac{2}{3}\ T^{-1/2} \qquad\qquad A_3' \cong 5 \cdot 10^{-4}\ T^{3/2}$$

$$A_2' \cong \frac{2}{3}\ T^{-1/2} \qquad\qquad A_4' \cong 7 \cdot 10^{-5}\ T^{-1/2}$$

The preceding values and expressions are the basis for the numerical solutions to be presented unless explicitly stated otherwise. As mentioned previously, published data on this process are not available, but these conditions are thought to be fairly typical.

Utilizing these standard values, the relation between the characteristics and the original independent variables (time and axial distance) can be illustrated better. Notice that, $\frac{G}{\rho_g \epsilon L} = 2.782\ \text{sec}^{-1}$, so that for

$$\theta = \xi - \frac{z}{L} = 2.782\ t - \lambda \qquad (3\text{-}65)$$

where t = sec, the following conditions exist,

λ	t(sec)	θ	θ/ξ
0	10	27.82	1.0
	36	100.00	1.0
	1800	5150.00	1.0
1	0.36	0.0	0.0
	10	26.82	0.965
	36	99.00	0.990
	1800	5149.00	0.9998

Thus for elapsed times greater than 36 seconds, $\theta = \frac{Gt}{\rho_g \epsilon L} = \xi$ to within one per cent.

In addition to the concentration and temperature profiles, parameters of interest for this study which can be obtained from these profiles are the maximum bed temperature attained, the breakthrough time, and the bed efficiency. The latter two parameters are described in terms of the following definitions.

Breakthrough Time: This is the time required for the sulfur dioxide level at the exit of the reactor to increase to 10% of its inlet concentration.

Bed Load, B: This is the amount of $CuSO_4$ contained in the bed at any given time.

$$B = \lim_{n \to \infty} \sum_{i=1}^{n} \left(\begin{matrix}\text{volume of} \\ CuSO_4 \text{ per} \\ \text{pellet}\end{matrix} \right) \left(\begin{matrix}\text{pellets} \\ \text{per unit} \\ \text{bed volume}\end{matrix} \right) \left(\begin{matrix}i^{th} \text{ differ-} \\ \text{ential bed} \\ \text{volume}\end{matrix} \right) \left(\begin{matrix}\text{pellet} \\ \text{density}\end{matrix} \right) \left(\begin{matrix}\text{weight} \\ CuSO_4 \text{ per} \\ \text{volume of } CuSO_4\end{matrix} \right)$$

$$= \int_0^L \left[\frac{4\pi}{3}(R^3 - r_c^3) \right] \left[\frac{3(1-\epsilon)}{4\pi R^3} \right] \left[\frac{\pi D_B^2}{4} \, dZ \right] \left[W_7 \rho_s \right]$$

$$= \frac{\pi}{4} (1-\epsilon) \rho_s W_7 L D_B^2 \int_0^1 (1-\omega^3) d\lambda$$

which can be integrated numerically using the trapezoidal rule and profile information.

Bed Efficiency, η: This is the cumulative fraction of sulfur dioxide removed from the flue gas which has passed through the bed up to any given time, t_E.

$$\eta = \frac{B\chi'}{W' t_E}$$

where W' = inlet mass flow rate of SO_2, g/sec

χ' = stoichiometric constant

$= M_2 \, \gamma_{22} / M_7 \, \gamma_{27}$ = g SO_2/g $CuSO_4$

When comparing two alternative processes or modes of operation which possess equivalent breakthrough times, the one having the larger bed efficiency would be preferred, since this indicates that a larger percentage of the SO_2 was removed. The bed efficiency can vary for processes with equal breakthrough times when the breakthrough curve of one is sharp and the other flat. In the former, the exit SO_2 concentration would remain very low until near breakthrough, and then rise to breakthrough concentration very rapidly. A rough idea of the bed loading at breakthrough can be obtained from the radius of the outer shrinking core at breakthrough, because fractional pellet utilization is given by $1-\omega^3$. The efficiency is only of secondary importance, however, since the critical criteria for a successful SO_2 removal process are the breakthrough time and the maximum bed temperature attained. Achieving the largest breakthrough time possible would be an important goal, since this would lead to less frequent regeneration and more economical operation. As mentioned previously, the maximum allowable bed temperature (peak temperature) will be 750°C in order to prevent degradation of the pellets.

5.2 Accuracy of the Numerical Solution Technique

The accuracy of the numerical integration technique presented in Section 4.1 can be ascertained through use of the analytical-comparison-algorithm developed in Section 4.2.2 and presented in Appendix D. The comparison algorithm yields the mean absolute fractional differences between the analytical and numerical values

of the independent variables for a given set of dependent variables. The variance in these two quantities is also computed. This algorithm can only be used to determine the numerical accuracy for the Model 2 characteristic equations using constant, "averaged" properties, since this is the only case which possesses an analytical solution.

Using the standard conditions defined in the preceding section, analysis of the effect of step sizes ($\Delta\theta$ and $\Delta\lambda$) on the accuracy of the predictor-corrector integration scheme for Model 2 with constant properties is shown in Table 4. For each case it was attempted to present an equal number of points for error evaluation to the comparison subroutine, because the number of samples can affect the mean and the variance. Thus, 300 points were usually transmitted to the comparison subroutine for evaluation of error.

From Table 4, the optimum $\Delta\theta$ for $\Delta\lambda = 0.05$ (20 discrete points in distance) occurs between 50 and 25. Employing Equation (3-65) and $\Delta\lambda = 0.05$ and $\Delta\theta = 25$, Δt corresponds to 13.5 seconds. For larger step sizes with distance, no reasonable $\Delta\theta$ could be obtained. When the distance step size was decreased to 0.025, $\Delta\theta$ had to be decreased in order to obtain stable numerical solutions. Numerical instability was inferred whenever abnormal oscillations in the profiles for any of the dependent variables occurred and/or whenever values for Y, S, ϕ, ω or η exceeded 1.0 or became negative (since each of these variables is normalized between 0.0 and 1.0). Also, values for the dimensionless temperatures, Ψ and μ, less than 1.0 indicate numerical instability as long as $T_i \geq T_o$, since the reactions

TABLE 4

Effect of Step Size on Accuracy of Numerical Solution
(Model 2)

Space Increment ($\Delta\lambda$)	"Time" Increment ($\Delta\theta$)	Mean Absolute Fractional Error in λ	Mean Absolute Fractional Error in θ	Variance of Absolute Fractional Error in λ	Variance of Absolute Fractional Error in θ	Numerical Stability
0.025	25	$0.6 \cdot 10^{-2}$	$2.73 \cdot 10^{-2}$	$0.27 \cdot 10^{-3}$	$0.59 \cdot 10^{-2}$	Yes
	50	-	-	-	-	Unstable
0.050	10	$1.43 \cdot 10^{-2}$	$5.08 \cdot 10^{-2}$	$1.26 \cdot 10^{-3}$	$1.68 \cdot 10^{-2}$	Yes
	25	$1.43 \cdot 10^{-2}$	$5.02 \cdot 10^{-2}$	$1.25 \cdot 10^{-3}$	$1.65 \cdot 10^{-2}$	Yes
	50	$1.40 \cdot 10^{-2}$	$4.91 \cdot 10^{-2}$	$1.19 \cdot 10^{-3}$	$1.57 \cdot 10^{-2}$	Yes
	100	$2.07 \cdot 10^{-2}$	$7.78 \cdot 10^{-2}$	$2.36 \cdot 10^{-3}$	$3.9 \cdot 10^{-2}$	Unstable
0.100	$1 \rightarrow 25$	-	-	-	-	Unstable

are exothermic.

For $\Delta\lambda = 0.05$ notice that a minimum exists in both the λ and θ deviations at $\Delta\theta = 50$. This phenomenon can be explained by considering truncation and roundoff errors. These two types of errors always occur in numerical integration. The latter is present because only a finite number of digits can be used to represent numbers in digital computers. Roundoff errors exist because the integration formulas are only approximate for finite step sizes. Therefore decreasing the step size usually reduces the truncation errors, but conversely increases the accumulated roundoff errors since more steps are needed to reach a given final point. Thus, optimum step sizes should exist at which the combined truncation and roundoff errors are minimized.

In conclusion, step sizes of $\Delta\theta = 50$ and $\Delta\lambda = 0.05$ will be used to develop the Model 2 profiles even though step sizes one half this size for each variable produced less deviation when compared to the analytical solution. Differences in the profiles obtained for either pair is negligible, and the former pair leads to execution times one-fourth that of the latter for equal final values of bed length and real-time operation of the bed (a single sorption cycle). Normally, a single sorption cycle would be the elapsed time between introduction of flue gas to the reactor and the point at which the exit SO_2 concentration reaches 10% of the inlet SO_2 concentration (breakthrough).

5.3 Model 2 Profiles

Results of the numerical solution of the Model 2 equations using the standard inlet and initial conditions and standard, "average" values for the physical properties are shown in Figures 4 through 8. These profiles were obtained using $\Delta\theta = 50$ and $\Delta\lambda = 0.05$.

Figure 4 is a plot of bed efficiency versus time elapsed since the flue gas was first introduced to the bed. Figure 5 presents the normalized bulk gas phase oxygen concentration versus the time-distance characteristic, θ, with the distance characteristic, λ, as a parameter. From Equation (3-65), it can be seen that for a fixed distance θ varies proportionally with the elapsed time from the instant that the flue gas first reaches this point in the bed. Thus the curves of Figure 5 are essentially a plot of O_2 concentration versus time at different points in the bed. Using θ as the ordinate instead of "real" time merely shifts the profiles-with-time for each point in the reactor to a common origin. If "real" time were used, the concentration profile at the outlet of the reactor with time would be offset from that at the reactor inlet by t_E, the time required by an inert to traverse the length of the bed.

The normalized bulk gas phase sulfur dioxide concentration versus θ with normalized distance, λ, as a parameter is presented in Figure 6. This figure contains the breakthrough curve which is defined as the SO_2 profile at the outlet of the reactor. From the relationships between λ, θ and t presented in Section 5.1, 30 minutes corresponds to a θ of 5150. Breakthrough ($S = 0.10$) occurs for

FIGURE 4. BED EFFICIENCY VERSUS ELAPSED TIME

..... MODEL 2, CONSTANT PROPERTIES

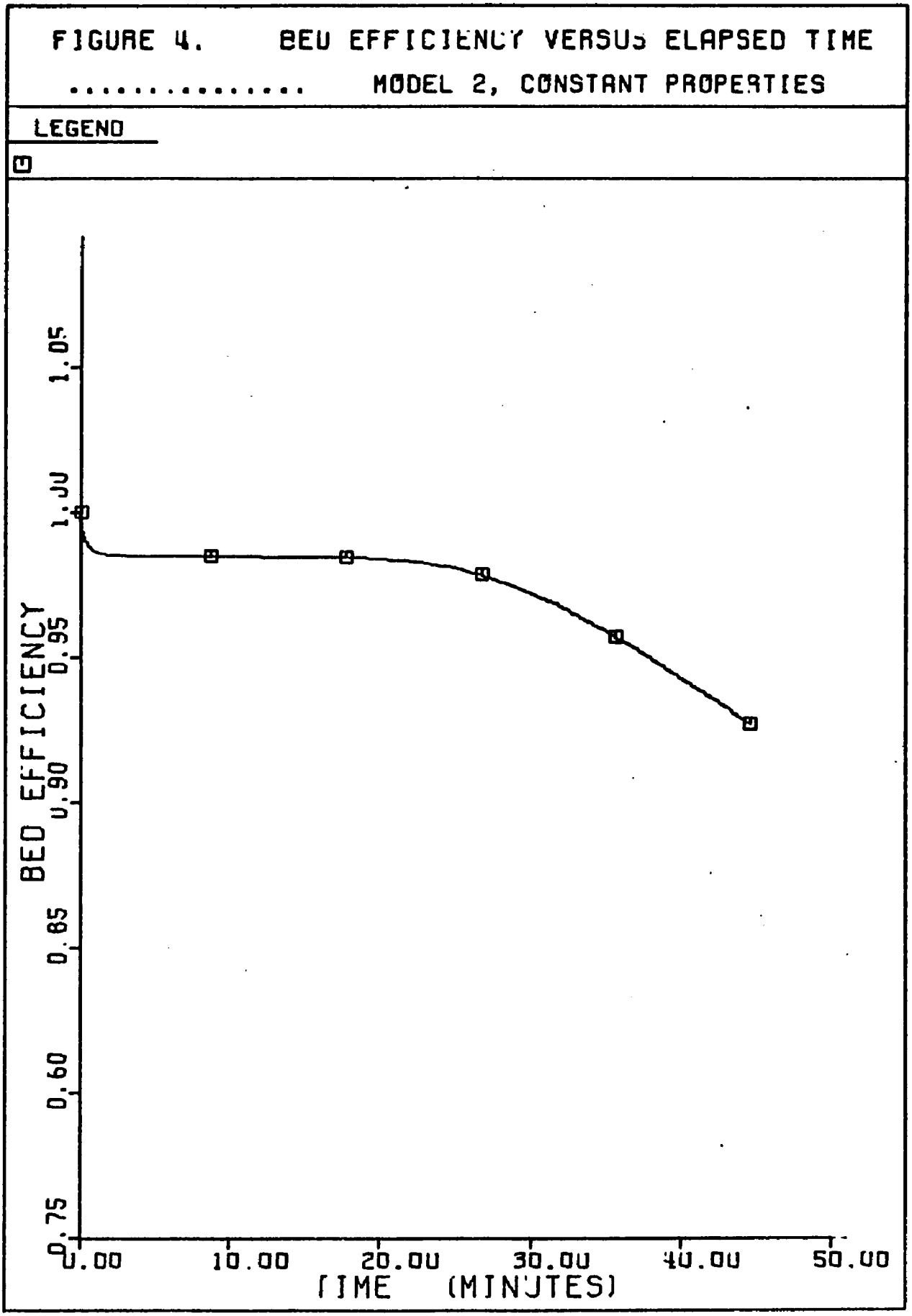

FIGURE 5. NORMALIZED OXYGEN PROFILE

..... MODEL 2, CONSTANT PROPERTIES

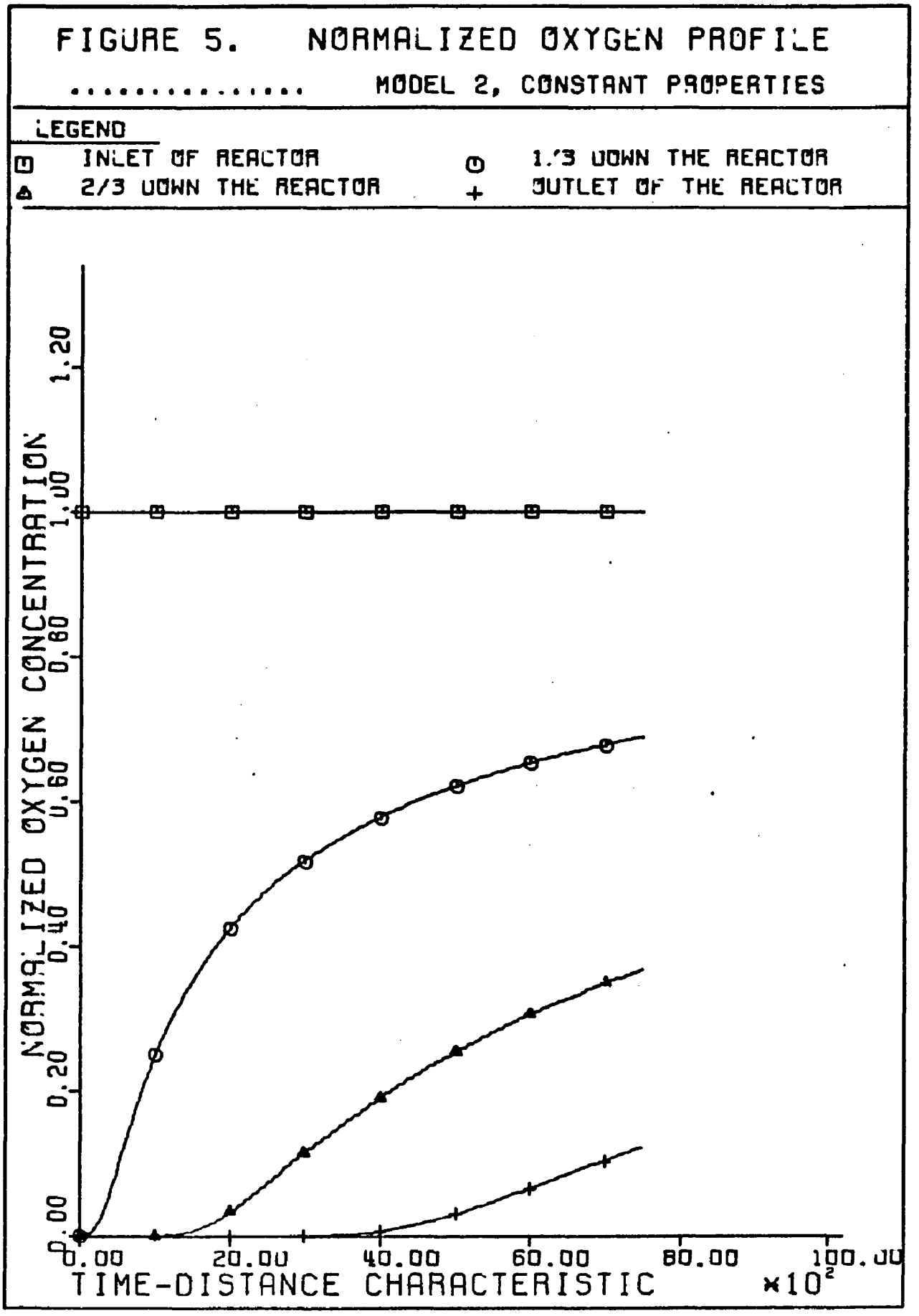

FIGURE 6. NORMALIZED SULFUR DIOXIDE PROFILE

..... MODEL 2, CONSTANT PROPERTIES

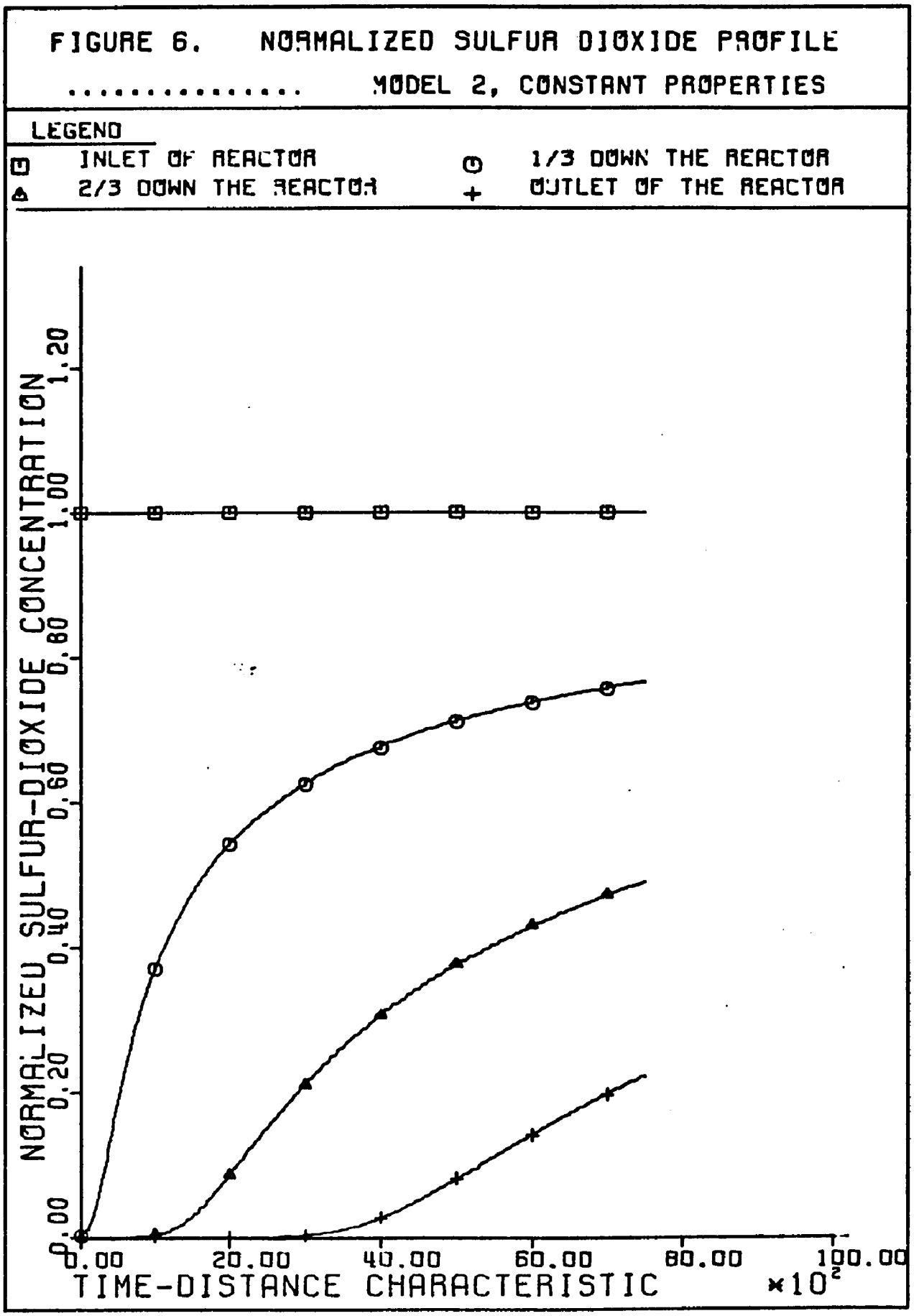

FIGURE 7. NORMALIZED SHRINKING-CORE RADIUS PROFILES

..... MODEL 2, CONSTANT PROPERTIES

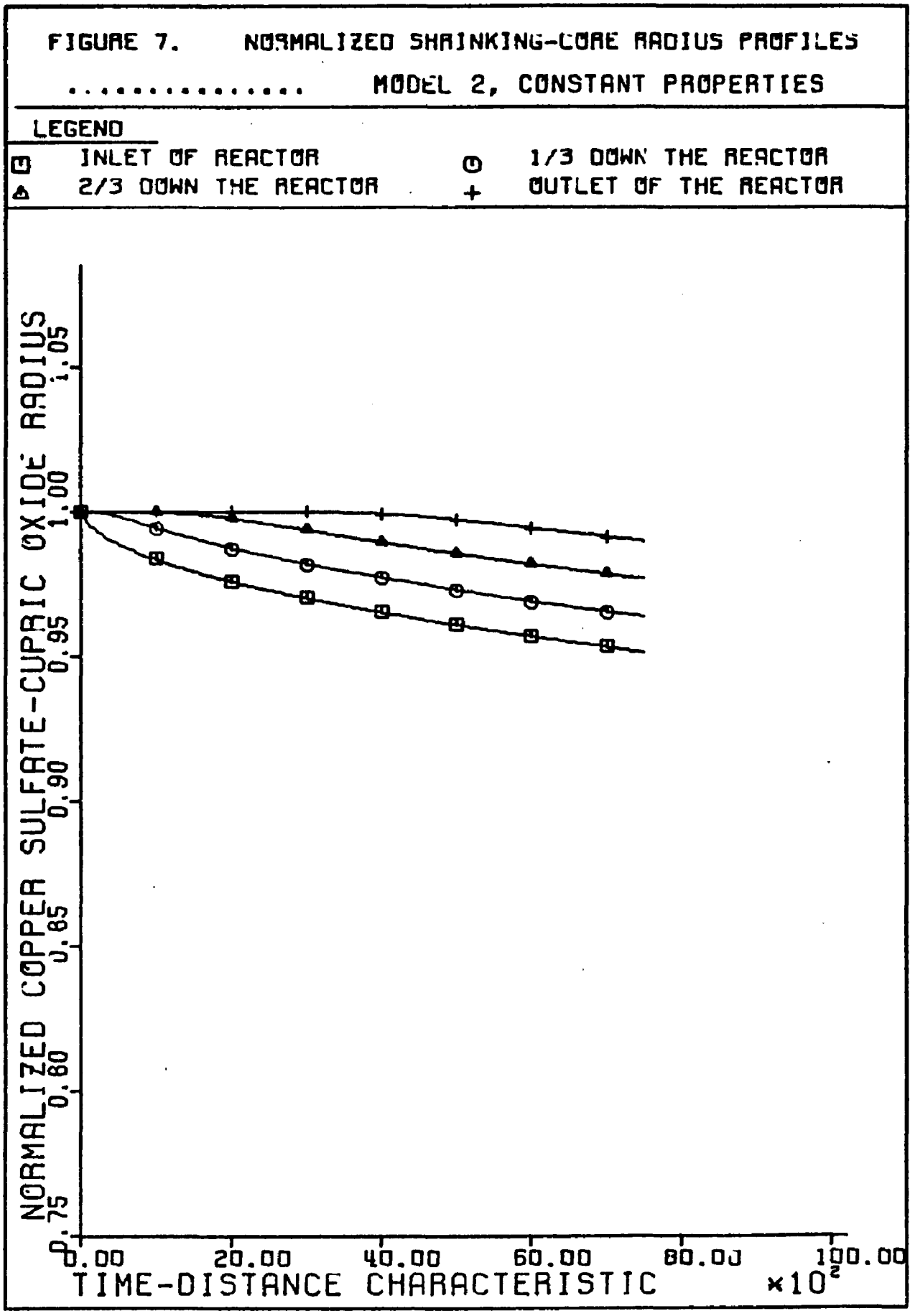

FIGURE 8. REACTOR TEMPERATURE PROFILE

..... MODEL 2, CONSTANT PROPERTIES

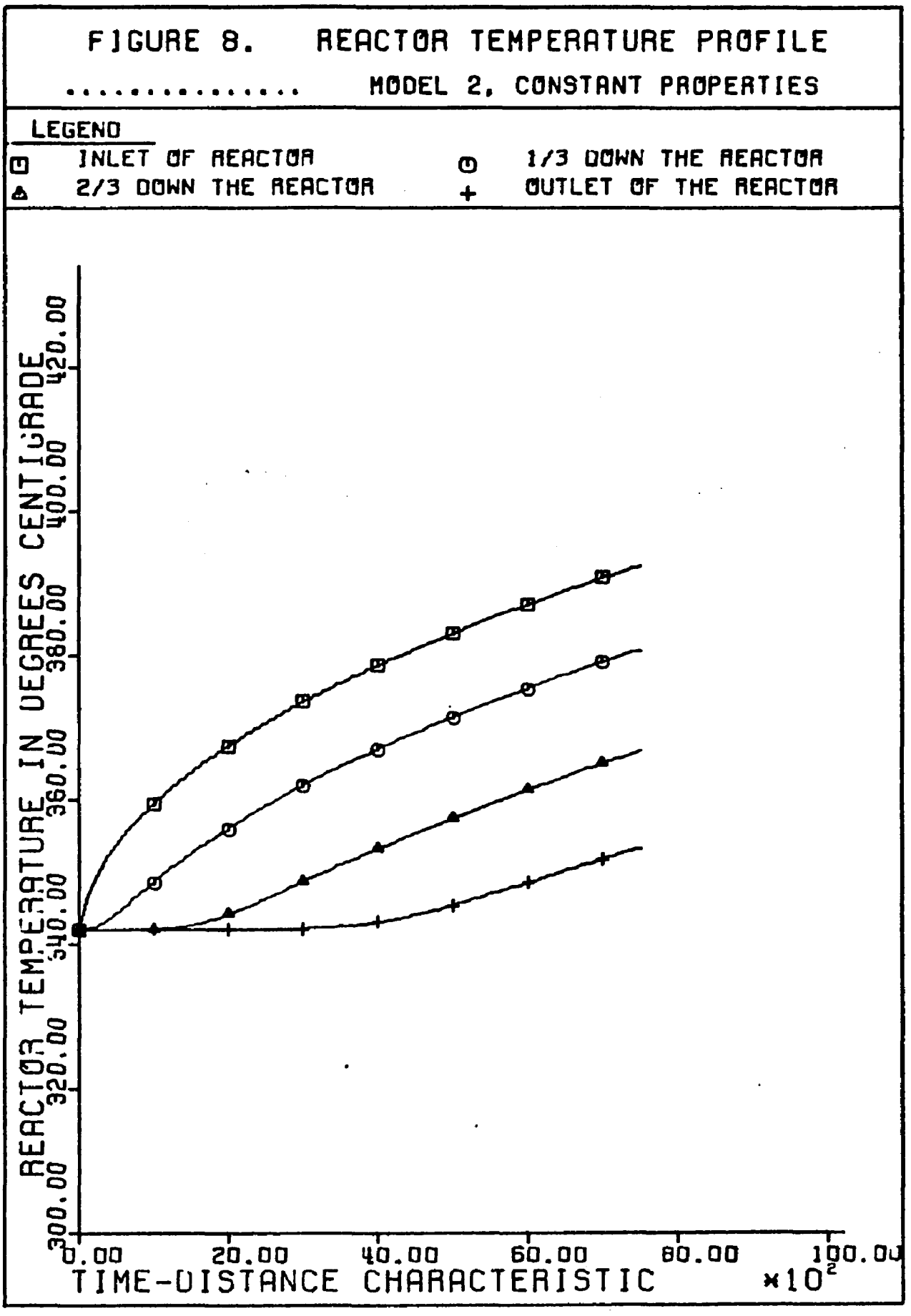

θ = 5700 which is equivalent to 33 minutes after sorption was initiated. Notice in Figures 4 and 6 that bed efficiency decreases refect outlet SO_2 increases.

Figure 7 illustrates the position of the unreacted-shrinking-core radius within a pellet at various positions in the bed as time of sorption varies. The normalized radius, ω, is presented and this can be related to conversion of solid reactant by Equation (3-36a). Notice that at breakthrough, the pellets at the bed outlet have hardly been utilized $\omega \approx 0.99$. Penetration of the sulfation reaction site at the bed inlet is also small. At breakthrough, it corresponds to a normalized radius of 0.95 which is only 14.5% conversion of the solid reactant at the bed inlet.

The reactor temperature at various locations and times within the bed is presented in Figure 8. Notice that reactor temperature is monotonically increasing at any given point in the bed and could conceivably melt the reactor if long sorption cycles were allowed and enough CuO were present during adiabatic operation. This feature is one of the major weaknesses of Model 2. Comparing the Model 2 reactor energy balance, Equation (3-105), with the pellet energy balance of Model 1, Equation (3-92), the model 2 balance is merely a pellet balance and no allowance of axial transport of heat is present. Thus, the temperature of the flue gas near the entrance jumps immediately to that of the very hot pellets at this point and, because pellet-bulk gas thermal equilibrium exists, the gas temperature decreases as the gas passes down the reactor, never carrying away any of the heat generated in the various segments of the bed. This is a very unrealistic feature and Model 2 cannot be expected

to generate very rigorous reactor temperature profiles. Therefore its use should be restricted to checking the accuracy of the numerical integration.

Figures 5 through 8 represent time profiles or what an observer sitting on a pellet sees as the flue gas flows past him or what goes on within the pellets at his axial location in the bed. Figures 9,10, and 11 represent "snapshot" profiles of the state of the SO_2, pellet unreacted-shrinking-core radius, and temperature along the length of the bed at a fixed instant of time. To be completely rigorous, they represent what an observer riding a nitrogen molecule sees as he passes through the reactor, but his journey is so fast (0.36 seconds at the "standard" conditions) that they approximate a snapshot of what is occurring throughout the bed at any instant. Therefore, these "snapshot" profiles can be obtained directly from the "time" or θ-profiles by merely placing a straight-edge perpindicular to the abscissa at a particular value of θ. These three figures illustrate the wave-like nature of the concentration and temperature profiles.

The effect of allowing the physical properties to vary with temperature is illustrated in Figure 12. Comparing Figure 6 with Figure 12, the results with variable properties show no appreciable change from those obtained by utilizing constant properties. A slight difference does exist, however, because breakthrough (θ = 5700) no longer corresponds to 33 minutes. In converting from θ to t,

FIGURE 9. AXIAL SULFUR DIOXIDE PROFILES

..... MODEL 2. CONSTANT PROPERTIES

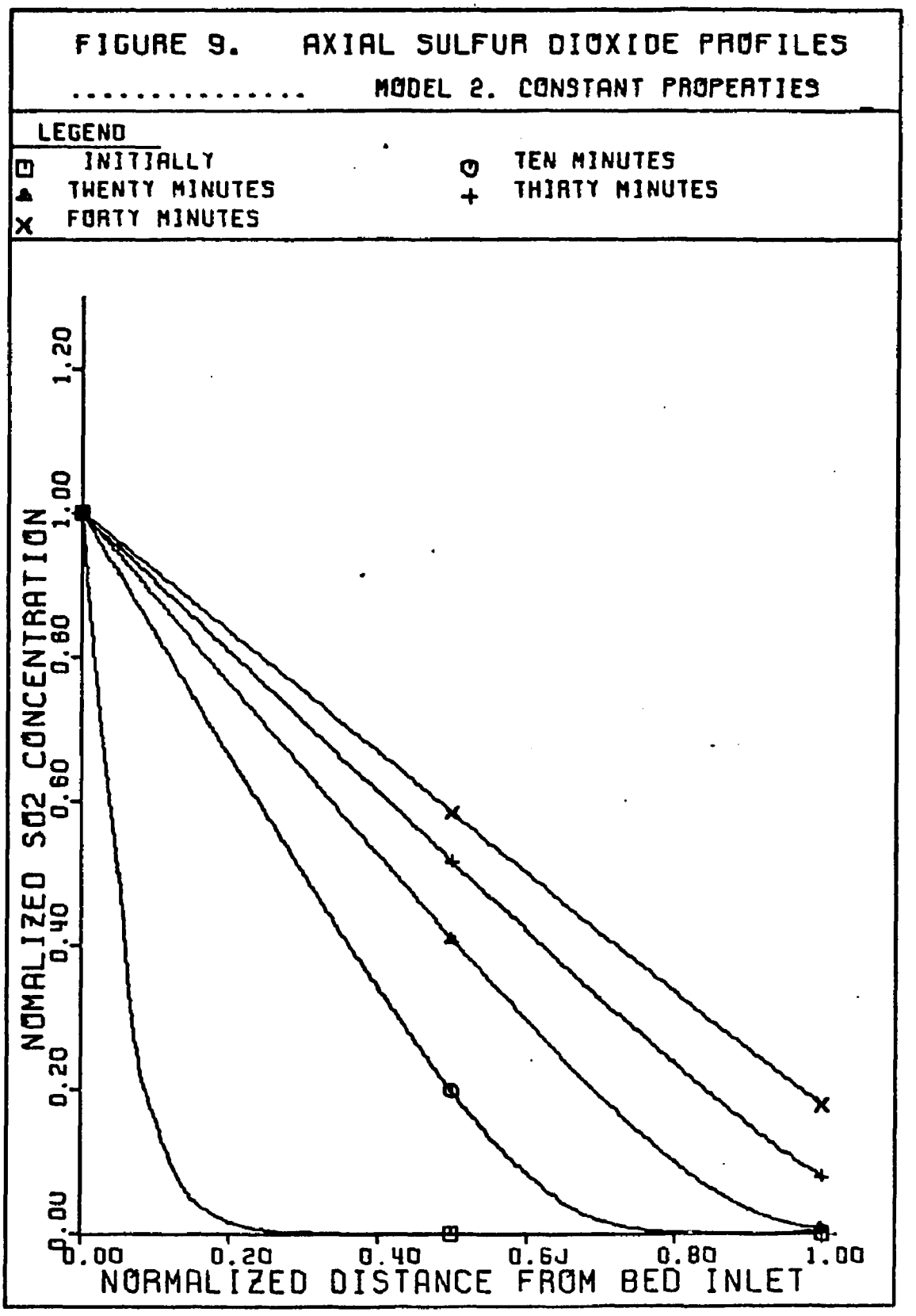

FIGURE 10. AXIAL UNREACTED-CORE RADIUS PROFILES
..... MODEL 2. CONSTANT PROPERTIES

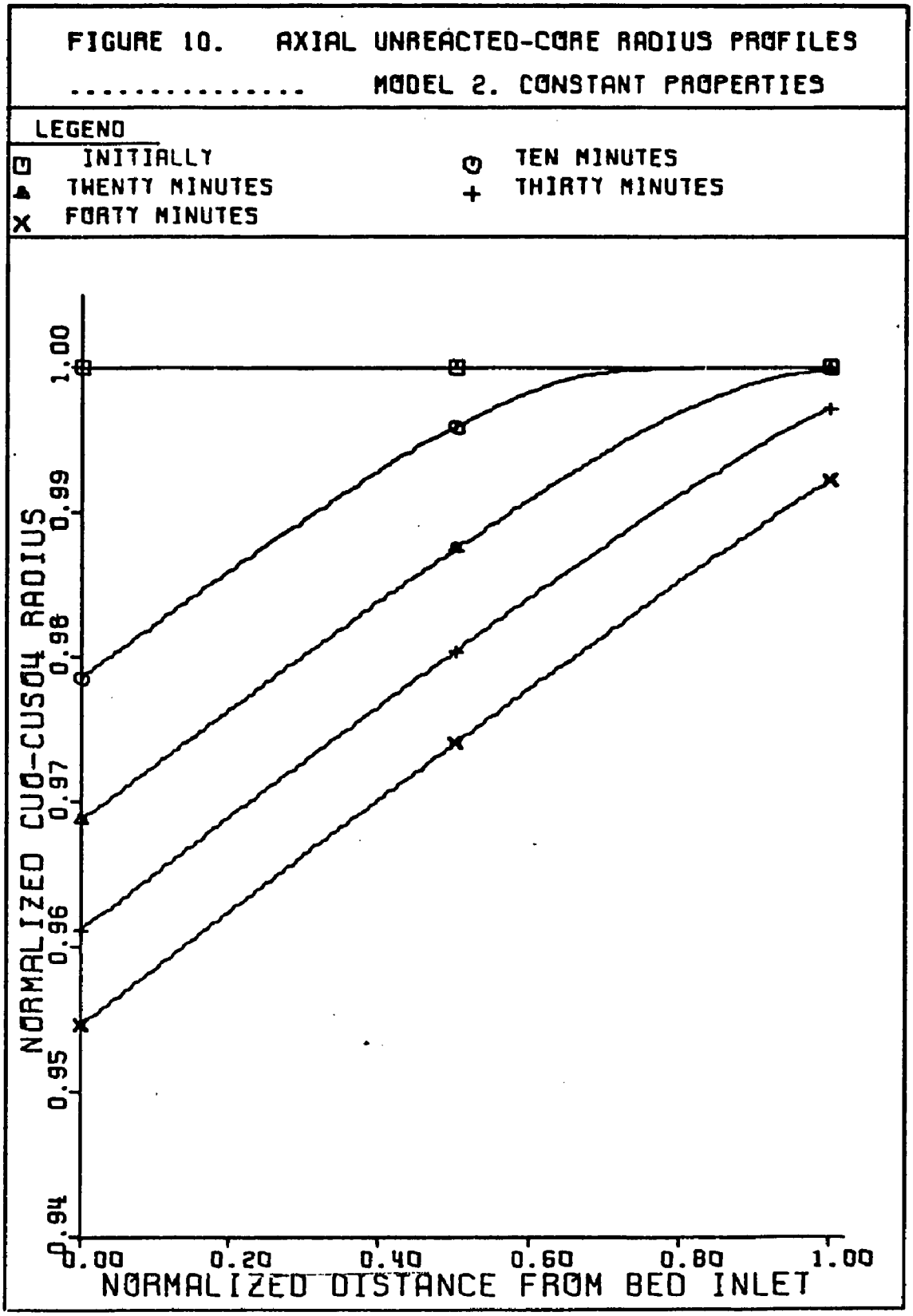

FIGURE 11. AXIAL TEMPERATURE PROFILES

..... MODEL 2. CONSTANT PROPERTIES

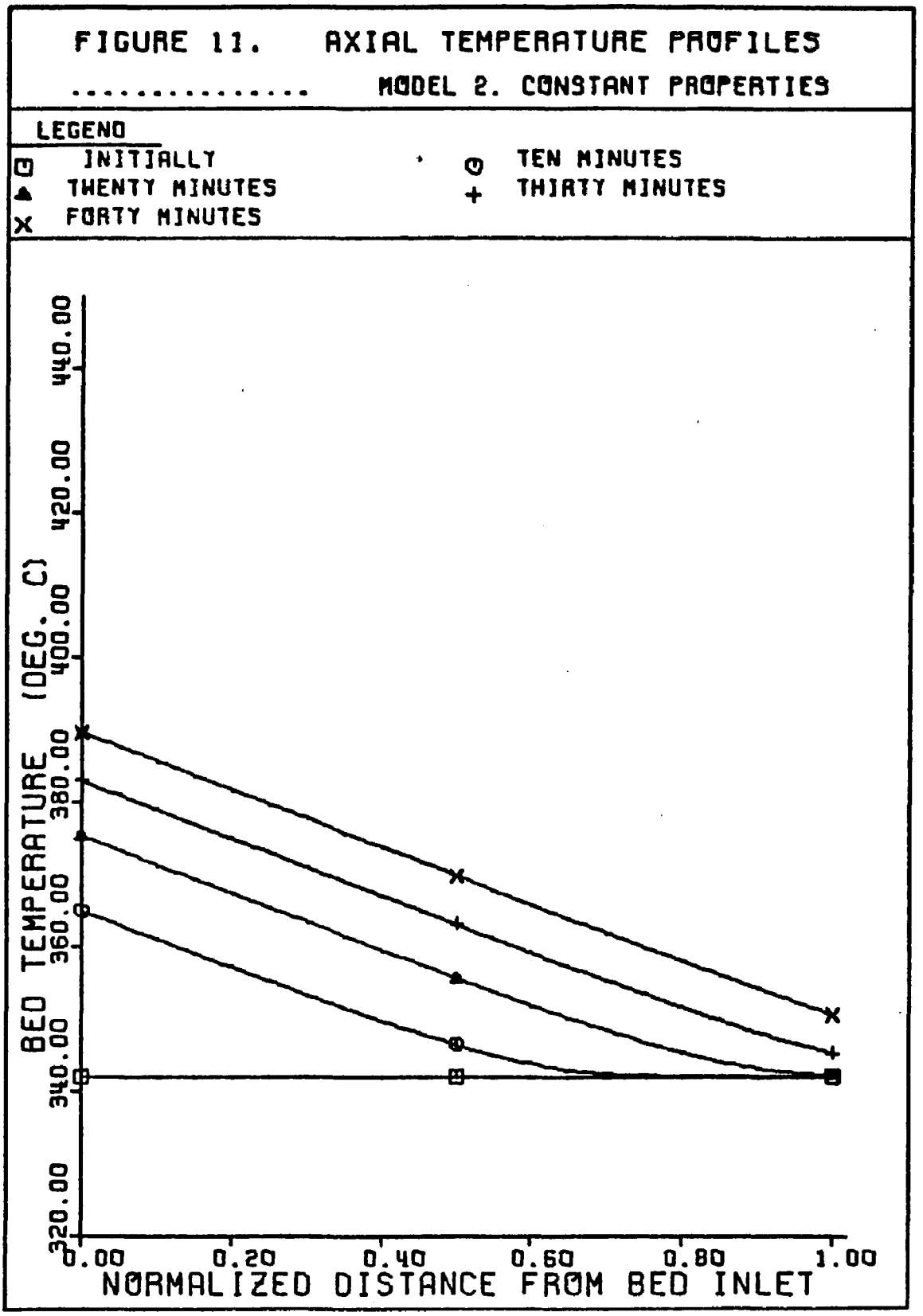

FIGURE 12. NORMALIZED SULFUR DIOXIDE PROFILE

..... MODEL 2, VARIABLE PROPERTIES

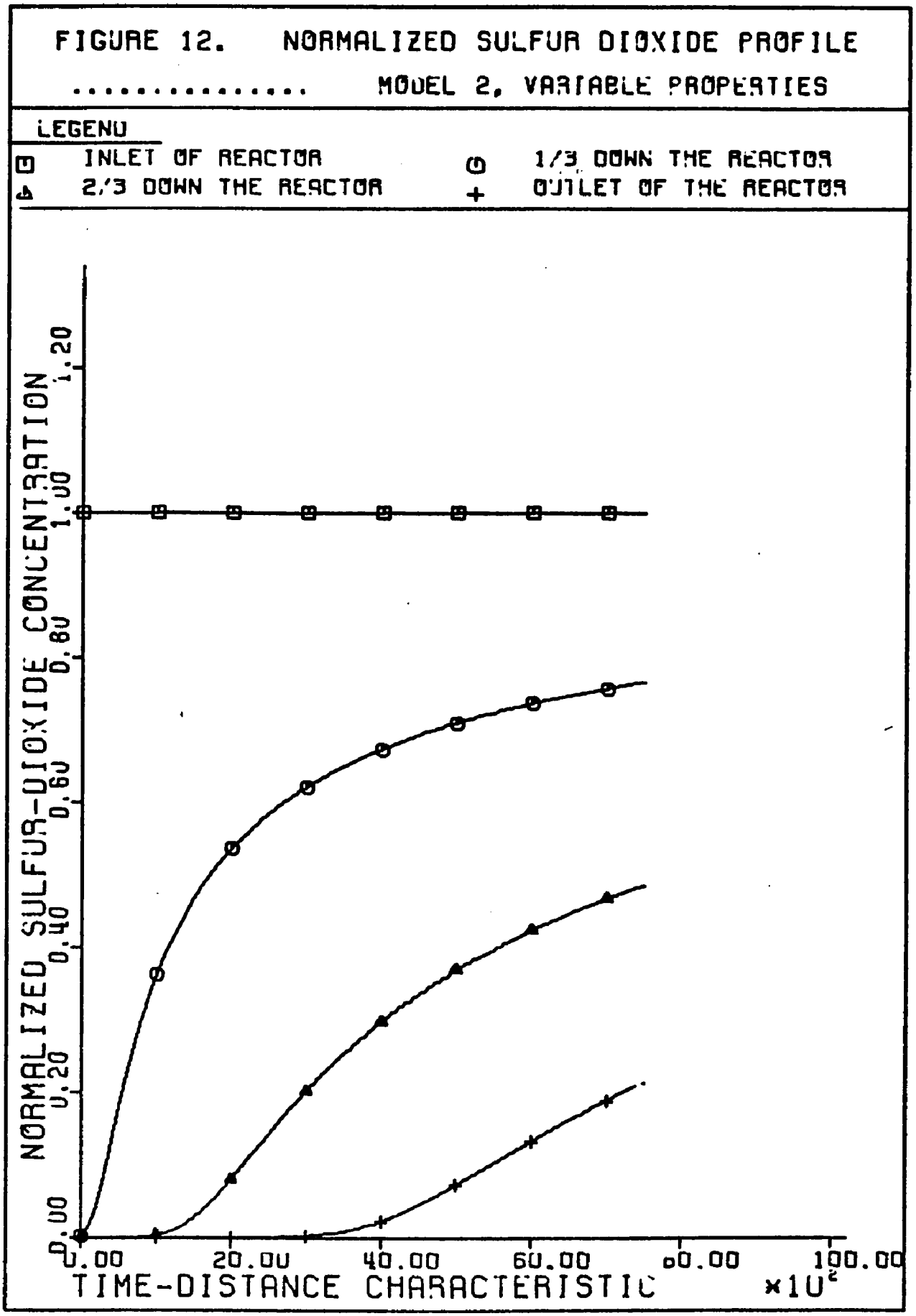

$$t = \frac{\rho_g \epsilon L}{G} (\theta - \lambda) \quad \alpha \quad \frac{1}{T}$$

since density decreases with temperature. Thus breakthrough for Model 2 with variable properties occurs at 36 minutes. The peak temperature for variable properties is 666.7°K (393.7°C) while that for constant properties is 665.5°K for Model 2. This represents a rise of 50°C in 45 minutes and is well below the 1025°K upper limit for peak bed temperature. In both cases the peak temperature location is the entrance to the bed which is to be expected for the energy balance utilized. As was the case for the SO_2 profiles, (see Figures 6 and 12), the shapes of the O_2, shrinking-core radius and temperature profiles for variable properties are identical to those for constant properties (see Figures 5, 7, and 8 respectively).

The increase in the peak temperature and the breakthrough time for the variable property case can be explained upon examination of the variation of the A_i' constants with temperature. The consumption of SO_2 and the generation of heat (determined by A_2' and A_4' respectively) increase as the temperature decreases. The average temperature in the bed for the variable properties run was about 640°K, whereas, the physical properties were evaluated at 675°K. Therefore the increase in the exit SO_2 concentration should be slower and the rise in the bed temperature greater for the conditions of the variable property case. Naturally the effects would not have been very substantial if the constant properties had been evaluated at a more proper average temperature (say 645°K rather than 675°K). In conclusion, however, allowing the physical properties to vary had

no appreciable effect upon Model 2.

Execution time for a 45 minute sorption cycle utilizing Model 2 with constant conditions was one minute and 10 seconds on the IBM 360-65. This represents a computer to real time ratio of 0.026. The ratio for the variable property solution was 0.108 for a 48 minute sorption cycle or 4.1 times greater than the constant property solution.

The penetration of the reaction zone into the pellets (solid reactant conversion) can be increased by increasing A_3'. For a given pellet diameter, this could be accomplished by reducing the initial CuO concentration, W_7, or by increasing the diffusion within the pores, D_{ei}. Since Knudsen diffusion predominates, the latter phenomenon varies in direct proportion to the size of the pellet pores. For both variable and constant properties, the furthest penetration of the sulfation reaction site at the "standard" conditions is 0.95R (14.5% pellet conversion) for Model 2. Referring to the latter case as the standard, the following results were obtained using constant properties for Model 2:

Operating Conditions	Maximum Reaction Penetration	Pellet Conversion	Peak Temp.(°K)	Break-through Time(min)
Standard	0.95R	14.5%	653	33.0
$D_{ei} = 2D_{ei}\big\|_{std.}$	0.935R	17.6%	680	46.0
$W_7 = \frac{1}{2} W_7\big\|_{std.}$	0.935R	17.6%	650	18.5
$\frac{D_{ei}}{W_7} = 4 \frac{D_{ei}}{W_7}\big\|_{std.}$	0.907R	26.0%	660	35.4

The maximum penetration in each case occurred at the reactor inlet. As expected, decreasing the CuO concentration increased pellet utilization, but reduced breakthrough time by 50% which is very undesirable. Doubling the effective pore diffusivity (increasing the size of pellet pores) increased breakthrough time by 39% and increased pellet utilization by 21%. In the extreme, therefore, only 26% of the pellet volume has been converted to $CuSO_4$.

5.4 Model 1 Profiles

5.4.1 Constant Properties

Results of the numerical integration of the Model 1 "characteristic" differential equations by the predictor-corrector scheme introduced in Section 4.1.3 are presented in Figures 13 through 19. To achieve stable solutions, it was necessary to reduce $\Delta\theta$ to 10.0 (from 50.0) for a distance step size of $\Delta\lambda = 0.05$. These step sizes will be used in the remainder of this chapter unless stated otherwise. The standard initial and inlet conditions were used, but the physical properties were evaluated at 640°K, instead of 675°K, in order to match the average temperature expected in the bed.

For a sorption cycle of 5 minutes, execution time on the IBM-360-65 was 1.81 minutes which corresponds to a computer/real time ratio of 0.36. This ratio is 13.9 times as great as the ratio for the standard conditions, constant property run of Model 2.

The breakthrough curve is the bottom curve in Figure 16. Instead of steadily increasing from 0.0 to the breakthrough point of 0.1 at the bed exit as in Model 2, the normalized SO_2 concentration

FIGURE 13. BED EFFICIENCY VERSUS ELAPSED TIME
..... MODEL 1, CONSTANT PROPERTIES

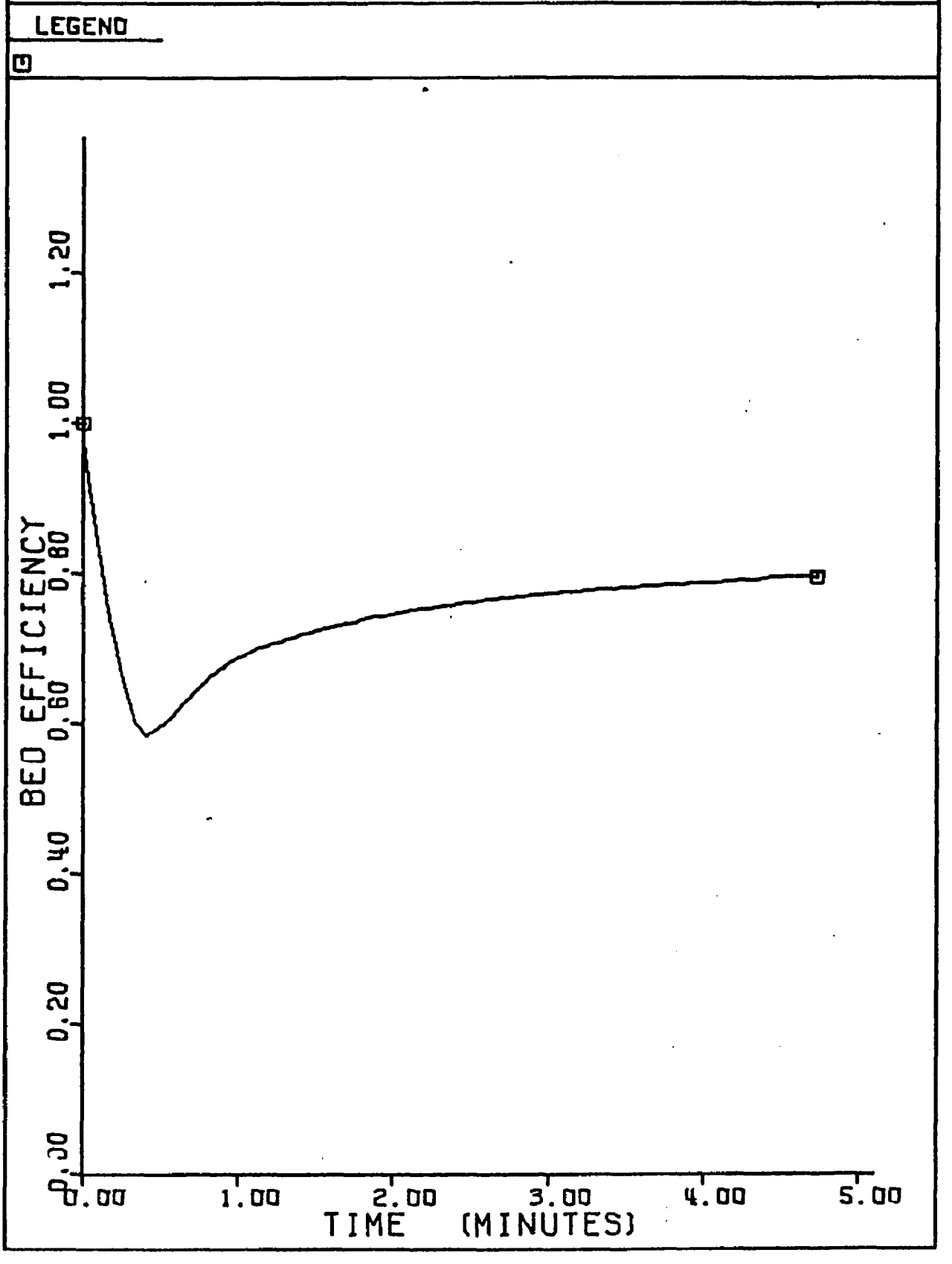

FIGURE 14. BULK GAS PHASE TEMPERATURE PROFILES

..... MODEL 1, CONSTANT PROPERTIES

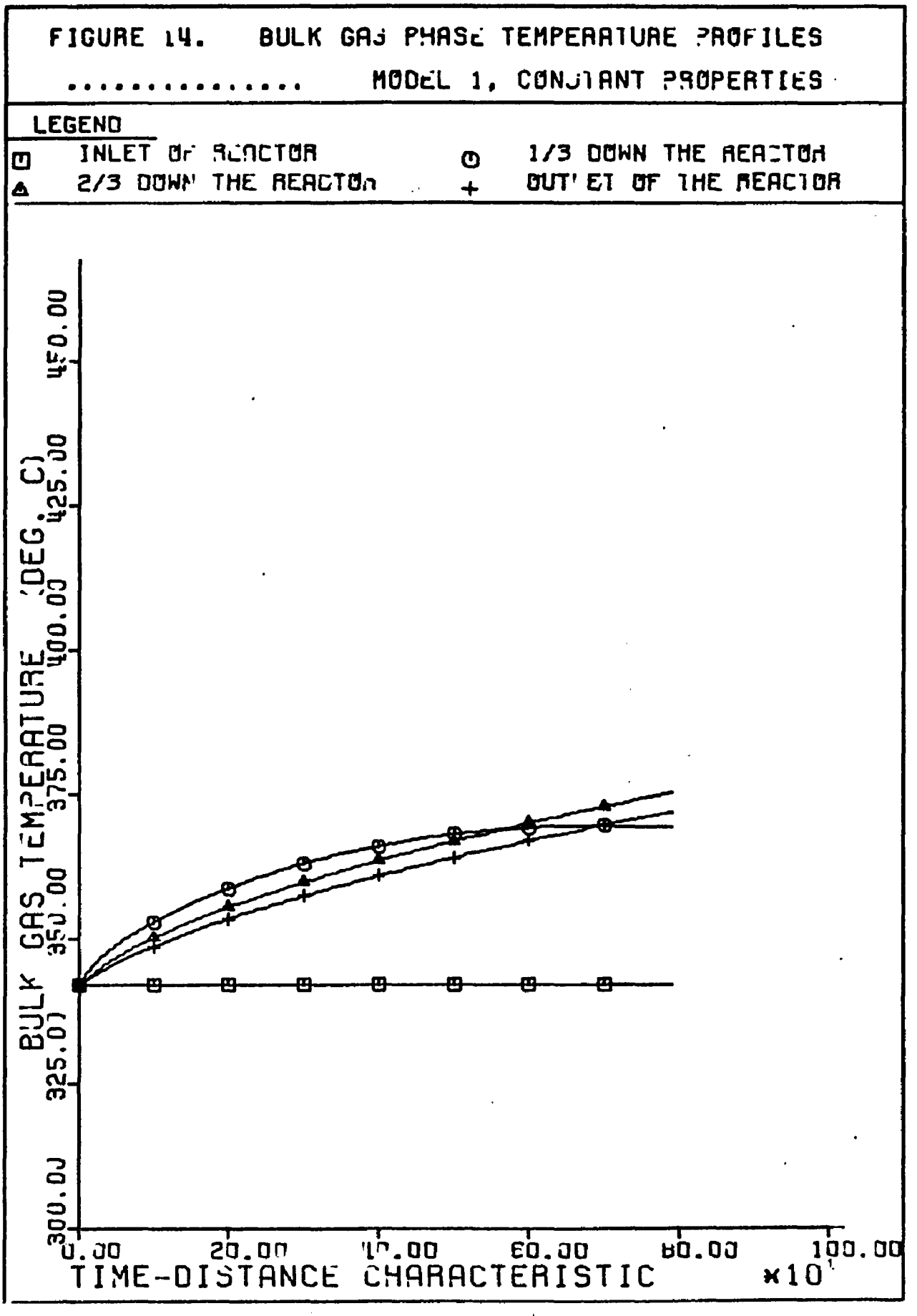

FIGURE 15. NORMALIZED OXYGEN PROFILE

..... MODEL 1, CONSTANT PROPERTIES

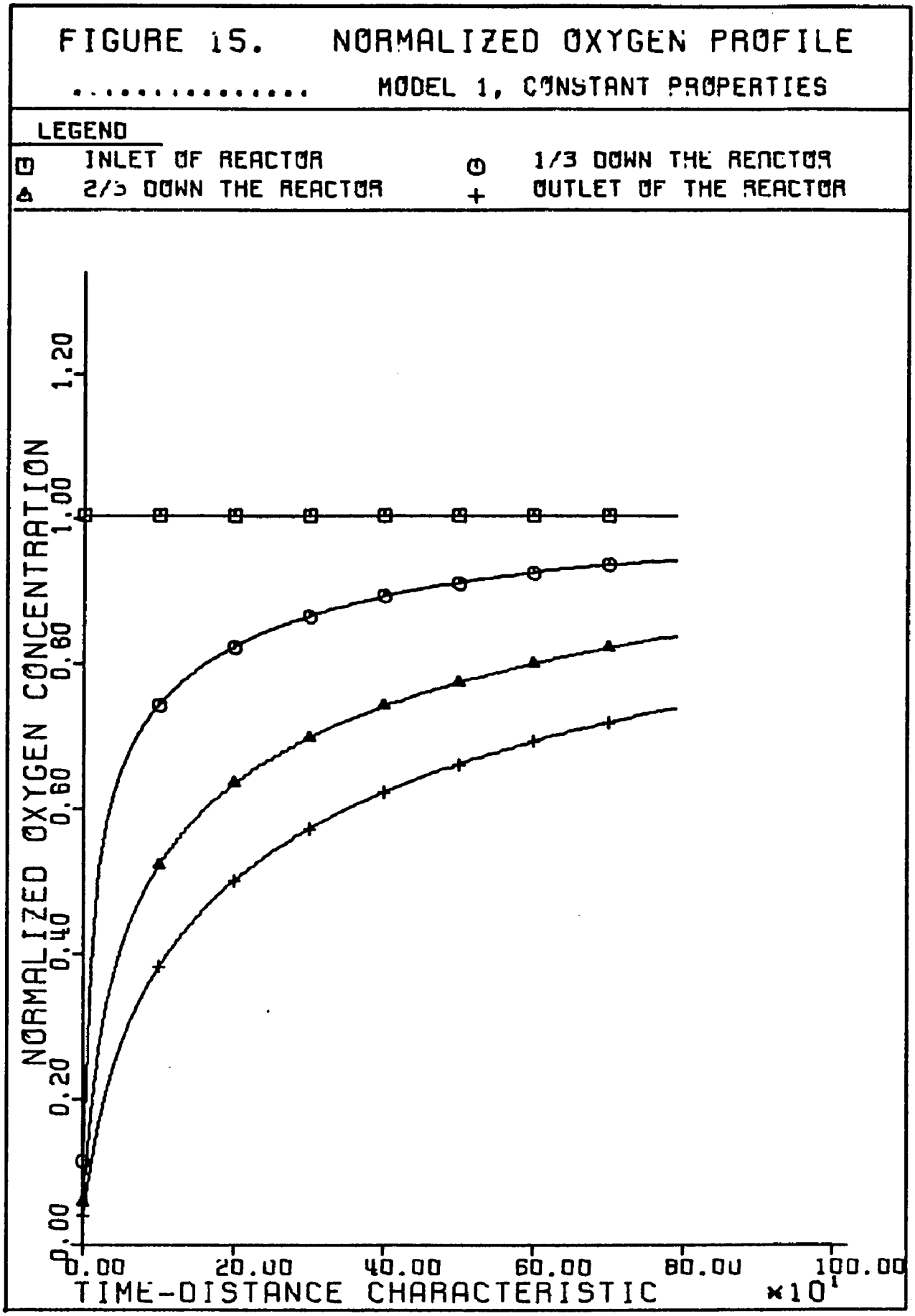

FIGURE 16. NORMALIZED SULFUR DIOXIDE PROFILE

..... MODEL 1, CONSTANT PROPERTIES

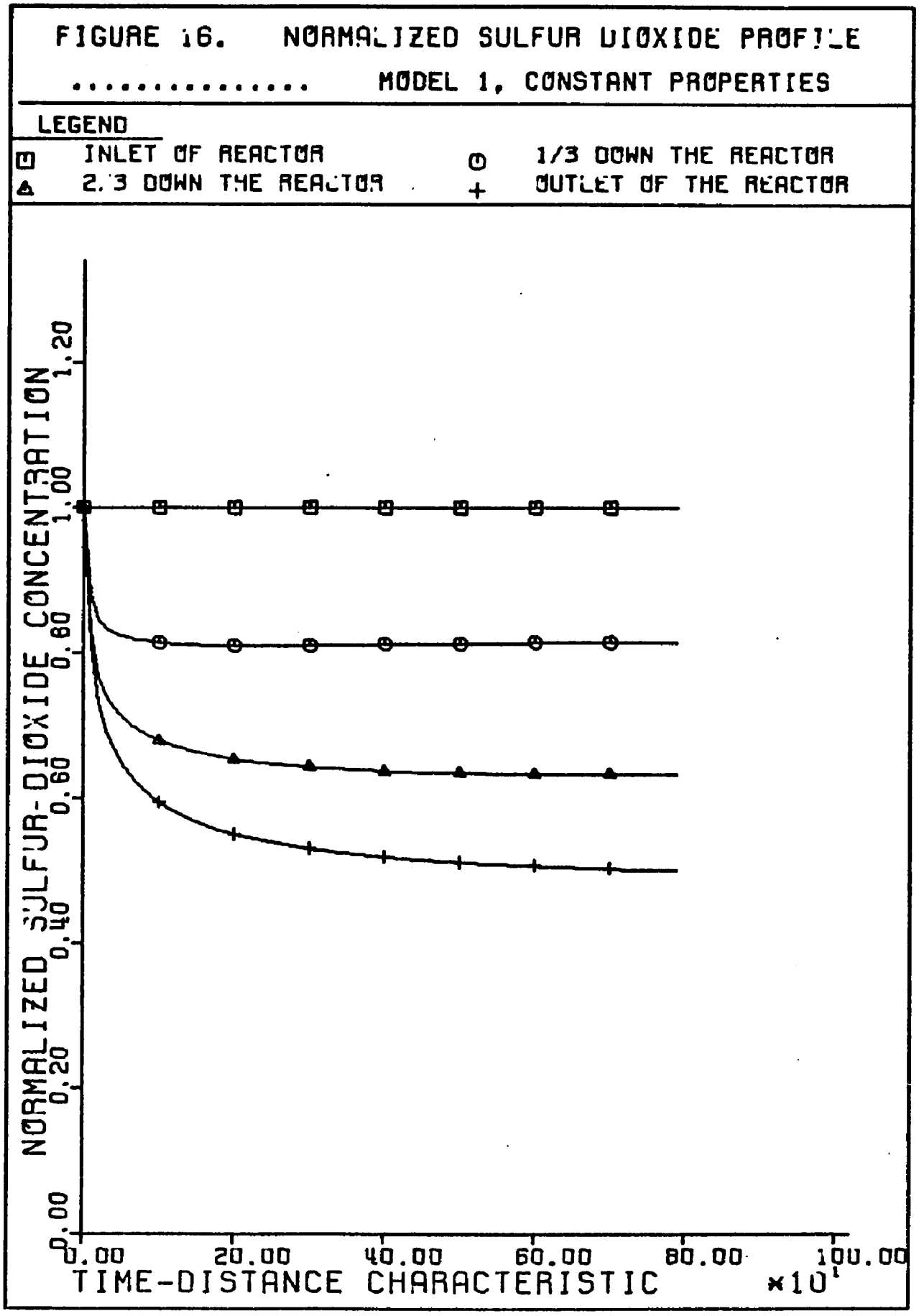

FIGURE 17. NORMALIZED OXIDATION REACTION SITE .... PENETRATION FOR MODEL 1, CONSTANT PROPERTIES

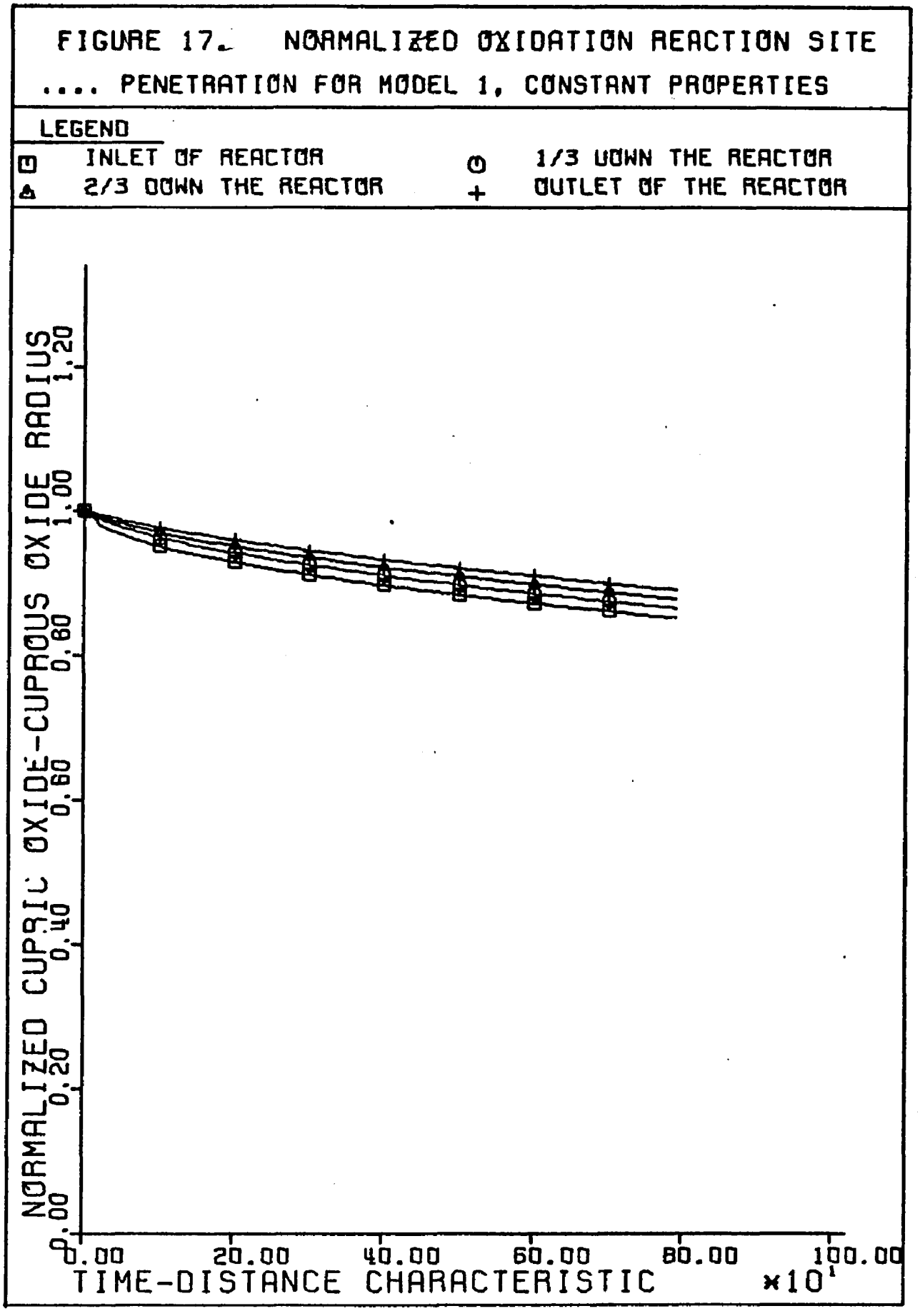

FIGURE 18. NORMALIZED SULFATION REACTION SITE .... PENETRATION FOR MODEL 1, CONSTANT PROPERTIES

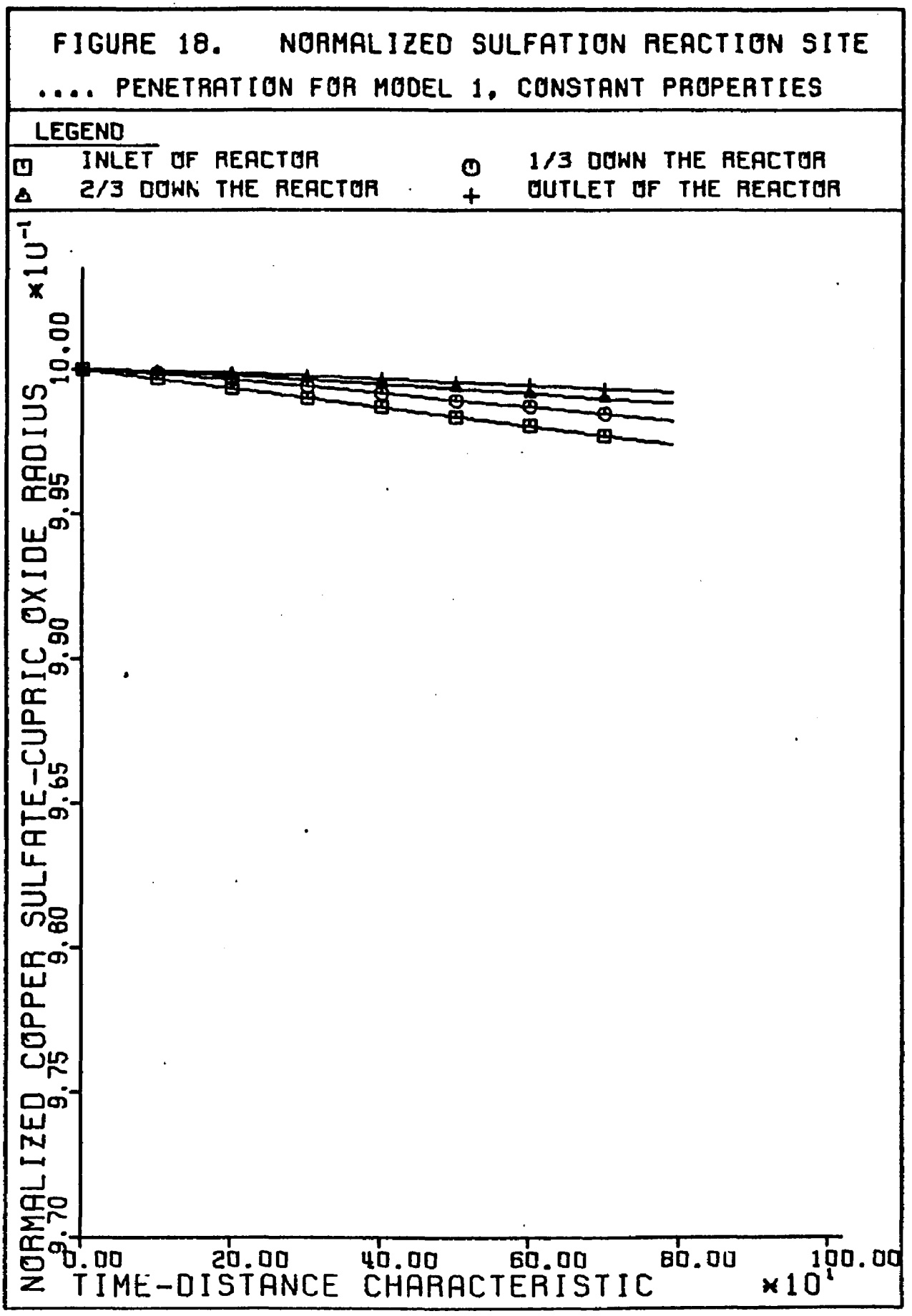

FIGURE 19. PELLET TEMPERATURE PROFILES

..... MODEL 1, CONSTANT PROPERTIES

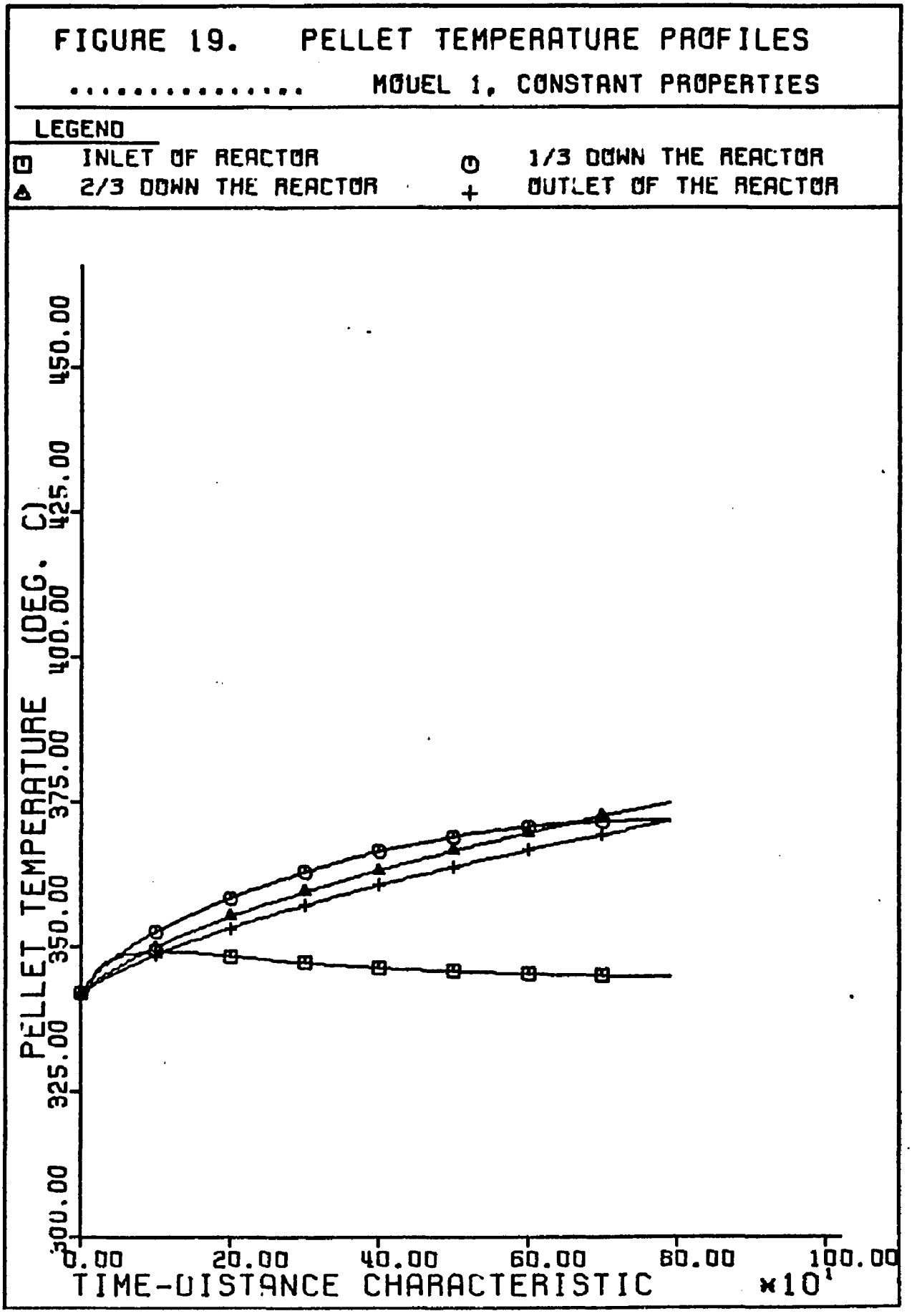

slowly falls from its inlet concentration to a normalized value of 0.4993 after 5 minutes (θ = 782). This can be explained by observing the exit O_2 concentration profile which is given by the bottom curve of Figure 15. It behaves as in Model 2 (see Figure 5) since it slowly increases from near 0.0, but at a much faster rate. Physically, this means that the sulfation reaction cannot start immediately because most of the O_2 is being consumed by oxidation and there is very little CuO for sulfation. As more oxygen becomes available, the oxidation reaction site penetration deepens, thereby allowing sulfation to occur. Thus, the consumption of SO_2 is delayed until the oxidation reaction penetration becomes significant.

Analysis of the dimensionless numbers evaluated at "standard" conditions will lend further insight to the Model 1, constant property results. The Sherwood numbers are both greater than 10^3 which means that resistance to diffusion of mass across the surface film surrounding each pellet is negligible compared to the resistance to mass transfer in the pellet pores. The modified Damkohler number for the oxidation reaction is on the order of 10^7 implying that the diffusion resistance in the pores is very large in comparison to resistance to the oxygen consumption at the oxidation reaction site. Thus, pore diffusion is the controlling resistance for the oxidation reaction at the "standard" conditions. The modified Damkohler numbers for the sulfation reaction possess orders of magnitude of 10^0 and 10^1. Thus, N_{D21}, N_{D22} and N_{sh2} indicate that pore diffusion <u>and</u> chemical reaction at the sulfation site influence the sulfation

reaction simultaneously, and that the film mass transfer resistance is negligible. Also since $\frac{N_{D2j}}{N_{D1}} > 10^5$, the oxidation reaction is much faster than sulfation as was expected.

From Figure 19, the peak temperature attained by the pellets is 648°K (375°C) which is a temperature rise of 33°C in 5 minutes. A 50°C rise in 45 minutes occurred in Model 2 at the same initial and inlet conditions. This means that the heat liberated by the oxidation reaction significantly increases bed temperatures. Comparing the shapes of the temperature profiles in Models 1 and 2 (Figures 8, 14 and 19), the effect of allowing heat to escape to the bulk gas phase and be carried down the reactor is very evident. Temperature "waves" are developed and the location of the maximum temperature moves down the bed with time rather than remaining at the entrance as in Model 2.

The peak temperature was determined from Figure 19. Notice the bed temperature is only shown at the bed inlet, Z = L/3, Z = 2L/3, and the bed outlet. A more detailed profile would show that the true peak temperature was 2°K higher and located at Z = 3L/5 rather than at 2L/3. Therefore the magnitude and location of the peak temperature obtained from the normal output of the computer program is only a general (but rather good) estimate of these quantities.

Another interesting phenomenon of Model 1 is that the bulk gas temperature can exceed the pellet temperature once the hot spot (peak temperature at any instant) is passed. This can be explained by examining the bulk gas energy balance, Equation (3-87) and

considering hitching a ride upon a nitrogen molecule. Such a ride is traced in the t, Z plane by a constant value of θ. The pellet temperatures observed during this ride can therefore be ascertained by examining Figure 19 at a constant value of θ. Between the bed entrance and the location of the hot spot, the nitrogen molecule observes $T_s > T_g$, and therefore its temperature increases. Once past the hot spot however, the nitrogen molecule has risen to very nearly $T_{s,\,max}$ and finds that the pellet temperature has dropped leaving $T_g > T_s$. Thus, this flue gas now preheats the remaining portion of the bed as heat is transferred to the pellets. Before the hot spot is reached, the pellets can be considered to preheat the flue gas before it reaches the point of maximum reaction rate. This phenomenon makes the Model 1 energy temperature profiles much more realistic than Model 2.

After 5 minutes of sorption, the maximum sulfation reaction site penetration is 0.997R (1.0% pellet utilization) and the maximum oxidation reaction penetration is 0.852R. Both conditions occur at the bed entrance as seen in Figures 17 and 18. At the same time and point for Model 2 (constant property run), the sulfation penetration was 0.979R (7% pellet utilization). Thus the addition of the chemical reaction resistance at the sulfation site decreased the pellet utilization by 70%.

Comparing Figures 4 and 13, the Model 1 efficiency is much lower and exhibits a gradual increase throughout the sorption cycle. This corresponds directly with the gradual decrease in the exit SO_2 profile. The maximum effeciency attained is 44.2% while the

minimum efficiency for Model 2 under similar conditions is 92%. Thus the addition of the chemical reaction resistance at the sulfation site is responsible for an average drop in bed efficiency of 67%.

By increasing the sorption cycle, the exit SO_2 profile reached a minimum normalized concentration of .4959 at 7.5 minutes and then began to rise. This indicates that the point of maximum sulfation had passed through the length of the bed and finally reached the exit of the bed at 7.5 minutes.

In studies of similar fixed bed systems, the accuracy of the numerical solution is usually determined by analytically integrating the solid phase material balances at the bed entrance since the gas phase concentrations remain constant at their inlet conditions. This is not possible in Model 1, since Equations (3-90, 91 and 92) are too complex.

5.4.2 Variable Properties

Allowing the physical properties to vary has a greater effect on the Model 1 profiles than it did for Model 2. This is expected since the reaction rate constants are more temperature dependent than the effective diffusivities. Figures 20 and 21 represent the variable property SO_2 and pellet temperature profiles respectively. For a 5 minute 2 second sorption cycle, the computer to real time ratio is 0.9 which is $2\frac{1}{2}$ times as great as for constant properties. As in the discussion for Model 2 with variable properties, note that the inclusion of variable gas density has varied the sorption time even though the final value of θ is the same in both the constant

FIGURE 20. NORMALIZED SULFUR DIOXIDE PROFILE

..... MODEL 1, VARIABLE PROPERTIES

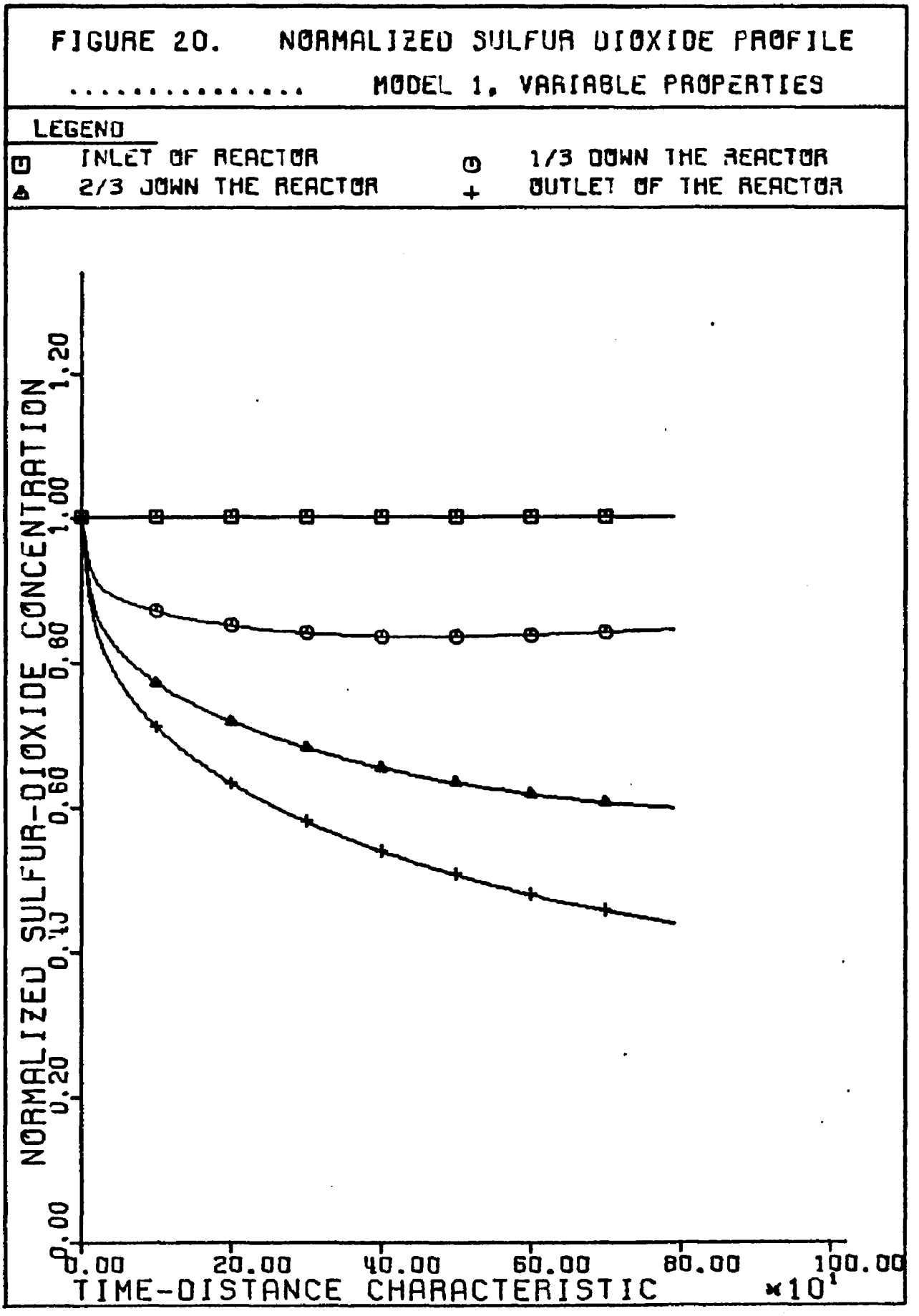

FIGURE 21. PELLET TEMPERATURE PROFILES

..... MODEL 1, VARIABLE PROPERTIES

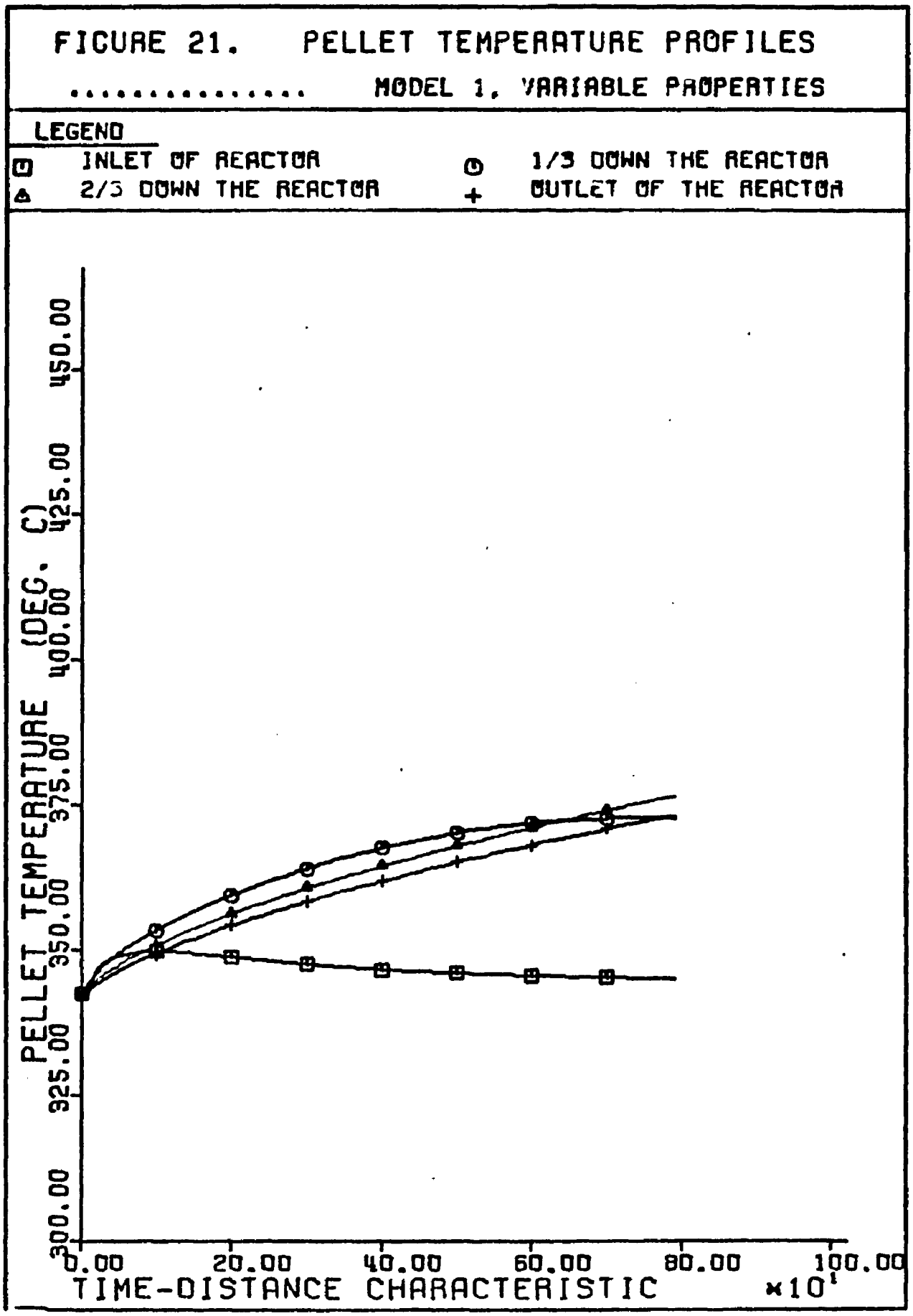

and variable property runs (2 seconds more for variable property). Again, this occurs since the temperature at the bed exit at the end of sorption is 644°K and the constant physical properties are evaluated at 640°K.

The peak temperature for variable properties is 642°K and occurs two-thirds down the length of the reactor from the inlet. Thus there is a slight increase (2°C) in the temperature profiles from the constant to the variable property case for Model 1.

The concentration profiles differ in that the SO_2 exit profile decreases to 0.46 rather 0.50 as in the constant property run. The increased consumption of SO_2 can be caused by the slightly higher temperature level maintained throughout the course of the sorption cycle, since one of the limiting resistances, $\frac{1}{k_{II}}$, increases strongly with temperature.

To achieve feasible breakthrough times, every possible advantage will have to be utilized. Therefore, the variation of properties will be included in the remaining studies even though execution times are more than doubled. The last case analyzed - Model 1, variable properties, 5 minute sorption cycle - will be termed Run 1 in the following sections.

5.4.3 Reaction Rate Constants

The effect of the reaction rate constants is investigated in Runs 2 through 4 as the frequency factors, k_j^o, are varied. The results are tabulated below:

Properties	Run 1	Run 2	Run 3	Run 4
k_I^o	10^7	10^{25}	10^2	10^7
k_{II}^o	10^{15}	10^{15}	10^{15}	10^{16}
ω_{min}	0.9985	0.9985	0.9985	0.9910
μ_{max}	1.050	1.055	1.055	1.056
$S(1,\theta)_{min}$	.438	.438	.438	0.014

where subscript "max" infers the maximum value attained and "min" the minimum value attained. The normalized sulfation reaction penetration is ω, the bed efficiency is η, the normalized pellet temperature is $\mu(=T_s/T_o)$, and the normalized SO_2 concentration at the exit is $S(1,\theta)$.

Each of the runs consisted of a 5 minute sorption cycle and locations for ω_{min} and μ_{max} are at the entrance and $\frac{2}{3}$ down the bed respectively and at the end of the cycle. Also in each case the minimum exit SO_2 concentration occurred at the end of the cycle.

As predicted earlier, the oxidation reaction rate constant had no appreciable effect as it was varied between 10^2 and 10^{25}. In Run 4, the sulfation rate constant exhibited its rate controlling behaviour as an increase of 10 times its reported value (see Appendix B-9) drastically changed the breakthrough curve. The shape of this curve was similar to the other runs as the exit SO_2 concentration decreased from its inlet concentration, but the rate of decrease was much faster with breakthrough concentration being passed (from higher concentrations - this is not the breakthrough time) after 0.48 minutes. Also, as in the other runs, the exit SO_2 was still

gradually decreasing after 5 minutes. This means that extra care must be taken in the experimental determination of the sulfation reaction rate constant. Runs 2 and 3 indicate that assuming the value of the oxidation rate constant, k_I, in Appendix B-9 was quite satisfactory.

5.4.4 Lumping Pellet Heat Transfer Resistance at Surface

The previous Model 1 runs neglected the internal resistance to heat transfer ($k_s \rightarrow \infty$) for the pellets. As mentioned in Section 3.1.8, the lumped (at the surface) pellet heat transfer resistance, h', can be approximated by

$$\frac{1}{h'} = \frac{1}{h} + \frac{R}{k_s}$$

which yields $\frac{h'}{h} = 0.1$ at 675°K. Assuming that this ratio is constant with temperature, the effect of including pellet internal resistance is studied in Run 5. The results for Runs 1 and 5 are given by:

Properties	Run 1	Run 5
h	$10^{-5}T^{1/2}$	$10^{-6}T^{1/2}$
ω_{min}	0.9985	0.9982
μ_{max}	1.050	1.0441
Position of μ_{max}	$\lambda = 2/3$, $\theta = \theta_f$	$\lambda = 1.0$, $\theta = \theta_f$
$S(1,\theta)_{min}$	0.438	0.6247 @ 4.88 min
$S(1,\theta_f)$	0.438	0.6248

where the subscript "f" refers to the end of the sorption cycle (5 minutes).

The maximum sulfation penetration is greater in Run 5 because the inlet pellet temperatures during the entire cycle averaged 5°C higher than those in Run 1. This coupled with the fact that the same amount of O_2 and SO_2 were available in both runs (inlet gas concentrations are constant) leads to increased sulfation at the inlet. From the location and magnitude of $T_{s,max}$ in these two runs, the temperature wave for Run 5 travels down the bed faster and with a smaller amplitude than in Run 1.

Reduction in the magnitude of the heat wave can be explained by the decreased value of h. Less heat is transferred from the hot pellets to the flue gas at the bed entrance with reduced h. Thus the entrance pellet temperatures are greater for Run 5. However, less preheating of the downstream pellets can occur if less heat was given to the gases at the entrance. Furthermore, what little heat that has been transferred to the gas will not transfer very readily to the cooler downstream pellets because of the increased surface resistance. Thus there is much less preheating of the downstream bed initially; and, as the reaction zone proceeds down the bed, less preheating of the flue gas takes place. Consequently the sulfation reaction (except at the entrance) is not as rapid, since k_{II} is strongly dependent on temperature and it is a rate controlling factor.

Results of Run 5 indicate that rapid transfer of heat between phases aids performance of the reactor. Unfortunately, large resistance to heat transfer between the phases is predicted for the present system (see Section 3.1.8). Thus the profiles of Run 5 are

more likely to occur than those of Run 1.

5.4.5 Greater Initial Bed Temperature

The effect of permitting the initial temperature of the pellets to be greater than the inlet gas temperature is studied in Run 6 shown below:

Properties	Run 1	Run 6
$T_s(\lambda,0)$	615°K	675°K
ω_{min}	0.9985	0.979
μ_{max}	1.050	1.154
Location of μ_{max}	$\lambda = 2/3$, $\theta = \theta_f$	$\lambda = 2/3$, $\theta = \theta_f$
$S(1,\theta)_{min}$	0.438	.077 @ 4.1 min
$S(1,\theta_f)$	0.438	.079

Both runs are for a sorption cycle of 5 minutes. Note that the velocity of the heat wave was not affected in Run 6 as it was in Run 5. A vastly improved breakthrough curve is obtained for Run 6. The exit SO_2 level decreases rapidly from its inlet level and passes down through breakthrough after 1.8 minutes, reaches a minimum level at 4.1 minutes, then gradually begins to increase again. The peak temperature attained is 710°K (437°C) which is well below the upper safety limit of 1020°K.

It is very likely that industrial application of this reactor would involve initial bed temperatures greater than the inlet temperatures (35). Therefore this improvement in operation can be expected to occur.

A solution with $T_s(\lambda,0) = 800°K$ was impossible to obtain due to instability even though step size was halved.

5.4.6 Inlet Conditions

The effects of various inlet conditions are illustrated in Runs 7, 8, 9 and 10 which are compared to Run 1 in Table 5. Each of these runs represents a sorption cycle of 5 minutes. Inlet gas temperature and initial pellet temperature were increased from 615°K to 675°K in Run 7. This corresponds to operating with a hotter flue gas. In Run 8, the inlet oxygen concentration is increased by 50%, while in Run 9 the inlet sulfur dioxide concentration doubled over that of Run 1.

The velocity of the heat wave has been slowed in Run 7, since the location of $T_{s,max}$ at 5 minutes is one-third down the bed versus two-thirds for Runs 8, 9, 10 and 1. Run 7 possesses the best breakthrough curve of all the cases studied. The exit SO_2 concentration decreased from its inlet level to the breakthrough level in ten seconds and reduced another tenfold in the next 20 seconds. It then gradually declined to a minimum normalized concentration of $1.8.10^{-4}$ after 2.5 minutes. At the end of the 5 minute sorption cycle it had only reached a level of $3.0.10^{-4}$. Therefore, obtaining a hotter flue gas greatly improves breakthrough. The flue gas temperature may be beyond the feasible control of the sorption unit operators however. Thus, this benefit may be difficult to achieve economically.

From the results of Runs 8, 9 and 10, it can be concluded that increasing the inlet oxygen concentration improves the reactor

TABLE 5

Effect of Inlet Conditions on Model 1

Properties	Run 7	Run 8	Run 9	Run 10	Run 1
Difference between Run 1	$T_i = T_o = 755°K$	$y_{10} = \frac{3}{2} y_{10}$ of Run 1	$y_{20} = 2y_{20}$ of Run 1	$y_{10} = \frac{3}{2} y_{10}$ $y_{20} = 2y_{20}$	None
ω_{min} [a]	0.9872	0.9978	0.9971	0.9957	0.9985
μ_{max}	1.0472 [b]	1.0687	1.0577	1.0724	1.0552
Location [c] of μ_{max}	$\lambda = 1/3$, $\theta = \theta_f$	$\lambda = 2/3$, $\theta = \theta_f$	$\lambda = 2/3$, $\theta = \theta_f$	$\lambda = 2/3$, $\theta = \theta_f$	$\lambda = 2/3$, $\theta = \theta_f$
$S(1,\theta_f)$	$3 \cdot 10^{-4}$ [d]	0.253	0.462	0.265	0.460

a) Occurs at the bed entrance at the end of the sorption cycle in each run. Maximum pellet utilization is obtained by $1-\omega_{min}$.

b) $\mu = T_s/T_o$

c) θ_f corresponds to 5 minutes.

d) Decreased below breakthrough at 10 seconds and reached a minimum level of $1.8 \cdot 10^{-4}$ at 2.5 minutes.

performance, while increasing the sulfur dioxide concentration has no appreciable effect. Increasing inlet O_2 concentration by 50% halved the exit SO_2 concentration at the end of the 5 minute cycle. This may be a very practical method to increase the SO_2 consumption, since the inlet O_2 concentration may be increased by combustion of the fuel with more excess air. This would also increase the sorber inlet temperature of the flue gas which is very desirable.

5.4.7 Bed, Pellet and Pore Dimensions

Parameters which the reactor designer has some measure of control over are the bed length L, the pellet radius R and, to some extent, the pore size. Increasing the pore size is equivalent to increasing the effective diffusivities in the present system, since Knudsen diffusion predominates. The effect of increasing diffusivity is given by Run 11, varying the pellet diameter is illustrated in Runs 12 and 13, and increasing bed length is studied in Run 14. These runs are compared to Run 1 in Table 6. To achieve numerical stability, the distance step size, $\Delta\lambda$, had to be halved in Runs 13 and 14.

In Run 11, the diffusivities are made ten times greater. Such a large increase is realistic when pore size is increased to the point where ordinary molecular diffusion predominates over Knudsen diffusion (see Appendices A-6 and B-6). From Table 6, it can be seen that the maximum utilization of the pellets ($1-\omega_m^3$) and the location of the peak temperature are equal between Runs 1 and 11. The latter fact indicates that the heat waves had equivalent velocities in each run. The peak temperature for larger pores is

TABLE 6

Effect of Physical Dimensions on Model 1

Properties	Run 11	Run 12	Run 13	Run 14	Run 1
Difference between Run 1	$D_{ei} = 10D_{ei}$ of Run 1	$R = \frac{4}{5} R$ of Run 1	R = R/2 of Run 1	L = 2L of Run 1	None
ω_{min} [a]	0.9982	0.9982	0.9971	0.9985	0.9985
μ_{max}	1.1181	1.0660	1.0967	1.0556	1.0552
Location of μ_{max}	λ = 2/3, 5 min	λ = 2/3, 5 min	λ = 1/3, 4.92 min	λ = 1/3, 5 min	λ = 2/3, 5 min
$S(1,\theta_f)$ [b]	0.153	0.324	0.070 [c]	0.260	0.438

a) This occurs at the bed entrance and at the end of the sorption cycle in each run. Maximum pellet utilization is $1-\omega_{min}$.

b) θ_f corresponds to 5 minutes

c) Decreased below breakthrough after 4.1 minutes.

39°C greater, however, which is due to the increased rates of reaction (pore diffusion was a rate limiting factor for sulfation). This caused the exit SO_2 level to be much lower at the end of the cycle (0.15 versus 0.44), but still not below the breakthrough concentration. As in Run 1, the exit SO_2 concentration continued to gradually decrease at the end of 5 minutes in Run 11. Thus while increasing the pore size improved the performance significantly, this factor alone will not produce practical breakthrough curves.

Reducing the pellet diameter from 1/2" to 1/4" is studied in Run 13 and to 2/5" is presented in Run 12. As mentioned in Appendix B-2, these sizes are within the practical range used in fixed bed reactors. As indicated in Table 6, reducing particle size vastly improves performance of the reactor. This is predicted by analysis of the dimensionless numbers, since rates of change of each of the system dependent variables (the constants, A_i, of Chapter III) varies inversely with R, and the Sherwood and Damkohler numbers are proportional to R. These last two numbers are the ratios of the pore diffusional resistance to film and reaction site resistances respectively, and a decrease in their value increases pore diffusion rates. Since pore diffusion is limiting, reducing R directly improves reaction rate according to the form of the differential equations.

In Run 12 a 20% reduction in pellet diameter resulted in a 30% drop in exit SO_2 concentration when compared to Run 1 at the end of 5 minutes. The maximum pellet utilization and velocity of the heat wave are the same as Run 1, but the peak temperature is 7°C higher

in Run 12. In Run 13 a 50% reduction in pellet diameter resulted in an 85% drop in exit SO_2 concentration. As in Run 1, the exit SO_2 was gradually decreasing at the end of the cycle. Maximum pellet utilization was slightly improved in Run 13. Also in relation to Run 1, the peak temperature is 25°C greater in Rum 13, and from the respective location of their peak temperatures, the velocity of the heat wave is slower in Run 13. These results indicate small pellets should be used in the present reactor. With regard to the numerical simulation, however, halving pellet diameter approximately doubles execution time, since $\Delta\lambda$ had to be halved in Run 13.

According to the dimensionless constants, A_i, increasing reactor length should increase the rate of change of each of the dependent variables in direct proportion. This criterion is met in Run 14, since doubling the reactor length reduced the exit SO_2 concentration of Run 1 by 44% at the end of equivalent length sorption cycles. The magnitude and velocity of the heat waves and the maximum pellet utilization of Runs 1 and 14 are equivalent. With regard to the numerical solution, increase in execution times are proportional to the increase in L, since $\Delta\lambda$ has to be halved in Run 14 in order to achieve stable solutions. The comparison between Runs 1 and 14 indicates that increasing reactor length improves reactor performance, but capital investment increases with reactor size also.

In conclusion, the results of Runs 11, 12, 13 and 14 demonstrate that increasing reactor length and pore size improve the reactor performance, but not to the degree that reducing pellet diameter achieves. Also, changing the size of the pellets is more reasonable

than increasing pore size or reactor length from both practical and economic considerations.

The length of the sorption cycle was increased for Run 13 and resulted in a breakthrough time of 18.2 minutes. The pellet temperature profile and sulfur dioxide profiles for this run are presented in Figures 23 and 22 respectively. The peak temperature is 442°C (715°K) which represents a temperature rise of 100°C in 17 minutes. This run was repeated with the exception that the lumped pellet heat transfer resistance, h', was used instead of h. The results strikingly indicate the controlling effect of the internal resistance, since the exit SO_2 concentration never dipped below the breakthrough level, and reached a minimum normalized concentration of 0.15 after 15 minutes, then slowly began to rise. Notice in Figure 22 that the breakthrough curve remains below the 10% level for 14 minutes out of the 18 minute sorption cycle.

5.4.8 Mass Velocity

The effect of reducing the mass velocity G is studied in Run 15, while increasing the velocity is incorporated in Run 16. The results of these studies are tabulated below and compared to the standard (Run 1):

Properties	Run 15	Run 16	Run 1
$G/G_{Run\ 1}$	1/2	3/2	1.0
ω_{min}	0.9985	0.9985	0.9985
μ_{max}	1.0555	1.0560	1.0552
Location of μ_{max}	$\lambda = 1/3$, $\theta = \theta_f$	$\lambda = 2/3$, $\theta = \theta_f$	$\lambda = 2/3$, $\theta = \theta_f$

FIGURE 22. NORMALIZED SULFUR DIOXIDE PROFILE

..... MODEL 1. RUN 13 (1/4" PELLETS)

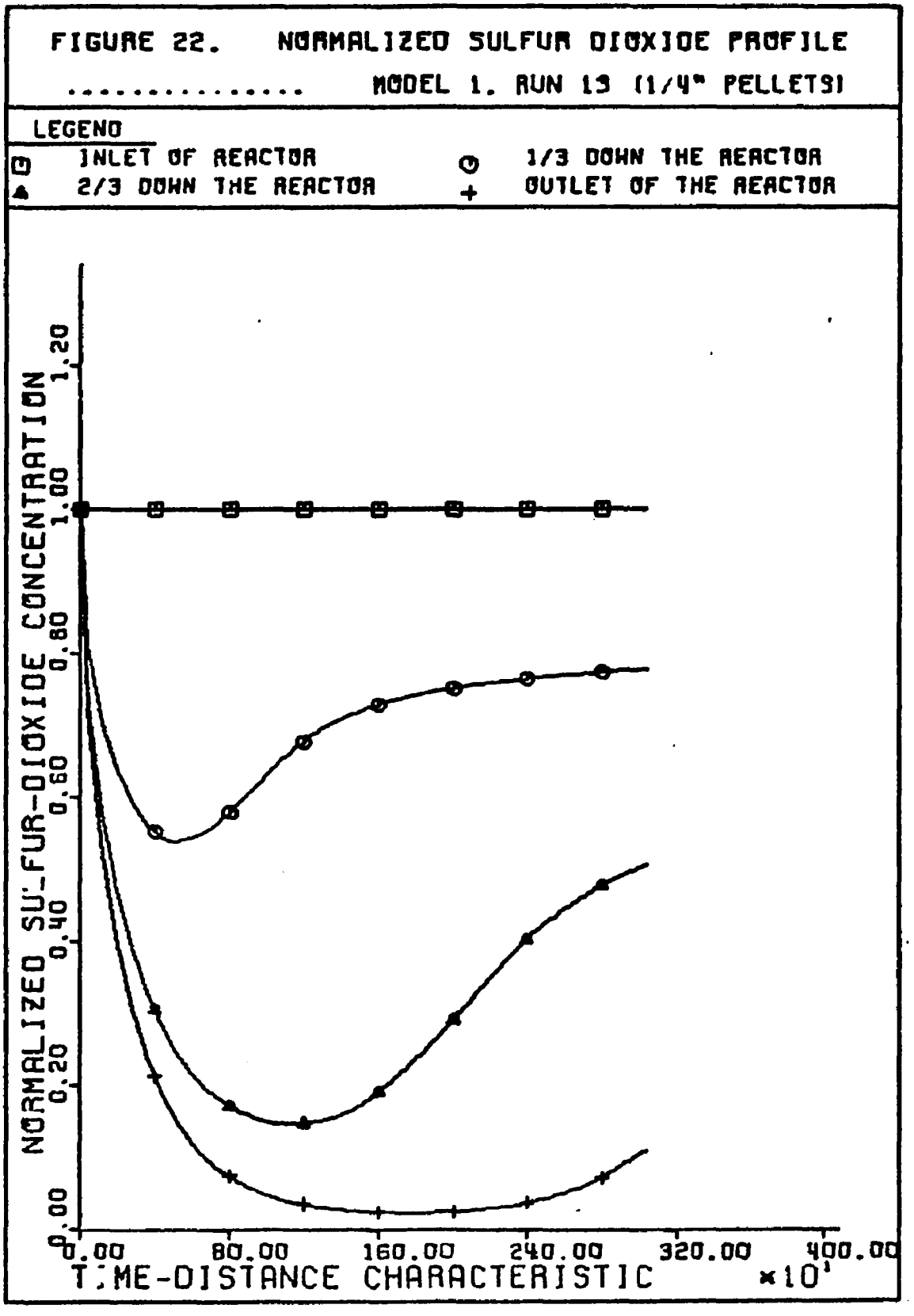

FIGURE 23. PELLET TEMPERATURE PROFILES

MODEL 1. RUN 13 (1/4" PELLETS)

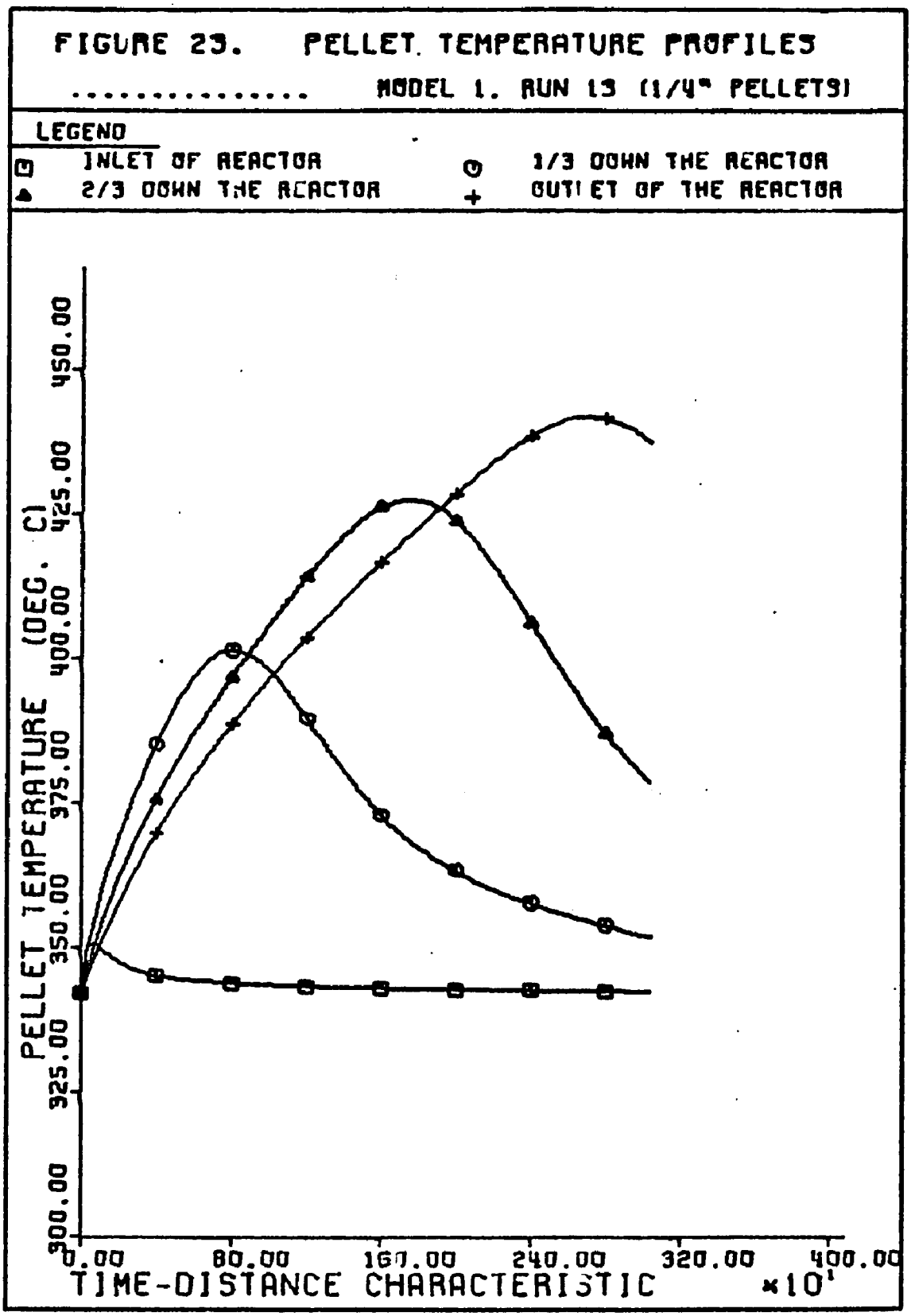

Properties	Run 15	Run 16	Run 1
$S(1,\theta_f)$	0.256	0.608	0.438

where θ_f represents a sorption cycle of 5 minutes. To achieve a stable numerical solution for Run 15 it was necessary to halve the distance step size.

Increasing the mass velocity corresponds to either increasing the mass flow rate of the gas or reducing the cross-sectional area of the bed. In Run 16, increasing the standard value of G from Run 1 by 50% reduced reactor performance, since the exit SO_2 level increased by 32% over that of Run 1 at the end of a 5 minute sorption cycle. Halving the standard value of G increased reactor performance by reducing the exit SO_2 level of Run 1 by 44%. The magnitude of the maximum pellet utilization ($1-\omega_{min}^3$) was not appreciably changed by varying G.

Notice from the results of Run 14 in Table 6 and Run 15 of this section that doubling the reactor length had the same effect as halving the mass velocity. This can be predicted from the system's dimensionless constants, since the ratio $\frac{L}{G}$ appears in A_1 through A_6. The maximum penetration of the sulfation reaction (ω_{min}), the magnitude and location of the peak temperature (μ_{max}), and the exit SO_2 concentration at the end of the sorption cycle are identical in Runs 14 and 15.

The mass flow rate of the flue gas will normally be beyond the control of the reactor designer, therefore varying G can only be accomplished by varying the bed diameter. Decreasing G by one-half corresponds to increasing bed diameter by 41% for a given gas mass

rate. Therefore this increase in performance can be achieved by increasing capital investment (larger reactor), but the increase in performance is not as significant as that produced by using smaller pellets or by increasing the bed temperature level.

5.5 Summary

For $\Delta\theta = 50$ and $\Delta\lambda = 0.025$, the numerical solutions generated by the predictor-corrector algorithm of the Model 2 differential equations were shown to match the analytical solutions to within approximately 3% at any point in time and distance. In order to assure numerical stability for the cases studied with Model 1, it was necessary to use step sizes of $\Delta\theta = 10.0$ and $\Delta\lambda = 0.025$. No analytical method was available to check the accuracy of the numerical solution of the Model 1 differential equations.

In Section 5.3, it was shown that the Model 2 energy balance is unrealistic, because the transfer of heat between the pellet and bulk gas phase cannot be neglected. Breakthrough time for the "standard" operating conditions was approximately 33 minutes for Model 2. Allowing the physical properties to vary with temperature had no appreciable effect with Model 2.

The temperature profiles and breakthrough curves of Model 1 are very different than those of Model 2. Analysis of the pertinent dimensionless numbers indicates that pore diffusion in the sulfation zone of the pellet and the chemical reaction at the sulfation site are the rate controlling steps at the expected operating conditions. Thus, Model 2 is not very realistic for the system under study,

while Model 1 is.

Allowing physical properties to vary with temperature affected the Model 1 breakthrough curves yielding improved performance. This feature should yield more realistic profiles, but its inclusion increased the computer to real time ratio 2.45 times that of the constant property case. For a five minute sorption cycle, this ratio is 0.88 for the IBM 360-65 using $\Delta\theta = 10$ and $\Delta\lambda = 0.05$. Therefore a thirty minute breakthrough would require 27 minutes of execution time on the IBM 360-65 for these step sizes.

Incorporating the oxidation reaction in Model 1 benefits reactor performance, since it generated higher bed temperatures which consequently increased the rate controlling factors D_{ei} and k_{II}. It also has a detrimental effect on performance (breakthrough), however, in that sulfation is delayed until the oxidation reaction site penetration is significant. Thus, even though penetration of the sulfate radius into the pellets was small for all the runs investigated, the Cu_2O should be dispersed throughout the pellets in order to gain full benefit of the heat generated by the oxidation reaction (which penetrates much deeper into the pellets).

Analyzing the system under study through use of the dimensionless constants and many simulations utilizing Model 1, it was found that:

1) Pore diffusion and chemical reaction in the sulfation layer of the pellets are the rate controlling factors.

2) Resistance to heat transfer within the pellets is significant, and including this resistance significantly worsens reactor performance.

3) Preheating of the downstream pellets by the flue gas (which is itself heated by the pellets at the inlet) at initial stages of a sorption cycle is significant and improves reactor performance. At later stages of the cycle, as the point of maximum reaction rate moves down the reactor, preheating of the flue gas by the preceding portions of the bed improves reactor performance appreciably.

4) Consumption of SO_2 by the bed is very sensitive to temperature and pellet radius. Therefore utilizing a bed still hot from regeneration, obtaining flue gas as hot as possible and use of 1/4" pellets or smaller are very desirable.

5) Accurate experimental determination of the sulfation activation energy and frequency factor are essential. Similarly, accurate estimation of the effective diffusivities for O_2 and SO_2, either experimentally or theoretically, is required.

6) Increasing pore size (so that molecular rather than Knudsen diffusion predominates), inlet oxygen concentration, and reactor size also improve reactor performance, but are not as significant or practical (ease of implementation and cost) as utilizing smaller pellet sizes and higher initial bed temperature and inlet flue gas temperature.

7) Incorporating the various factors (increasing L, D_B, T_i, T_o or decreasing R) which cause improvements in the reactor performance increases simulation time, since steeper gradients are encountered and/or the reactor length is increased ($\Delta\lambda$ had to be reduced).

Thus, development of a rigorous and efficient model capable of mirroring reality and development of an efficient algorithm to

solve the model's differential equations accurately has enabled the preceding analysis to be performed. This analysis emphasized the optimization of design aspects for the system under study, but could also serve in the analysis of experimental data from a pilot plant reactor.

From the various simulations performed, it can be concluded that removal of SO_2 from flue gas is feasible in fixed bed reactors if pellet diameters smaller than 1/4", inlet flue gas temperatures greater than 400°C and initial bed temperatures exceeding 440°C are utilized in conjunction with the remaining "standard" conditions defined in Section 5.1. Temperature rises of approximately 100°C and breakthrough times on the order of 20 minutes can be expected.

Simulations of the system using Model 3 were not included, since run-away temperature and hot spots did not arise for the conditions studied, and removal of heat would be detrimental to reactor performance.

CHAPTER VI

CONCLUSIONS AND RECOMMENDATIONS

A complex model capable of simulating the transient, non-isothermal operation of a large class of fixed bed reactors has been developed. The most complete model incorporated two coupled, nonlinear solid-fluid reactions described by the unreacted-shrinking-core mechanism. Intraparticle resistances to mass transfer included n^{th} order type reaction rate expressions, pore diffusion and film transfer through an external gas film surrounding each pellet. All resistance to energy transfer between the reaction sites within the pellet and the bulk gas phase are lumped at the pellet surface. The model utilizes an analytical solution to the pellet gas phase material balances after the pseudosteady state approximation is applied. The model has industrial importance and is applied to the removal of sulfur dioxide from flue gases over fixed beds containing copper oxides.

A numerical integration scheme based on the predictor-corrector technique is developed to solve the system of equations

$$\frac{\partial u_i}{\partial z_1} = F_i(\underline{u}, \underline{v}) \quad ; \quad i = 1,2,\ldots n$$

$$\frac{\partial v_j}{\partial z_2} = F_i(\underline{u}, \underline{v}) \quad ; \quad j = 1,2,\ldots m$$

where

$$\underline{u} = u_1, u_2, \ldots u_n$$

$$\underline{v} = v_1, v_2, \ldots v_n$$

The digital computer algorithm developed to implement the integration allows the physical properties of the system to vary with temperature.

Utilizing the characteristic transformation, the differential equations developed in the preceding model were transformed to the above form. For a limiting case, analytical solutions were obtained and utilized to determine the accuracy of the numerical solutions. The numerical and analytical solutions agreed to within 3% using step sizes of 0.025 for dimensionless distance and 50.0 for the dimensionless "time" characteristic.

Models incorporating multiple solid reactants in solid-fluid reactions have not appeared in the literature. Therefore the development, solution and application of such a model to an industrial application fills a void which currently exists in fixed bed reactor simulations. Also, the inclusion of all three intraparticle mass transfer resistances and intraparticle heat effects simultaneously in a fixed bed model is not reported in the literature. The author's model accomplishes both of the preceding qualities.

Analyzing the flue gas sulfur removal process through use of many simulations with the above model, it was found that internal heat transfer resistance and pore diffusion and chemical reaction control the rate of the sulfation reaction. Increasing flue gas inlet temperature, initial temperature of the bed and using small diameter pellets vastly improve reactor performance. Using 1/4" diameter pellets or smaller, initial bed temperatures greater than 400°C, inlet flue gas temperatures exceeding 340°C and the "standard" conditions given in Section 5.1, Model 1 predicts that the removal

of SO_2 from flue gas by Cu_2O is feasible in fixed bed reactors. Breakthrough times of approximately 20 minutes and 100°C temperature rises can be expected.

It was shown that accurate values are required for the effective diffusivity coefficients for O_2 and SO_2, the sulfation reaction rate constant (frequency factor and activation energy), the dependency of the sulfation reaction rate on O_2 and SO_2 concentration, and the effective thermal conductivity within the pellets. The general model (Model 1) should be reliable, because the reaction rate constant, order of the sulfur dioxide concentration dependency, the heat of reaction, and verification of the shrinking core mechanism were determined via experimental data for the sulfation reaction in a published report (35). In addition, established techniques are available to predict the effective diffusivities.

As a result of this research, several possibilities of future work are evident. Experimental data on fixed bed reactors involving gas-solid reaction systems involving multiple solid reactants is not available. The present work and that of Parsons et al (35) indicate that the removal of sulfur dioxide from flue gas by reaction with copper oxide or iron oxide is practical. Therefore it would be interesting to build an experimental reactor to verify the observations made through use of the models in Chapter V. Also, the development of an efficient solution technique for the rigorous incorporation of temperature variation of the physical properties represented by equations (3-2), (3-12), (3-33), (3-34), (3-30), (3-31) and (3-58) deserves some attention. As mentioned in Chapter III,

a tractable representation of the pellet energy balance which accounts for both radial gradients of temperature within the pellets and accumulation of energy in the pellets is needed, since both of these phenomena are important and rigorous inclusion of only one of them at a time is now possible.

It should also be mentioned that the numerical integration algorithm was written in a very general fashion and can be applied to a wide variety of problems by merely changing the boundary condition section and reading in new data. The total number of partial differential equations, the number having partials in distance, and the stoichiometric coefficients are considered data, rendering the algorithm very versatile.

NOMENCLATURE

a_c	=	radial position within pellet at which oxidation reaction is oocurring, cm
A	=	cross-sectional bed area, sq.cm.
A_i	=	dimensionless system parameters for Model 1 equations
A_i'	=	dimensionless system parameters for Model 2 equations
B	=	bed load = weight of $CuSO_4$ contained in the bed at any instant, g
c_i	=	molar heat capacity of i^{th} component, cal/ g mole-°C
C_g	=	gas mixture heat capacity, cal/g-°C
C_s	=	pellet heat capacity, cal/g-°C
D_B	=	bed diameter, cm
D_i	=	molecular diffusivity, sq.cm.
D_{ei}	=	effective diffusivity, sq.cm.
ΔE_i	=	activation energy for i^{th} reaction, cal/g mole
f,F,F_i,F_j'	=	some function
g,h	=	some function
G	=	mass flux or mass velocity, g/sq cm-sec
h	=	heat transfer coefficient at pellet surface, cal/sq cm-sec-°C
h'	=	lumped (internal and surface) pellet heat transfer coefficient, cal/sq cm-sec-°C
h_i	=	partial molal enthalpy of component i, cal/g mole

h_w	=	heat transfer coefficient at bed wall cal/sq cm-sec-°C
H_g	=	gas phase intensive enthalpy, cal/g
H_s	=	pellet phase intensive enthalpy, cal/g
ΔH_i	=	heat of reaction for reaction i, cal/g mole
i,j,k,l,m,n_1,n_2	=	indices used in discrete variable notation and in numerical algorithms
I	=	Legendre transform
J	=	energy conversion factor, cal/cm^3-atm.
k_j	=	j^{th} reaction's rate constant: Reaction I = cm/sec Reaction II = cm^4/g mole-sec
k_g	=	gas phase thermal conductivity, cal/cm-sec-°C
k_s	=	effective pellet thermal conductivity, cal/cm-sec-°C
k_j^o	=	frequency factor for reaction j (same units as k_i)
k_i'	=	film mass transfer coefficient at pellet surface for component i, g mole/sq cm-sec
k_j''	=	reaction rate constant for reaction j
K_i	=	film mass transfer coefficient of component i, cm/sec
L	=	bed length, cm
M	=	gas mixture molecular weight, g/g mole
M_i	=	molecular weight of component i, g/g mole
N_i	=	molar flux of component i, g mole/cm^2-sec
$\underline{N}_i$	=	weight of component i per pellet, g/pellet
N_{Bi}	=	Biot number for heat transfer

N_{Di}	=	Damkohler number
N_{Re}	=	Reynolds number
N_{sh}	=	Sherwood number
P	=	bed pressure, atm
Q	=	potential function
r	=	radial distance in pellet, cm
r_c	=	radial position within pellet at which sulfation reaction is occurring, cm
R	=	pellet outer radius, cm
R_i	=	overall reaction rate for i^{th} reaction
R'	=	universal gas constant, 82.06 cm^3 atm/g mole °K
S	=	normalized SO_2 concentration = $\frac{y_2}{y_{20}}$
t	=	time, sec
T	=	temperature, °K
u,v	=	some dependent variables
U	=	intensive internal energy, cal/g
V	=	volume, cc
W_i	=	weight fraction of component in the solid pellet
x_i	=	bulk gas phase mole fraction for component i
$\underline{x}_i$	=	weight fraction for bulk gas phase component i
X_i	=	pellet gas phase mole fraction for component i
y_i	=	bulk gas phase molar concentration for component i, g mole/cc
y_{si}	=	pellet gas phase molar concentration for component i, g mole/cc
Y	=	normalized oxygen concentration = $y_1 / y_{1.0}$

Z = axial distance from bed entrance, cm

z_1, z_2 = some independent variables

α = stoichiometric constant = $\left|\frac{\gamma_{27}M_7}{\gamma_{22}}\right|$ = 159.5 g $CuSO_4$/g mole SO_2

β = stoichiometric constant = $\frac{\gamma_{16}M_6}{\gamma_{11}}$ = 286 g Cu_2O/g mole O_2

γ = stoichiometric constant = γ_{21}/γ_{22} = moles O_2/mole SO_2 for sulfation reaction

γ_{ij} = stoichiometric coefficient for i^{th} reaction, j^{th} component

ϵ = bed void fraction

ϵ_s = pellet void fraction

η = bed efficiency = cummulative fraction of SO_2 removed from flue gas

θ = a normalized characteristic direction = $\frac{Gt}{\rho_g \epsilon L} - \frac{Z}{L}$

λ = normalized distance = $\frac{Z}{L}$

μ = normalized pellet temperature = T_s/T_o

ξ = dimensionless time = $\frac{Gt}{\rho_g \epsilon L}$

ρ_g = gas density, g/cc

ρ_s = pellet density, g/cc

σ = convergence criteria in numerical algorithm

ϕ = normalized oxidation reaction radius, $\frac{a_c}{R}$

Φ = transformed sulfation reaction radius = $\omega^3/3$

χ = transformed SO_2 concentration = $\frac{\alpha y_{20} \epsilon S}{3(1-\epsilon)\rho_s W_7}$

Ψ = normalized bulk gas phase temperature = T_g/T_o

ω = normalized sulfation reaction radius = $\frac{r_c}{R}$

Subscripts

g = external or bulk gas phase

i = designates i^{th} component; i^{th} reaction, or initial conditions

j = designates j^{th} component or j^{th} reaction

s = internal or pellet gas phase

S = solid pellet phase

0 = inlet condition

1 = O_2

2 = SO_2

3 = N_2

4 = CO_2

5 = H_2O

6 = Cu_2O

7 = $CuSO_4$

8 = CuO

I = oxidation reaction

II = sulfation reaction

BIBLIOGRAPHY

1. Acrivos, A., Ind. Eng. Chem., 48, 703 (1956).

2. Ames, W. F., Nonlinear Partial Differential Equations in Engineering, pp. 37-40, Academic Press, New York, 1965.

3. Bares, J., Marecek, J., Mocek, K., and Erdos, E., Coll. Czech. Chem. Commun. (Prague), 35, #6, 1628 (1970).

4. Bienstock, D., Brumm, L. W., Haynes, W. P., and Benson, H. E., Bur. Mines Inform. Circ. #7836 (1958).

5. Bischoff, K., Chem. Eng. Sci., 18, 711 (1963).

6. Bischoff, K., Ind. Eng. Chem. Fund., 8, 665 (1969).

7. Blackemore, J. E., and Corcoran, W. H., Ind. Eng. Chem. Proc. Des. Dev., 8, 206 (1969).

8. Conte, S. D., Elementary Numerical Analysis, p. 228, McGraw-Hill, New York, 1965.

9. Courant, R. and Friedrichs, K. O., Supersonic Flow and Shock Waves, pp. 37-87, Interscience Publishers, New York, 1948.

10. Deans, H. A. and Lapidus, L., A.I.Ch.E. Journal, 6, 656 (1960).

11. Eteson, D. C. and Zwiebel, I., A.I.Ch.E. Journal, 15, 124 (1969).

12. Godfrey, T. G., Ernst, W. S., Tennery, V. J., and Harris, L. A., "Characterization and Behaviour of Alkalized Alumina During the Sulfur Dioxide Sorption-Regeneration Process - A Summary Report", ORNL-TM-3210, 1969.

13. Gonzalez, L. A., and Spencer E. H., Chem. Eng. Sci., 18, 753 (1963).

14. Hlavacek, V., Can. J. Chem. Eng., 48, 656 (1970).

15. Johnson, B. M., Froment, G. F., and Watson, C. C., Chem. Eng. Sci., 17, 835 (1962).

16. Kardos, P. W. and Stevens, W. F., A.I.Ch.E. Journal, 17, 1090 (1971).

17. Katell, S., Chem. Eng. Prog., 62, (1966).

18. Kramers, H. and Alberda, G., Chem. Eng. Sci., 2, 173 (1953).

19. Lamb, D. E., and Wilhelm, R. H., Ind. Chem. Eng. Fund., 2, 173 (1963).

20. Levenspiel, O., Chemical Reaction Engineering, pp. 338-357, John Wiley, New York, 1962.

21. Liu, S. and Amundson, N. R., Ind. Eng. Chem. Fund., 1, 200 (1962).

22. Luss, D. and Amundson, N. R., A.I.Ch.E. Journal, 15, 194 (1969).

23. Masamune, S., and Smith, J. M., A.I.Ch.E. Journal, 10, 246 (1964).

24. Maurin, P. G., and Janakin, J., Chem. Engr., 77, #9, 173 (1970).

25. McCracken, D. D. and Dorn, W. S., Numerical Methods and Fortran Programming, p. 322, John Wiley, New York, 1964.

26. McGuire, M. L. and Lapidus, L., A.I.Ch.E. Journal, 11, 85 (1965).

27. Newell, J. E., Chem. Eng. Prog., 62, 67 (1966).

28. Norman, J. R., and Wood, D. G., Inst. Engrs., Australia: Mech. Engr. Trans., ML-4, #11, 118 (1968).

29. Olson, J. H., Ind. Eng. Chem. Fund., 7, 185 (1968).

30. Olson, K. E., Ph.D. Thesis, U. of Minn., 1962.

31. Olson, K. E., Luss, D., and Amundson, N. R., Ind. Eng. Chem. Proc. Des. Dev., 7, 96 (1968).

32. Ozawa, Y., Ind. Eng. Chem. Proc. Des. Dev., 8, 378 (1969).

33. Ozawa, Y., Chem. Eng. Sci., 25, 529 (1970).

34. Paris, J. R. and Stevens, W. F., Can. J. Chem. Eng., 48, 100 (1970).

35. Parsons, T., Schroeder, G. D., Deberry, D., Nat. Air Poll. Control Admin. Contract #PH 86-68-68, July 31, 1969. (Tracor Document No. 69-579-U)

36. Petersen, E. E., Chemical Reaction Analysis, p. 15, Prentice-Hall, Englewood Cliffs, New Jersey, 1965.

37. Ramirez, R., Chem. Engr., 77, #9, 173 (1970).

38. Scott, C. D., A.I.Ch.E. Journal, 15, 116 (1969).

39. Shen, J. and Smith, J. M., Ind. Eng. Chem. Fund., 4, 293 (1965).

40. Sladek, K. J., Lowell, P. S., Schwitzgebed, K., and Parsons, T. B., Ind. Eng. Chem. Proc. Des. Dev., 10, 384 (1971).

41. Smith, J. M., Can. J. Chem. Eng., 48, 142 (1970).

42. Van Deemter, J. J., Ind. Eng. Chem., 45, 1227 (1953).

43. Vanderveen, J. W., Luss, D., Amundson, N. R., A.I.Ch.E. Journal, 14, 636 (1968).

44. Von Rosenberg, D. U., Methods for the Numerical Solution of Partial Differential Equations, American Elsevier, New York, 1969.

45. Wall, J. D., Hydroc. Proc., 50, 158 (1971).

46. Wen, C. Y., Ind. Eng. Chem., 60, 34 (1968).

47. Wen, C. Y. and Wei, L. Y., A.I.Ch.E. Journal, 16, 848 (1970).

48. Wen, C. Y. and Wei, L. Y., A.I.Ch.E. Journal, 17, 272 (1971).

49. Wen, C. Y. and Wang, S. C., Ind. Eng. Chem., 62, 30 (1970).

50. Yulish, J., Chem. Engr., 78, #13, 58 (1971).

APPENDIX

APPENDIX A

ESTIMATION OF PHYSICAL PROPERTIES FOR BULK GAS PHASE

1. Inlet Temperature Range

For convenience and easy reference, the range of the typical inlet temperatures for a fixed bed flue gas sulfur removal process (19,26,29) is given below along with the conversions to other temperature scales.

	°C	°K	°R	°F
Minimum Inlet Temperature	342	615	1110	650
Average Inlet Temperature	402	675	1210	750
Maximum Inlet Temperature	482	755	1360	900

2. Inlet Flue Gas Composition

A typical flue gas composition is nonexistant, since it depends on the type of fuel used (coke, fuel oil, natural gas, etc.), the composition of the fuel, the amount of excess air present, and the temperature of combustion. The inlet flue gas composition for this study is based on the following criteria (12):

1) Flue gas is a combustion product of the following coal:

Component	Weight Per Cent
Carbon	70.1
Oxygen	6.6
Hydrogen	4.9
Nitrogen	1.4
Sulfur	3.0
Ash	12.7
Moisture	1.3

2) Combustion conditions:

Excess air = 20%
Heating value = 12800 BTU/pound

3) Sulfur in the coal:

Burns to SO_3: 2%

Burns to SO_2: 98%

4) Practically no ash in the flue gas.

5) Flue gas analysis:

Component	Inlet Weight Fraction	Inlet Mole Fraction
O_2	.0340	.0304
SO_2	.0025	.0011
N_2	.7615	.7805
CO_2	.1420	.0926
H_2O	.0600	.0954

Assuming that only a tenth of the original sulfur dioxide and oxygen remain in the flue gas at the outlet of the reactor, the following outlet composition for the flue gas exists for the above inlet composition.

Component	Outlet Weight Fraction	Outlet Mole Fraction
O_2	.00352	.00314
SO_2	.00026	.00012
N_2	.78739	.80303
CO_2	.14680	.09529
H_2O	.06203	.09842

The effect of composition on the physical properties will be determined by using both the inlet and outlet compositions and then comparing the resulting correlations.

3. Flue Gas Molecular Weight

Based on the preceding flue gas composition range, the mixture molecular weight of the gas stream varied by less than 0.25%. Thus the gas mixture molecular weight, obtained by mole fraction averaging, is 28.6 g/g mole.

4. Gas Density

A volume balance on a given weight of gas of known composition renders the following relation between the mixture density, composition, and species' densities,

$$\rho \text{ mixture} = \rho_g = \frac{1}{\sum_{i=1}^{5} \frac{x_i}{\rho_i}} \qquad \text{(A-4.1)}$$

where x_i is the weight fraction of specy i and ρ_i is the density of gaseous specy i. Assuming ideal temperature effect of gases and using data available in the literature (13,20), the expression below was obtained to represent the gas density.

$$\rho_g = 21.9\ T^{-1}\ \#/\text{cft}$$
$$= 0.351\ T^{-1}\ \text{gr/cc}$$

where T is temperature in degrees Kelvin. This expression predicts flue gas density to within 0.5% of that obtained by using Equation (A-4.1) over the composition range to be expected in this study.

5. Mixture Viscosity

Due to the greater influence of the heavier molecules in collisions, mixture viscosities often deviate positively from that

predicted by simple mole-fraction averaging. The mixture viscosity may even be greater than the viscosity of any pure component. This phenomenon frequently occurs in mixtures of polar and nonpolar gases having a wide range of molecular weights but equivalent pure component viscosities.

Using the Chapman-Enskog theory, as recommended in Reid and Sherwood (22) and given below, to predict the pure component viscosities, the preceding situation is approached for the flue gas. The Chapman-Enskog theory yields the following expression for viscosity,

$$\mu_i = 2.669.10^{-3} \sqrt{M_i T} / (\sigma_i^2 \Omega_V) \text{ , cp}$$

where T is temperature in degrees. Kelvin, M_i is molecular weight of specy i, σ_i is the molecule diameter in angstroms for specy i, and Ω_V is the appropriate collision integral. The molecular weights vary between 18 and 64, while the viscosity ranges from 0.024 cp and 0.037 cp at 675°K.

The Wilke (34) estimation method was utilized to predict mixture viscosity because of its ease of application and agreement with experimental data (22) at low pressures. The equations involved are,

$$\mu_g = \sum_{i=1}^{n} \mu_i \Big/ \left[1 + \sum_{\substack{j=1 \\ j\neq i}}^{n} \phi_{ij} (x_j/x_i)\right] \qquad \text{(A-5.1)}$$

$$\phi_{ij} = \left[1 + (\mu_i/\mu_j)^{1/2} (M_j/M_i)^{1/4}\right]^2 \Big/ \left\{\sqrt{8(1+(M_i/M_j))}^{1/2}\right\}$$

where μ_g = mixture viscosity

μ_i = pure component viscosity

M_i = molecular weight of specy i

x_i = mole fraction of specy i

Generating values with the preceding formulas, the following expression was arrived at for the variation of mixture viscosity with temperature,

$$\mu_g = 6.9.10^{-4} T^{0.637}, cp$$

where T is temperature in degrees Kelvin. This expression predicts flue gas viscosity to within 2.5% of that given by Equation (A-5.1) over the range of compositions and temperatures expected in this study.

6. Bulk Gas Mixture Diffusivities

The theory of diffusion in multicomponent systems is complex, with the diffusivity expressions depending upon the geometry of the system, the direction(s) of diffusion, and the number of components diffusing and remaining stagnant. A rigorous but complex, analysis of diffusion in multicomponent gas systems is given in Hirschfelder et al (9). A simplifying approximation can be made, however, by introducing a mixture diffusion coefficient, D_{im}, for component i of the mixture. Such a treatment is given in Chapter 21 of Bird, Stewart and Lightfoot's text (3), and it will be considered to be adequate for the present problem.

In their analysis, the mixture diffusivity is defined by Fick's law as,

$$I_i = - \frac{\rho_g}{M} D_{im} \nabla x_i$$

where I_i is molar flux for species i relative to the molar average

velocity in a multicomponent mixture. By definition the sum of the molar fluxes, I_i, is zero, yielding the following expression for D_{im} in an n-component mixture,

$$\sum_{i=1}^{n} D_{im} \nabla x_i = 0$$

The relationship between the molar flux relative to a stationary boundary, N_i, and I_i is,

$$I_i = N_i - x_i \sum_{j=1}^{n} N_j \qquad \text{(A-6.1)}$$

Using Hirschfelders and Curtiss' expression for ∇x_i (6) and Equation (A-6.1), the equation for D_{im} becomes (3,4),

$$D_{im} = \frac{N_i - x_i \sum_{j=1}^{n} N_j}{\sum_{j=1}^{n} \frac{N_i x_j - N_j x_i}{D_{ij}}} \qquad \text{(A-6.2)}$$

Once the ratios and directions of the N_i's are known, D_{im} can be predicted easily using Equation (A-6.2).

The binary diffusion coefficient, D_{ij}, will be estimated by (22),

$$D_{ij} = 1.858.10^{-3} T^{3/2} \sqrt{\frac{M_i + M_j}{M_i M_j}} \Big/ (P \sigma_{ij}^2 \Omega_D) \qquad \text{(A-6.3)}$$

where D_{ij} is in cm^2/sec, T in °K, P is pressure in atmospheres, M_i is the molecular weight of component i, σ_{ij} is the Leonnard-Jones force constant for a mixture in $\mathring{A}$, and Ω_D represents the Lennard-Jones potential function for diffusion.

Basing the molar flux ratios on stoichiometry and using Equations (A-6.2) and (A-6.3), the mixture diffusivities are determined and presented below for various temperatures.

Temperature, °K	D_{1m} (cm^2/sec)	D_{2m} (cm^2/sec)
615	0.726	0.452
675	0.835	0.561
755	1.010	0.666

7. Bulk Gas Heat Capacity

None of the available prediction methods for the heat capacity of gas mixtures has been sufficiently tested, and the methods for polar mixtures are known to be unreliable (22). There is also wide disagreement among the standard reference books on the data for common gases.

For these reasons and because of their ease of implementation, the empirical relations developed in Hougen et al (11) for the pure component molal heat capacities were deemed acceptable.

The mixture heat capacity obtained by simple mole fraction averaging of the pure components is given by

$$C_g = 2.78 + 8.33.10^{-5}T + 3.04.10^{-9}\ T^2$$

where C_g is the mixture heat capacity in cal/g-°K, and the absolute temperature T is expressed in °K.

8. Bulk Gas Mixture Thermal Conductivity

The thermal conductivity of a gas mixture is usually a nonlinear function of composition (22). Compared to the mole fraction averaging of the pure component conductivities, a positive deviation results if the molecules possess widely different polarities, whereas the mixture conductivity is less than this average for polar

mixtures. Some mixtures, such as N_2-CO_2, show positive deviations at high temperatures but exhibit negative deviations at low temperatures (14).

The flue gas mixture contains both polar and nonpolar molecules, therefore simple mole fraction averaging cannot be utilized. For this type of mixture, either the Lindsay and Bromley formulation or the Cheung, Bromley and Wilke method are recommended (22) based on a compromise of accuracy versus ease of application. Both of these methods utilize the Wassiljewa mixture equation,

$$P_m = \sum_{i=1}^{n} P_i \Big/ \left[1 + \sum_{\substack{j=1 \\ j \neq i}}^{n} A_{ij} (x_j / x_i) \right]$$

where P_m is the mixture property, P_i is the property for component i, A_{ij} is a function to be specified and x_i is the mole fraction for the i^{th} component. This is the same form as the mixture viscosity equation in Appendix A-5.

The Lindsay-Bromley method will be used for the flue gas mixture since it has been tested more extensively and is easier to implement. The method consists of the following pair of equations (22),

$$k_g = \sum_{i=1}^{n} k_i \Big/ \left[1 + \sum_{\substack{j=1 \\ j \neq i}}^{n} A_{ij} (x_j / x_i) \right] \qquad \text{(A-8.1)}$$

where k_g is the mixture thermal conductivity and k_i is the pure-component thermal conductivity. The function A_{ij} was developed by utilizing a Sutherland model for a gas and is expressed by,

$$A_{ij} = \frac{1}{4}\left(1 + \left\{(\mu_i/\mu_j)(M_j/M_i)^{3/4}\left[\left(1 + S_i/T\right)/\left(1 + S_j/T\right)\right]\right\}^{1/2}\right)^2$$

$$\left[\left(1 + S_{ij}/T\right)/\left(1 + S_i/T\right)\right] \qquad \text{(A-8.2)}$$

where $S_i = 1.5\ T_{bi}$

$S_{ij} = 0.733\ (S_i S_j)^{1/2}$

T_{bi} = normal boiling point of component i

Values for the thermal conductivity of the pure components in the flue gas were taken from the literature (27). Data at three temperatures (600°K, 700°K, and 800°K) was fitted to a second-order polynomial expression in temperature for each component.

A computer program was developed to determine the polynomial coefficients and the mixture thermal conductivity at various temperatures and compositions using Equations (A-8.1) and (A-8.2). Based on these conductivities, the following expression for mixture thermal conductivity as a function of temperature was found to be valid to within 1.2% over the entire temperature and composition range expected,

$$k_g = 4.45.10^{-7}\ T^{.866}\ \text{cal/cm-sec°K}$$

where temperature, T, has units of degrees Kelvin.

9. Fixed Bed Heat and Mass Transfer Coefficients

Due to the complex flow paths and geometry in fixed beds, it has been necessary to develop semiempirical correlations for mass

and heat transfer rates between the pellets and the flowing fluid. The dimensionless groups selected for correlation are based on analysis of the pertinent conservation equations. For forced convection in fixed beds, the significant dimensionless groups for heat and mass transfer are the Chilton-Colburn j-factors, void fraction of the bed, and the Reynolds, Schmidt and Prandtl numbers (4).

At negligible interphase transfer rates, advantage can be taken of the analogy between heat and mass transfer which, for multi-component diffusion, is conveniently expressed by the j-factors as (4),

$$\left.\begin{aligned} j_D &= \frac{K_i^o \rho_g}{G} N_{Sci}^{2/3} \\ j_H &= \frac{h^o}{C_g G} N_{Pr}^{2/3} \end{aligned}\right\} = \text{same function of } N_{Re} \text{ and } \epsilon \qquad \text{(A-9.1a)} \quad \text{(A-9.1b)}$$

where $N_{Sci} = \frac{\mu_g}{\rho_g D_{im}}$ = Schmidt number for component i

$N_{Pr} = \frac{C_g \mu_g}{k_g}$ = Prandtl number

$N_{Re} = \frac{2RG}{\mu_g}$ = Reynolds number

K_i^o = mass transfer coefficient for component i at negligible interphase mass transfer rates

h^o = heat transfer coefficients at negligible interphase heat transfer rates.

Equation (A-9.1) is especially valid if the Prandtl and Schmidt numbers exceed 0.5 and the flow velocity is high. Each of these conditions is met, since it will be shown that

$$N_{Pr} \approx 1.0,\ N_{Sc} \geq 1.0,\ v \approx 16000 \text{ ft/hr}$$

where v = fluid velocity.

The transfer coefficients are defined by

$$N_i = K_i(y_i - y_{si})$$
$$Q = h(T_g - T_s)$$

where N_i is the molar flux of component i perpendicular to the solid-fluid interface, Q is the heat flux perpendicular to the interface, the subscripts "g" and "s" represent conditions in the ambient fluid and at the pellet surface respectively. It should be emphasized that all of the parameters in Equation (A-9.1) are local and represent conditions only at a single cross-section of the bed.

The first j-factor correlation in general use was by Gamson Thodos and Hougen (7), and since then there have been numerous investigations (2,4,5,10,17,21,35) and correlations published. The data for these correlations was obtained in various ways: dissolving soluble solids into flowing streams, evaporating liquids from porous pellets into gas streams, extracting misicible liquids from pellets into fluid streams and sublimating volatile solids into air. Ten of these correlations were compared over a wide range of Reynolds numbers and had a mean deviation of $\pm$ 28% (15,28). This indicates the large differences which exist among the various correlations. Possible reasons for these deviations include axial mixing effects, wall effects, and ambiguity over the vapor pressures and diffusivities to be used in the calcuations.

Petrovic and Thodos' recent correlation (21) was chosen for

this study, since it matches closely many of the experimental correlations (McCune and Wilhelm, Gamson et al, Wilke and Hougen) and Carberry's theoretical analysis for conditions existing in this study. Their correlation is given by,

$$\epsilon j_D = 0.357\ N_{Re}^{-0.59} \qquad \text{(A-9.2)}$$

which is valid for $3 < N_{Re} < 2000$. This correlation is based on new data and correction of various earlier studies by Thodos for axial mixing.

Using the results of the preceding sections in conjunction with Equation (A-9.1), the following expressions are developed for the transfer coefficients at negligible transfer rates.

$$h^o = 8.85.10^{-5}\ T^{0.445}, \quad \text{cal/sq cm-sec-°K} \qquad \text{(A-9.2)}$$

$$K_1^o = 2.16.10^{-3}\ T^{1.31}, \quad \text{cm/sec} \qquad \text{(A-9.3)}$$

$$K_2^o = 8.09.10^{-4}\ T^{1.42}, \quad \text{cm/sec} \qquad \text{(A-9.4)}$$

where T is in °K. The mass transfer correlations are valid to within 2.7% and the heat transfer correlations to within 0.8% in comparison to Equations (A-9.1) over the expected temperature range. The Schmidt numbers varied between 1.0 and 1.6, Prandtl numbers equaled 1.0, and the Reynolds number varied between 135 and 155. In developing these expressions, j_H and j_D were considered equal.

Bird, Stewart and Lightfoot present approximate methods to correct the above values for high mass transfer rates (3,4) using either the film theory, penetration theory, or boundary layer theory. The authors correlated correction factors, θ, versus either flux ratios, R, or rate factors, ϕ, using each of the aforementioned

theories. For mixtures, these quantities are defined in Table A-1.

TABLE A-1

Summary of Coordinates for Mass Transfer Correction Plots (4)

Process	Diffusivity Ratio, Λ	Flux Ratio, R	Rate Factor, ϕ	Correction Factor, θ
Heat transfer	N_{Pr}	$R_T = \frac{\Sigma_j N_j C_{gj}}{h}$	$\phi_T = \frac{\Sigma_j N_j C_{gj}}{h^o}$	$\theta_T = \frac{h}{h^o}$
Mass transfer	N_{sci}	$R_{im} = \frac{\Sigma_j N_j}{k_i}$	$\phi_{im} = \frac{\Sigma_j N_j}{k_i'}$	$\theta_{im} = \frac{k_i'}{k_i'^o} = \frac{K_i}{K_i^o}$
		$= \frac{x_{is} - x_{ig}}{N_i/\Sigma_j N_j - x_{is}}$		

In Table A-1, h and k_i' represent heat and mass transfer coefficients, respectively, at significant transfer rates. The following relationship applies for the mass transfer coefficients, k_i' and K_i

$$k_i' = K_i \frac{\rho_g}{M}$$

These correlation charts are given on p. 675 of Bird et al (4).

By utilizing stoichiometry to approximate the ratios of the molar fluxes, N_i/N_j, and the fact that y_{si} is always less than or equal to y_i, it can be shown that,

$$-.06 \leq R_{im} \leq 0$$

for i = 1,2. The R -θ chart in Bird, Stewart, and Lightfoot yields,

$$1.0 \leq \theta_{im} = \frac{k_i'}{k_i'^o} = \frac{K_i}{K_i^o} \leq 1.04 \qquad \text{(A-9.5)}$$

for the conditions of this study regardless of which of the three transfer theories is utilized.

From the definition of ϕ_{im} one obtains,

$$N_i = \frac{k_i'^{o}\phi_{im}}{(\Sigma_j N_j/N_i)} \qquad \text{(A-9.6)}$$

and from the film theory analysis

$$\phi_{im} = \ln(R_{im} + 1) = R_{im} - \frac{1}{2} R_{im}^2$$

$$\cong R_{im} \qquad \text{(A-9.7)}$$

for small values of R_{im}. One can combine Equations (A-9.6) and (A-9.7) to obtain,

$$N_i = \frac{k_i'}{\Sigma_j N_j/N_i} R_{im}$$

$$= \frac{k_i'^{o}(x_{ij}-x_{is})}{1-x_{is}\Sigma_j N_j/N_i} \qquad \text{(A-9.8)}$$

Combining Equation (A-9.2) with the definition of the thermal rate factor, ϕ_T, yields

$$\phi_T = \frac{k_1'^{o}}{h^o} \frac{x_{1s}-x_{1g}}{1-x_{1s}\Sigma_j \frac{N_j}{N_1}} \Sigma_j \frac{N_j}{N_1} C_{gj}$$

which has the following limits,

$$-.09 \leq \phi_T \leq 0.0$$

For this range of conditions, the ϕ-θ chart in Bird, Stewart and Lightfoot (4) predicts

$$1.0 \leq \theta_T = \frac{h^o}{h} \leq 1.07$$

regardless of whether the film, penetration or boundary layer theory is utilized.

Thus the interphase mass transfer rate in the reactor under study will not appreciably affect the coefficients obtained in Equations (A-9.2), (A-9.3) and (A-9.4).

APPENDIX B

ESTIMATION OF PHYSICAL PROPERTIES FOR PELLETS

1. Physical Characterization of Pellets

In order to predict effective diffusivity the following pellet characteristics for permeability must be known:

1) pore size distribution

2) pellet void fraction

3) shapes and path directions of the pores.

Pore size distribution is important since it largely determines the mechanism of mass transport in the pores. Knudsen diffusion predominates in the pores when the mean free path between intermolecular collisions is much greater than the pore diameter, while molecular or "ordinary" diffusion occurs when the pore diameter is much larger than the mean free path. Hence pore size distribution is important since only one of these mechanisms will apply or both. Both may apply in the transition region, which is a range of pore sizes and/or molecular concentrations in which both collisions of molecules with the pore walls and collisions between molecules are equally important. Also, a pore structure involving a system of large macropores, each leading to much smaller micropores, could exhibit ordinary diffusion in the large pores and Knudsen diffusion in the micropores. Such a structure is common when pellets are made by compacting fine porous powders.

The shape and direction of the pores is also important. A pellet with many bottle-neck pores, for example, would be

characterized by an effective radius much smaller than the average pore radius. The path the pores take in the pellet determines the area of intersection at the surface. Also a pore that twists and bends, merges with other pores, becomes a dead-end, or runs into another outside surface causes varying effects on the rate of diffusion.

The void fraction is determined by the shape, path and size of the pores.

The following sections quantitize this qualitative introductory section on the pellet properties.

2. Inert Pellet Carrier and Pellet Dimensions

Alumina is one of the most widely used catalyst supports, because it is structurally stable up to temperatures of 590°C, inert in most reacting environments, and available in many forms with surface areas varying between 1 and 300 m^2/g. Furthermore, an announced industrial fixed bed process (29) and an experimental moving bed process (19) to remove SO_2 from flue gas both utilize inert alumina as the support for copper oxide sorbents. For these reasons, alumina is the chosen as the pellet support for the present investigation.

The metal oxide sorbent could be distributed onto the pores of the carrier by the simple and widely used method described in Satterfield's text (23). It consists of immersing the carrier in an appropriate solution, followed by drying and then possibly reducing or calcining the product. Parsons et al (19) use this

technique with calcination to prepare the metal oxide sorbent and give a detailed discussion. The metal hydroxides are dispersed on the carrier by precipitation, followed by several filterings and washings. The moist product is dried at low temperature for several days and then calcined at relatively low temperatures to avoid sintering. The final product had surface areas of 50 m^2/g and density of 1.6 g/cc.

Catalytic and noncatalytic pellets can be manufactured in various sizes and shapes. In fixed beds the pellets normally are irregular granules, short cylindrical extrudates, cylinders, spheres, and saddles with the mean diameter for these particles varying between $\frac{1}{16}$ " and $\frac{1}{2}$". If the particles are too large, diffusional resistance becomes prohibitive and the interior surface becomes ineffective. Particles smaller than $\frac{1}{16}$ " are usually mechanically weak, difficult to make, and/or responsible for excessive pressure drop. For these reasons spherical pellets in the above diameter range will be investigated. Simple shapes, such as a sphere, are necessary in analytical reactor studies if tractable solutions are to be obtained. Also there exists both theoretical (1) and experimental (17) evidence on the applicability of mathematical models with spherical pellets to systems containing other pellet geometry without loss of accuracy.

3. Pore Size

A study by Weisz and Schwartz (30) on 59 different catalyst pellets resulted in average pore sizes varying between 9 Å and 250 Å.

Thus, a mean pore radius of 100 Å will be selected for this study.

4. Pellet Density

In Weisz and Schwartz' study (30), the density of various alumina pellets varied between 0.9 and 1.6 g/cc. The copper oxide-inert alumina pellets prepared by Parsons et al (19) possessed an average density of 1.6 g/cc. The latter value is considered acceptable for this study.

5. Pellet Heat Capacity

No literature data was available on the heat capacity of alumina pellets. However Perry (20) lists expressions for the molar heat capacities of alumina, cupric oxide and cupric sulfate as a function of temperature. The expressions are based on U.S. Bureau of Mines Bulletin #371 published in 1934. Parsons (19) derives similar expressions for the heat capacities of the oxides and sulfates of copper using more recent data, however, and these will be utilized for Cu_2O, CuO and $CuSO_4$. The expressions are of the form

$$C_{pi} = A_i + B_i T + C_i T^{-2} \quad \text{cal/g-°K}$$

Utilizing a weight fraction averaging technique and the fact that the maximum initial concentration of cuprous oxide is 10%, the solid heat capacity can be expressed as

$$C_s = 0.207 + 8.14.10^{-5} T - 3.13.10^{3} T^{-2} \text{ cal/g-°K}$$

for the copper-alumina pellets. This expression is valid to within ± 2.3% over the expected solids composition range.

6. Effective Pore Diffusivities

Experimental evidence indicates that pores are interstices between ill-fitting crystallites, possessing highly irregular cross-sections and can be considered an array of randomly oriented cylinders with rough walls and many intersections with other pores.

There are three possible mechanisms for mass flow in these pellet pores:

1) Diffusion in the void area due to concentration differences.

2) Forced flow due to pressure differences.

3) Surface migration of adsorbed molecules on the pore wall due to specialized conditions allowing thick, physically adsorbed layers to form.

Flow in pores due to pressure differences can arise for two reasons. A pressure drop can develop when a volume change exists in a gas phase reaction; i.e., the volume contraction due to reaction can cause the interior of a pellet to be at a lower pressure than the surface. Pressure differences for this effect are usually negligible. Secondly, axial pressure drop in the reactor can cause significant pressure gradients across a pellet. This effect does not have to be considered for the present study, because there is negligible pressure drop in the reactor under investigation. Surface migration is rarely significant (23,33), especially at low pressures, and will not be included.

As mentioned in an earlier discussion, mass diffusion in the pores can occur by two mechanisms - ordinary diffusion and Knudsen diffusion. Knudsen diffusion occurs when the gas density is low

and/or when the pores are quite small. The diffusion coefficient per unit cross-sectional area of pore for component i in Knudsen flow is (23,33),

$$D_{iK} = 9.7.10^3 \, r \sqrt{\frac{T}{M_i}} \text{ sq cm/sec}$$

where r is the pore radius in cm, T the temperature in °K, and M_i the molecular weight of the i^{th} component. The diffusivity, D_{iM}, for ordinary diffusion is discussed in Appendix A-6. It occurs when molecule-molecule collisions predominate rather than molecule-wall collisions. To account for flow in the transition region where both diffusion mechanisms are significant, several expressions have been developed (23,25,33). Wheeler's intuitive relation is given by

$$D_i = D_{iM}\left[1 - \exp(-D_{iK}/D_{iM})\right] \qquad \text{(B-6.1)}$$

where D_i is the diffusivity in the transition region. The complexity involved in the application of the other techniques ususally cannot be justified. It should be noted that when ordinary diffusion predominates ($D_{iK} \gg D_{iM}$), the exponential term approaches zero and $D_i \cong D_{iM}$; whereas, when Knudsen flow predominates ($D_{iK} \ll D_{iM}$). Subsequent expansion of Equation (B-6.1) leads to,

$$D_i = D_{iK} - \frac{D_{iK}^2}{2D_{iM}} + \frac{D_{iK}^3}{6D_{iM}^2} - \cdots\cdots\cdots$$

$$\cong D_{iK}$$

Equation (B-6.1) will be utilized to predict pore diffusivity because of its generality and accuracy in all three regions of pore

diffusion.

The effective diffusivity, D_{ie}, will be less than the ideal pore diffusivity, D_i, for two reasons. First, for a given cross-section of porous material, the amount of free space available for diffusion is equal to the volume void fraction ϵ_s, if the pores are randomly oriented. Secondly, a tortuosity factor, χ, must be introduced to account for the winding path, irregular shape, and varying cross-section of the pores. These three factors all tend to reduce the diffusivity. Constrictions offer resistances which cannot be offset by enlargements. Also the devious pore path is longer than a straight line parallel to the mean direction of mass flow. Wheeler develops a theoretical value of 0.5 for χ by assuming pores to be cylinders of a fixed diameter which intersect any plane at an average angle of 45°. Satterfield (23) cites experimental data for all types of pellets in which χ ranged between 0.1 and 1.0.

Based on the foregoing discussion, an expression relating the effective diffusivity to the ideal pore diffusion coefficient is,

$$D_{ie} = \epsilon_s \chi D_i$$

Values for ϵ_s and χ for this study are chosen from the data obtained by Gorring and de Rosset (8) for alumina spheres

$$\epsilon_s = 0.7$$

$$\chi = 0.5$$

These values are used because alumina was chosen as the support, the tortuosity agrees with Wheeler's prediction and the pellets are

spherical.

Calculations with various compositions over the temperature range of 600°K-800°K indicate the following expression is valid for effective diffusivities,

$$D_{1e} = 3.69.10^{-4}\ T^{0.562},\ cm^2/sec$$

$$D_{2e} = 3.71.10^{-4}\ T^{0.509},\ cm^2/sec$$

where T is temperature in degrees Kelvin. These two relations are valid to within 0.7% over the range of conditions (both temperature and composition) expected.

Knudsen diffusion predominates, especially for the sulfur dioxide, as the temperature coefficients are approximately equal to 1/2. The SO_2 should tend towards Knudsen flow before the O_2, since the molecules are larger and are more likely to hit the pore walls.

7. Heats of Reaction

The standard heat of reaction is defined as the heat of reaction at 25°C and 1 atm of pressure. It can be predicted from the standard heats of formation of the products and reactants according to the following expression,

$$\Delta H_r\Big|_{25°C} = \Sigma \left[\Delta H_f \text{ Products}\right]_{25°C} - \Sigma \left[\Delta H_f \text{ Reactants}\right]_{25°C}$$

Using the standard heats of formation pertaining to the copper system (19,32), standard heats of reaction for the two reactions are

$$\Delta H_{rI}\Big|_{25°C} = -74.2 \text{ K cal/g mole}$$

$$\Delta H_{rII}\Big|_{25°C} = -75.94 \text{ K cal/g mole}$$

where ΔH_I, is the heat evolved per mole of oxygen converted in the first (or oxidation) reaction. ΔH_{rII} is the heat evolved per mole of sulfur dioxide converted in the second (or sulfation) reaction.

Heat of reaction is usually strongly dependent on temperature, therefore a relation must be derived to extrapolate these values to values which will apply at the high temperatures expected in this investigation. According to Levenspiel (16), the heat of reaction temperature T_2, ΔH_r^2, is related to a known heat of reaction at temperature T_1, ΔH_r^1, as follows,

$$\Delta H_{rj}^2 = \Delta H_{rj}^1 + \int_{T_1}^{T_2} \nabla C_{pj} dT \qquad j=1,2 \qquad \text{(B-7.1)}$$

where

$$\nabla C_{pj} = \sum_{k=1}^{8} \gamma_{j,k} C_{pi} \qquad j=1,2$$

and the heat capacities of the gases, C_{pi} (i=1,2...5), are given in Hougen et al (11) and those for the solids, C_{pi} (i=6,7,8), are given in Appendix B-5. The $\gamma_{j,k}$ are the stoichiometric coefficients defined in Section 3.1.1. Note that Equation (B-7.1) is not valid if phase changes occur.

Expressions for the heats of reaction at temperature T can be obtained from Equation (B-7.1) as,

$$\Delta H_{rI} = -125576 + 4.74\ T + 5.36.10^{-4}T^2 + 3.34.10^{-7} + 3.02.10^{5}T^{-1} \qquad \text{(B-7.2)}$$

$$\Delta H_{rII} = -136220 + 3.22T - 1.52.10^{-2}T^2 + 4.29.10^{-6}T^3 - 1.51.10^{5}T^{-1} \qquad \text{(B-7.3)}$$

where ΔH_r is in cal/g mole and T is in °K. Equations (B-7.2) and (B-7.3) can be simplified to,

$$\Delta H_{rI} = 5.22T - 135000, \quad \text{cal/g mole } O_2$$

$$\Delta H_{rII} = 7.41T - 138640, \quad \text{cal/g mole } SO_2$$

where T is in °K. These last two correlations match Equations (B-7.2) and (B-7.3) to within $\pm$ 0.02% over the temperature range of interest.

8. Pellet Thermal Conductivity

Satterfield (23) provides an excellent review on the thermal conductivity of porous particles in fixed beds and states that relatively little data has been published in this area. "A priori" prediction of this property can be ruled out, because the data reported thus far yields no significant correlation between conductivity of the pure solid and that of the porous material. Instead, geometrical considerations predominate, and these factors are different to quantitize.

For these reasons, the data reported by Mischke and Smith (23) for alumina pellets with air in the pores will be considered satisfactory. The conductivity is given as $5.2.10^{-4}$ cal/sec-cm-°C at 50°C for a pellet density and pressure equivalent to that being using in the present study.

The conductivity of gases varies approximately linearly with temperature, while the temperature effect of the porous solid is not stated in the literature. Evidence that the porous solid conductivity varies inversely with temperature (18) leads to the

following relation

$$k_s = k_o T^{-1.8}$$

Utilizing this relation and the preceding data point, the thermal conductivity of the porous alumina pellet is given by

$$k_s = 13.5\ T^{-1.8} \quad \text{cal/sec-cm-°C}$$

where T is in °K.

9. Reaction Rate Constants

Parsons et al (19) performed experimental analyses in order to define the reaction kinetics of the sulfation reaction using various metal oxides. Utilizing a TRACOR TGA-3C thermal balance in their isothermal kinetic measurements, data was obtained in the form of solid product (metal sulfate) weight gain as a function of time. This raw data was converted to product conversion, X', versus time by dividing the weight gain by the maximum theoretical weight gain.

For very small diameter particles of 44-88 microns, it was postulated that

$$\frac{dX'}{dt} = k\ (1-X')^n (x_2 P) \qquad \text{(B-9.1)}$$

for the sulfation reaction. If n = 2/3, this expression describes the shrinking core mechanism with chemical reaction rate controlling (31). For n = 1/3, the external film mass transfer controls a shrinking core reaction (31). A more complex expression for pore diffusion controlling the shrinking core was also tested. The data for CuO fit the chemical reaction rate controlling, n = 2/3, expression very well. This could be expected for such small particle

sizes. A value of 40 min^{-1} atm^{-1} for k was determined at 482°C with initial concentrations of 0.034 and .003 mole per cent for the oxygen and sulfur dioxide respectively.

The relation between the Tracor sulfation reaction rate constant, k, and that introduced in Equation (3-33), k_{II}, can be determined by the following arguments.

For chemical reaction controlling, the shrinking core mechanism developed in Section 3.1.5 becomes,

$$\frac{\partial r_c}{\partial t} = \frac{\alpha k_{II}}{\rho_s W_7} y_{s1} y_{s2}\Big|_{r_c} \qquad (3\text{-}33)$$

or

$$\frac{\partial \omega}{\partial t} = \frac{-\alpha k_{II}}{R\rho_s W_7} y_1 y_2 \qquad (B\text{-}9.2)$$

since $y_{si}(z,r,t) = y_i(z,t)$ for $r \geq r_c$ in this case.

Parsons and coworkers define the product conversion, X′, as the weight gain of $CuSO_4$ divided by the theoretical stoichiometric weight gain. Thus the relation between this conversion and the radius of the shrinking core is

$$X' = \frac{\text{weight gain}}{\text{max.wt.gain}} = 1-\omega^3 \qquad (B\text{-}9.3)$$

and therefore

$$\frac{dX'}{dt} = -3\omega^2 \frac{d\omega}{dt} \qquad (B\text{-}9.4)$$

Combining Equations (B-9.1) through (B-9.4) and Equation (3-5) (which relates mole fraction and concentration) and using Parsons' conditions (19) for pellet size, pellet density, temperature, oxygen

concentration and product concentration yields

$$k_{II} = 1.53 \cdot 10^{7} \quad \frac{cm^4}{mole\text{-}sec}$$

at 482°C (775°K).

For an Arrhenius temperature dependency, the rate constant becomes

$$k_j = k_j^o \quad \exp(-\Delta E_j/RT)$$

where T is evaluated in °K. The activation energy for the sulfation reaction is reported (19) as 27 K cal/mole, therefore

$$k_{II} = 8.917.10^{14} \exp(-13500/T) \quad cm^4/sec\text{-}mole\ SO_2$$

for the sulfation reaction.

$$CuO + 1/2\ O_2 + SO_2 \rightarrow CuSO_4$$

Data is not available on the oxidation reaction,

$$Cu_2O + 1/2\ O_2 \rightarrow CuO$$

but if its activation energy is assumed to be one tenth that of the sulfation reaction and if $k_I = k_{II}$ at 402°C, then

$$k_I = 9.15 \cdot 10^{6} \exp(-1350/T),\ cm/sec$$

where T = °K.

BIBLIOGRAPHY FOR APPENDICES

1. Aris, R., Chem. Eng. Sci., 6, 262 (1957).

2. Bar-Ilan, M. and Resnick, W., Ind. Eng. Chem., 49, 313 (1957).

3. Bird, R. B., Stewart, W. E. and Lightfoot, E. N., Notes on Transport Phenomena, pp. 386-430, John Wiley, New York, 1958.

4. Bird, R. B., Stewart, W. E., and Lightfoot, E. N., Transport Phenomena, pp. 411-420, 571, 646, 656-678, John Wiley, New York, 1960.

5. Carberry, J. J., A.I.Ch.E. Journal, 6, 460 (1960).

6. Curtiss, C. F., and Hirschfelder, J. O., J. Chem. Phys., 17, 550 (1949).

7. Gamson, B. W., Thodos, G., and Hougen, O. A., Trans. A.I.Ch.E., 39, 1 (1943).

8. Gorring, R. L. and de Rosset, A. J., J. Catalysis, 3, 341 (1964).

9. Hirschfelder, J. O., Curtiss, C. F., and Bird, R. B., Molecular Theory of Gases and Liquids, pp. 514-610, John Wiley,New York, 1954.

10. Hobson, M. and Thodos, G., Chem. Eng. Prog., 45, 517 (1949).

11. Hougen, O. A., Watson, K. M., and Ragatz, R. A., Chemical Process Principles, Part I, 2nd ed., pp. 255, 311, John Wiley, New York, 1959.

12. Katell, S., Chem. Eng. Prog., 62, 67 (1966).

13. Keenan, J. H., and Keyes, F. G., Thermodynamic Properties of Steam, p. 41, John Wiley, New York, 1936.

14. Keyes, F. G., Trans. A.S.M.E., 74, 1303 (1952).

15. Kramers, H., Chem. Eng. Sci., 8, 45 (1958).

16. Levenspiel, O., Chemical Reaction Engineering, pp. 204 -205, John Wiley, New York, 1962.

17. McCune, L. K., and Wilhelm, R. H., Ind. Eng. Chem., 41, 1124 (1949).

18. Olson, K. E., Ph.D. Thesis, U. of Minn., 1962.

19. Parsons, T., Schroeder, G. D., and Deberry, D., Nat. Air Poll. Control Admin., Contract #PH 86-68-68, July 31, 1969.

20. Perry, J. H., Chemical Engineers' Handbook, 4th ed., pp. 3-71, 3-116 to 121, McGraw-Hill, New York, 1963.

21. Petrovic, L. J., and Thodos, G., Ind. Eng. Chem. Fund., 7, 274 (1968).

22. Reid, R. C., and Sherwood, T. K., The Properties of Gases and Liquids, 2nd ed., pp. 323, 398-399, 421-426, 481-488, 523-543, McGraw-Hill, New York, 1966.

23. Satterfield, C. N., Mass Transfer in Heterogeneous Catalysis, pp. 21-23, 37-67, 169-173, MIT Press, Cambridge, Mass., 1970.

24. Scott, C. D., A.I.Ch.E. Journal, 15, 116 (1969).

25. Scott, D. S., and Dullien, F. H. L., A.I.Ch.E. Journal, 8, 113 (1962).

26. Sladek, K. J., Lowell, P. S., Schwitzegekel, K., and Parsons, T. B., Ind. Eng. Chem. Proc. Des. Dev., 10, 384 (1971).

27. Svehla, R. A., NASA TR R-132, 1962.

28. Thornes, D., and Kramers, H., Chem. Eng. Sci., 8, 271 (1958).

29. Wall, J. D., Hydroc. Proc., 50, 158 (1971).

30. Weisz , P. B., and Schwartz, A. B., J. Catalysis, 1, 399 (1962).

31. Wen, C. Y., Ind. Eng. Chem., 60, 34 (1968).

32. Wheast, R. C., ed., Handbook of Chemistry and Physics, pp. D-38 to D-49, Chemical Rubber Co., Cleveland, Ohio, 1968.

33. Wheeler, A., Catalysis, Vol. II, pp. 105-131, Reinhold Publ. Corp., New York, 1955.

34. Wilke, C. R., J. Chem. Phys., 18, 517 (1950).

35. Wilke, C. R., and Hougen, O. A., Trans. A.I.Ch.E., 41, 445 (1945).

APPENDIX C

PREDICTOR CORRECTOR ALGORITHM IN FORTRAN IV

```
C
C
C*************************************************************************
C
C    *****  PREDICTOR-CORRECTOR PDE SOLUTION ALGORITHM  *****
C
C
      DIMENSION XX(10,150),YY(10,150),Y(4,101,6),KD(10)
      DIMENSION ABC(6),WXY(6)
      DOUBLE PRECISION U
      DOUBLE PRECISION ER
      DOUBLE PRECISION DZ,DT
      DOUBLE PRECISION HOLD
      DOUBLE PRECISION SAV(6)
      COMMON U(42,3,6),N,I,J
      COMMON  /MO/ ER(6),KOUNT,IPC
      COMMON /OM/ JJ
      COMMON  /MSPC/ DZ,DT,NN,NN1
      COMMON  /MP/ HOLD(6)
      COMMON /MFPP/ G(50),Q(20),GG(25)
      DOUBLE PRECISION DABS
      DIMENSION TITLE(20)
      DOUBLE PRECISION AAA(6)
      DO1 I=1,20
    1 Q(I)=0.0E00
      READ(5,10) TITLE
   10 FORMAT(20A4)
      WRITE(6,20) TITLE
   20 FORMAT(10X,'*****',5X,20A4,5X,'*****'//)
C
C       IPC= PRINT CONTROL PARAMETER     PC=0, SENSE SWITCH CONTROLS PRINTING
C                                        PC .GT. 0, PRINT EVERY PC GRID POINTS
C                                        PC .LT. 0, NO INDIVIDUAL PRINTING
C       IR = NUMBER OF DISTANCE STEPS
C       N = NUMBER OF PDE'S
```

```
C       NN = NUMBER OF PDE'S WITH PARTIAL WRT DISTANCE CTX
C
C       FOR MODEL 1 -
C         U(I,J,1)=PSI(II,JJ),  U(I,J,2)=Y(II,JJ),  U(I,J,3)=S(II,JJ),
C         U(I,J,4)=PHI(II,JJ),  U(I,J,5)=W(II,JJ),  U(I,J,6)=MU(II,JJ)
C              WHERE  II=I-1  AND  JJ=J-1
C         I=DISTANCE CTX
C         J=TIME-DIST CTX
C
C
C       CONSTANTS
C
      READ(5,100) G,GG
  100 FORMAT(8E10.3)
      G(15)=G(14)*G(32)/G(31)
      G(16)=G(27)/G(28)
      G(18)=G(18)*G(50)/28.6
      G(19)=G(19)*G(50)/28.6
      G(39)=G(29)/G(28)*G(32)
      G(40)=G(26)/G(27)*G(31)
      IPC=G(41)+0.1
      IR=G(35)+0.1
      IR1=IR+1
      N=G(37)+0.1
      NN=G(38)+0.1
      NN1=NN+1.1
      NM1=N-1
      ABC(1)=G(42)
      WXY(1)=G(43)
      DO102 I=2,NN1
      ABC(I)=0.0E00
  102 WXY(I)=0.2E00
      ABC(N)=G(44)
      WXY(N)=G(45)
      ABC(NM1)=G(46)
```

```
      WXY(NM1)= G(47)
      DT=G(34)
      TOL=G(17)
      KOUNT=0
      DZ=1.0D00/IR
      DO105 I=1,N
  105 AAA(I)=675.0/G(22)
      CALL PPROP(AAA)
      G(18)=G(18)*G(4)/G(50)
      G(19)=G(19)*G(4)/G(50)
      Q(20)=(1.0-G(2))*G(5)*G(15)*G(20)/G(1)*G(28)*G(30)/G(33)/G(32)/G(2
     19)
      ITIM=G(36)*Q(19)/DT+0.01
      IT1=ITIM+1.1
      NTP=IT1/102
      NTP=NTP+1.1
      NTP1=NTP+1
      NTP2=NTP1+NTP
      ND=2.1
      XX(1.1)=0.0
      YY(1.1)=1.0
      KET=1
      JJMIN=Q(19)*60.0/DT
      JTEST=JJMIN
C
C       END OF CONSTANTS
C
      WRITE(6,110) N,IPC,IR,ITIM,NTP1,NTP2
      WRITE(6,120)
      WRITE(6,130) G,GG,Q,DZ,DT,TOL
  110 FORMAT(/10X,'NO. OF PDE = ',I2,10X,'PRINT CONTROL = ',I4,/10X,
     1 'LENGTH STEPS = ',I3,10X,'TIME STEPS = ',I4,
     210X, 'STORE AT TIME STEPS 1,',I2,',',I2,',ETC.'//)
  120 FORMAT(10X,'SYSTEM PARAMETERS EVALUATED AT 675 DEGREES KELVIN'/)
  130 FORMAT(9(2X,E11.4)/)
```

```
      DO135K=1,N
      ER(K)=0.0D00
      DO135I=1,IR1
      DO135J=1,3
  135 U(I,J,K)=0.0D00
C
C       BOUNDARY AND INITIAL CONDITIONS
C          THIS SECTION MAY NEED TO BE CHANGED FOR DIFFERENT PROBLEMS
C
      DO200 K=1,NN
      DO200 J=1,3
  200 U(1,J,K)=1.0D00
      DO300 I=1,IR1
      U(I,1,N)=G(21)/G(22)
      DO300 K=NN1,NM1
  300 U(I,1,K)=1.0D00
C
C       END OF BC'S
C
      WRITE(6,310)
  310 FORMAT(1H1)
      WRITE(6,320)
  320 FORMAT(2X,'I',2X,'J',4X,'PSI',15X,'Y',16X,'S',16X,'PHI',15X,'W',15
     1X,'MU'/)
      K=1
      WRITE(6,350) K
  350 FORMAT(/ 1X,'*** STEP',I2/)
C
C *****  STEP 1  *****
C       COMPUTE PSI(1,0),Y(1,0) AND S(1,0)
C
      I=2
      J=1
      JJ=1
      CALL START(1)
```

```
      CALL OUTPUT
C
C      COMPUTE PHI(0,1),W(0,1) AND MU(0,1)
C
      I=1
      J=2
      JJ=2
      CALL START(2)
      CALL OUTPUT
      K=2
      WRITE(6,350) K
C
C *****  STEP 2  *****
C      COMPUTE PSI(I,0),Y(I,0,) AND S(I,0)  I.GT.1
C
      J=1
      JJ=1
      DO500 I=3,IR1
      L=1
      CALL PRED(L)
      CALL CORR(L)
  400 KEY=0
      DO410 K=1,NN
  410 SAV(K)=U(I,J,K)
      CALL COR(L)
      DO490 K=1,NN
      TEST=DABS((U(I,J,K)-SAV(K))/SAV(K))
      IF(TEST.GE.TOL) KEY=1
  490 ER(K)=(HOLD(K)-U(I,J,K))/5.0
      IF(KEY.GT.0) GOTO400
      CALL OUTPUT
  500 CONTINUE
      K=3
      WRITE(6,350) K
C
```

```
C *****  STEP 3  *****
C       COMPUTE PSI,Y,S,PHI,W AND MU AT (1,1)
C
        I=2
        J=2
        JJ=2
        DO780 M=NN1,N
  780 U(I,J,M)=U(I,J-1,M)
        CALL START(1)
        CALL START(2)
        DO790 L=1,N
  790 HOLD(L)=U(I,J,L)
        CALL CORR(1)
        CALL CORR(2)
  800 KEY=0
        DO810 L=1,N
  810 SAV(L)=U(I,J,L)
        CALL COR(1)
        CALL COR(2)
        DO815 L=1,N
        TEST=DABS((U(I,J,L)-SAV(L))/SAV(L))
  815 IF(TEST.GE.TOL) KEY=1
        IF(KEY.GT.0) GOTO800
        DO830  L=1,N
  830 ER(L)=(HOLD(L)-U(I,J,L))/5.0
        CALL OUTPUT
        K=4
        WRITE(6,350) K
C
C *****  STEP 4  *****
C       COMPUTE PSI,Y,S,PHI,W AND MU AT (I,1)  I.GT.1
C
        DO1000 I=3,IR1
        CALL PRED(1)
        CALL START(2)
```

```
      DO860 M=NN1,N
  860 HOLD(M)=U(I,J,M)
      CALL CORR(1)
      CALL CORR(2)
  900 KEY=0
      DO910 L=1,N
  910 SAV(L)=U(I,J,L)
      CALL COR(1)
      CALL COR(2)
      DO970 L=1,N
      TEST=DABS((U(I,J,L)-SAV(L))/SAV(L))
  970 IF(TEST.GE.TOL) KEY=1
      IF(KEY.GT.0) GOTO900
      DO990  L=1,N
  990 ER(L)=(HOLD(L)-U(I,J,L))/5.0
      CALL OUTPUT
 1000 CONTINUE
      JJ=2
C
C       COMPUTE AVERAGE BED EFFICIENCY VERSUS TIME
C
      IF(JJ.LT.JTEST) GOTO1080
      KET=KET+1
      JTEST=JTEST+JJMIN
      XX(1,KET)=(JJ-1)*DT/Q(19)/60.0
      K=N-1
      YY(1,KET)=(1.0-U(1,J ,K)**3)/2.0
      DO1050 I=2,IR
 1050 YY(1,KET) =YY(1,KET)+(1.0-U(I,J ,K)**3)
      YY(1,KET)=(YY(1,KET)+(1.0-U(IR1,J ,K)**3)/2.0)*Q(20)/XX(1,KET)*DZ
     1/60.0
 1080 CONTINUE
C
C       END OF BED EFFICIENCY CALCULATIONS
C
```

```
C
C       STORE DEPENDENT VARIABLES  FOR PROFILE INFORMATION
C
      NT=0
      NTPT=1
      DO1110 JJ=1,2
      IF(JJ.LT.NTPT) GOTO1110
      NTPT=NTPT+NTP
      NT=NT+1
      KT=0
      DO1100 II=1,43,14
      KT=KT+1
      I=II-1
      IF(II.EQ.1)I=1
      DO1100 M=1,N
      Y(KT,JJ,M)=U(I,JJ,M)
 1100 CONTINUE
 1110 CONTINUE
C
C       END OF STORAGE
C
C
C
C ***********  START OF THETA(TIME) LOOPS  ****************************************
C
C
      J=3
      DO2500JJ=3,IT1
C
C ****  TIME STEP 1  ****
C       COMPUTE PHI(0,J), W(0,J) AND MU(0,J)  J.GT.1
C
      DO1200 L=1,NN
 1200 ER(L)=0.0D00
      I=1
```

```
      CALL PRED(2)
      CALL CORR(2)
 1550 KEY=0
      DO1600 L=NN1,N
 1600 SAV(L)=U(I,J,L)
      CALL COR(2)
      DO1650 L=NN1,N
      TEST=DABS((U(I,J,L)-SAV(L))/SAV(L))
      IF(TEST.GE.TOL) KEY=1
 1650 ER(L)=(HOLD(L)-U(I,J,L))/5.0
      IF(KEY.GT.0)GOTO1550
      CALL OUTPUT
C
C ****  TIME STEP 2  ****
C       COMPUTE PSI,Y,S,PHI,W AND MU AT (1,J)  J.GT.1
C
      I=2
      CALL PRED(2)
      CALL START(1)
      DO1690 K=1,NN
 1690 HOLD(K)=U(I,J,K)
      CALL CORR(1)
      CALL CORR(2)
 1700 KEY=0
      DO1710 L=1,N
 1710 SAV(L)=U(I,J,L)
      DO1720 L=1,ND
 1720 CALL COR(L)
      DO1770 L=1,N
      TEST=DABS((U(I,J,L)-SAV(L))/SAV(L))
 1770 IF(TEST.GE.TOL) KEY=1
      IF(KEY.GT.0) GOTO1700
      DO1800 L=1,N
 1800 ER(L)=(HOLD(L)-U(I,J,L))/5.0
      CALL OUTPUT
```

```
C
C ****  TIME STEP 3  ****
C       COMPUTE PSI.Y.S.PHI.W AND MU AT (I.J)  I.J BOTH .GT. 1
C
       DO2000 I=3.IR1
       DO1810 L=1.ND
 1810  CALL PRED(L)
       DO1820 L=1.ND
 1820  CALL CORR(L)
 1825  KEY=0
       DO1827 L=1.N
 1827  SAV(L)=U(I.J.L)
       DO1830 L=1.ND
 1830  CALL COR(L)
       DO1850 L=1.N
       TEST=DABS((U(I.J.L)-SAV(L))/SAV(L))
 1850  IF(TEST.GE.TOL) KEY=1
       IF(KEY.GT.0) GOTO1825
       DO1900 M=1.N
 1900  ER(M)=(HOLD(M)-U(I.J.M))/5.0
       CALL OUTPUT
 2000  CONTINUE
C
C       COMPUTE AVERAGE BED EFFICIENCY VERSUS TIME
C
       IF(JJ.LT.JTEST) GOTO2080
       KET=KET+1
       JTEST=JTEST+JJMIN
       XX(1.KET)=(JJ-1)*DT/Q(19)/60.0
       K=N-1
       YY(1.KET)=(1.0-U(1.J .K)**3)/2.0
       DO2050 I=2.IR
 2050  YY(1.KET) =YY(1.KET)+(1.0-U(I.J .K)**3)
       YY(1.KET)=(YY(1.KET)+(1.0-U(IR1.J .K)**3)/2.0)*Q(20)/XX(1.KET)*DZ
      1/60.0
```

```
 2080 CONTINUE
C
C       END OF BED EFFICIENCY CALCULATIONS
C
C
C       STORE DEPENDENT VARIABLES  FOR PROFILE INFORMATION
C
       IF(JJ.LT.NTPT) GOTO2110
       NTPT=NTPT+NTP
       NT=NT+1
       KT=0
       DO2100 II=1,43,14
       KT=KT+1
       I=II-1
       IF(II.EQ.1)I=1
       DO2100 M=1,N
       Y(KT,NT,M)=U(I,J,M)
 2100 CONTINUE
 2110 CONTINUE
C
C       END OF STORAGE
C
       DO2400 JK=1,2
       JL=JK+1
       DO2400 K=1,N
       DO2400 I=1,IR1
 2400 U(I,JK,K)=U(I,JL,K)
       DO2450 K=1,N
       DO2450 I=1,IR1
 2450 U(I,J,K)=0.0D00
       DO2500 K=1,NN
       U(1,J,K)=1.0D00
 2500 CONTINUE
C
C
```

```
C ************  END OF THETA(TIME) LOOPS  ****************************************
C
C
C
C       LIST DEPENDENT VARIABLE PROFILES
C
      WRITE(6,2550) (YY(1,JJ),XX(1,JJ),JJ=1,KET)
 2550 FORMAT((10X,2( 3X,D15.7)/))
      DO2580 KT=1,4
      DO2580 JJ=1,NT
 2580 WRITE(6,2600) KT,JJ,(Y(KT,JJ,M),M=1,N)
 2600 FORMAT(1X,I1,1X,I3,6(5X,E13.5)/)
C
C       PLOT BED EFFICIENCY
C
      KD(1)=KET
      ABCD=0.0
      WXYZ=0.20
      LAST=0
      CALL MPLOT(XX,YY,KD,1,1,1,0,LAST,ABCD,WXYZ)
      NPLT=4
      K=1
      RATIO=1.0
      DO2700 I=1,10
 2700 KD(I)=NT
      DO3000 KT=1,4
      DO3000 JJ=1,NT
 3000 XX(KT,JJ)=(JJ-1)*DT*NTP
C
C       PLOT N DEPENDENT VARIABLES
C
      DO4000 M=1,N
      IF(M.EQ.N) LAST=1
      DO3800 KT=1,4
      DO3800 JJ=1,NT
```

```
      IF(M.EQ.1.OR.M.EQ.N) Y(KT,JJ,M)=Y(KT,JJ,M)*G(22)-273.0
 3800 YY(KT,JJ)=Y(KT,JJ,M)
      ABCD=ABC(M)
      WXYZ=WXY(M)
C
C       PLOT NPLT CURVES FOR EACH DEPENDENT VARIABLE
C
      CALL MPLOT(XX,YY,KD,NPLT,K,RATIO,LAST,ABCD,WXYZ)
 4000 CONTINUE
      STOP
      END
```

```
      SUBROUTINE OUTPUT
      INTEGER SENSE
      DOUBLE PRECISION U
      DOUBLE PRECISION ER
      COMMON U(42,3,6),N,I,J
      COMMON  /MO/ ER(6),KOUNT,IPC
      COMMON /OM/ JJ
      DATA SENSE/0/
      IF(IPC) 2200,2000,2100
2000  CONTINUE
      IF(SENSE.EQ.1) WRITE(6,2050)I,JJ,(U(I,J,K),ER(K),K=1,N)
2050  FORMAT(2(1X,I3),6(1X,F6.4,1X,D9.2))
      RETURN
2100  KOUNT=KOUNT+1
      IF(KOUNT.LT.IPC) GOTO2200
      WRITE(6,2050)I,JJ,(U(I,J,K),ER(K),K=1,N)
      KOUNT=0
2200  RETURN
      END
```

```
      SUBROUTINE START(L)
C
C       STARTER FORMULAS
C
      DOUBLE PRECISION U
      DOUBLE PRECISION DZ,DT
      DOUBLE PRECISION S1,A(6),B(6)
      COMMON U(42,3,6),N,I,J
      COMMON  /MSPC/ DZ,DT,NN,NN1
      GOTO(200,400) ,L
C
C       INTEGRATE IN DISTANCE DIRECTION (LAMBDA CHARACTERISTIC)
C
  200 II=I-1
      DO210 K=1,N
  210 A(K)=U(II,J,K)
      DO220 K=NN1,N
  220 B(K)=(U(II,J,K)+U(I,J,K))/2.0
      DO230 K=1,NN
      CALL FUN(A,S1,K)
  230 B(K)=U(II,J,K)+DZ*S1/2.0
      DO250 K=1,NN
      CALL FUN(B,S1,K)
  250 U(I,J,K)=U(II,J,K)+DZ*S1
      RETURN
C
C       INTEGRATE ALONG THETA CHARACTERISTIC
C
  400 JJ=J-1
      DO410 K=1,N
  410 A(K)=U(I,JJ,K)
      DO420 K=1,NN
  420 B(K)=(U(I,JJ,K)+U(I,J,K))/2.0
      DO430 K=NN1,N
      CALL FUN(A,S1,K)
```

```
430 B(K)=U(I,JJ,K)+DT*S1/2.0
    DO450 K=NN1,N
    CALL FUN(B,S1,K)
450 U(I,J,K)=U(I,JJ,K)+DT*S1
    RETURN
    END
```

```
      SUBROUTINE  PRED(L)
C
C       PREDICTOR FORMULAS
C
      DOUBLE PRECISION U
      DOUBLE PRECISION DZ,DT
      DOUBLE PRECISION HOLD
      DOUBLE PRECISION A(6),F
      COMMON U(42,3,6),N,I,J
      COMMON  /MSPC/ DZ,DT,NN,NN1
      COMMON  /MP/ HOLD(6)
      GOTO (200,400),L
C
C       INTEGRATE IN DISTANCE DIRECTION (LAMBDA CHARACTERISTIC)
C
  200 DO210 K=1,N
  210 A(K)=U(I-1,J,K)
      DO250 K=1,NN
      CALL FUN(A,F,K)
      U(I,J,K)=U(I-2,J,K)+2.0*DZ*F
  250 HOLD(K)=U(I,J,K)
      RETURN
C
C       INTEGRATE ALONG THETA CHARACTERISTIC
C
  400 DO410 K=1,N
  410 A(K)=U(I,J-1,K)
      DO450 K=NN1,N
      CALL FUN(A,F,K)
      U(I,J,K)=U(I,J-2,K)+2.0*DT*F
  450 HOLD(K)=U(I,J,K)
      RETURN
      END
```

```
      SUBROUTINE  CORR(L)
C
C       CORRECTOR FORMULAS
C
      DOUBLE PRECISION U
      DOUBLE PRECISION DZ,DT
      DOUBLE PRECISION F1,S(6),A(6)
      COMMON U(42,3,6),N,I,J
      COMMON  /MSPC/ DZ,DT,NN,NN1
      GOTO(200,400),L
      ENTRY COR(L)
      GOTO(250,450),L
C
C       INTEGRATE IN DISTANCE DIRECTION (LAMBDA CHARACTERISTIC)
C
  200 II=I-1
      DO210 K=1,N
  210 A(K)=U(II,J,K)
      DO220 K=1,NN
      CALL FUN(A,F1,K)
  220 S(K)=F1
  250 DO260 K=1,N
  260 A(K)=U(I,J,K)
      DO280 K=1,NN
      CALL FUN(A,F1,K)
  280 U(I,J,K)=U(II,J,K)+DZ*(S(K)+F1)/2.0
      RETURN
C
C       INTEGRATE ALONG THETA CHARACTERISTIC
C
  400 JJ=J-1
      DO410 K=1,N
  410 A(K)=U(I,JJ,K)
      DO420 K=NN1,N
      CALL FUN(A,F1,K)
```

```
420 S(K)=F1
450 DO460 K=1,N
460 A(K)=U(I,J,K)
    DO480   K=NN1,N
    CALL  FUN(A,F1,K)
480 U(I,J,K)=U(I,JJ,K)+DT*(S(K)+F1)/2.0
    RETURN
    END
```

```
      SUBROUTINE FUN(A,F,L)
C
C
C      EVALUATE RHS OF PARTIAL DIFFERENTIAL EQUATIONS
C
C
      DOUBLE PRECISION DSQRT
      DOUBLE PRECISION U
      DOUBLE PRECISION A(6),B(14) ,YRC,SRC,F
      COMMON U(42,3,6),N,I,J
      COMMON /MFPP/ G(50),Q(20),GG(25)
      CALL PPROP(A)
      B(1)=A(5)+Q(9)*A(5)**2
      B(2)=A(5)+Q(10)*A(5)**2
      B(3)=A(4)+Q(9)*A(4)**2+Q(11)
      B(4)=A(4)*(1.0-(A(4)/A(5)))+Q(11)
      B(5)=B(2)*B(3)
      B(6)=B(3)/Q(12)+B(4)*(Q(14)*B(1)-A(2)*B(2))
      B(7)=-B(4)/Q(12)*A(2)
      SRC=B(6)**2-4.0*B(5)*B(7)
      IF(SRC.GE.0.0D00) GOTO50
      WRITE(6,9998) SRC
 9998 FORMAT(/10X,'COMPLEX NUMBERS',5X,D15.7,2X,'=B2-4AC'//)
   50 YRC=-B(6)+DSQRT(SRC)
      YRC=YRC/2.0/B(5)
      SRC=-B(6)-DSQRT(SRC)
      SRC=SRC/2.0/B(5)
      KEY=0
      IF(YRC.GE.0.0D00.AND.YRC.LE.1.0D00) KEY=1
      IF(SRC.GE.0.0D00.AND.SRC.LE.1.0D00) KEY=KEY+2
      IF(KEY.EQ.2) YRC=SRC
      B(8)=1.0+Q(12)*YRC*B(2)
      SRC=A(3)/B(8)
      B(9)=A(4)-A(4)**2+Q(11)
      B(10)=B(9)+Q(13)*SRC*B(4)*(A(5)-A(5)**2)
```

```
      B(11)=B(3)+Q(13)*SRC*B(1)*B(4)
      B(12)=A(6)/A(1)
      B(13)=B(8)-(1.0+Q(12)*YRC*(A(5)-A(5)**2))*B(12)
      B(14)=A(2)*(B(11)-B(10)*B(12))/B(11)
      GOTO (100,200,300,400,500,600),L
  100 F=-Q(1)*(A(1)-A(6))
      RETURN
  200 F=-Q(2)*A(2)*B(14)
      RETURN
  300 F=-Q(3)*A(3)*B(13)/B(8)
      RETURN
  400 F=-Q(4)*A(2)/B(11)
      RETURN
  500 F=-Q(5)*A(3)*YRC/B(8)
      RETURN
  600 F=-Q(6)*(       (A(6)-A(1))+Q(7)*B(14)+Q(8)*A(3)*B(13)/B(8))
      RETURN
      END
```

```
      SUBROUTINE PPROP(A)
C
C      EVALUATE PHYSICAL PROPERTIES AS A FUNCTION OF TEMPERATURE
C
      DOUBLE PRECISION U
      COMMON U(42,3,6),N,I,J
      DOUBLE PRECISION A(6)
      COMMON /MFPP/ G(50),Q(20),GG(25)
      A6=A(N) *G(22)
      A1=A(1)*G(22)
      IF(N.EQ.4) A1=A6
      G(4)=GG(1)/A1
      G(6)=GG(2)+GG(3)*A1+GG(4)*A1**2
      G(7)=GG(5)+GG(6)*A6+GG(7)/A6**2
      G(8)=GG(8)*EXP(GG(9)/A6)
      G(9)=GG(10)*EXP(GG(11)/A6)
      G(10)=GG(12)*A6**GG(13)
      G(11)=GG(14)*A6**GG(15)
      G(12)=GG(16)*A6**GG(17)
      G(13)=GG(18)*A6**GG(19)
      G(23)=GG(20)*A6+GG(21)
      G(24)=GG(22)*A6+GG(23)
      G(25)=GG(24)*A6**GG(25)
      Q(1)=3.0*(1.0-G(2))*G(20)*G(25)/G(1)/G(3)/G(6)
      Q(2)=3.0*(1.0-G(2))*G(4)*G(10)*G(20)/G(1)/G(3)
      Q(3)=3.0*(1.0-G(2))*G(4)*G(11)*G(20)/G(1)/G(3)
      Q(4)=G(2)*G(4)*G(40)*G(12)*G(18)*G(20)/G(1)/G(3)/G(3)/G(5)/G(14)
      Q(5)=G(2)*G(4)*G(39)*G(9) *G(18)*G(19)*G(20)/G(1)/G(3)/G(5)/G(15)
      Q(6)=3.0*G(2)*G(4)*G(20)/G(1)/G(3)/G(5)/G(7)*G(25)
      Q(7)=G(10)*G(18)*G(23)/G(22)/G(25)
      Q(8)=G(11)*G(19)*(G(24)-G(16)*G(23))/G(22)/G(25)
      Q(9)=G(12)/G(3)/G(10)-1.0
      Q(10)=G(13)/G(3)/G(11)-1.0
      Q(11)=G(12)/G(3)/G(8)
      Q(12)=G(3)*G(9)*G(18)/G(13)
```

```
Q(13)=G(3)*G(9)*G(16)*G(19)/G(12)
Q(14)=Q(13)/Q(12)
Q(19)=G(1)/G(2)/G(4)/G(20)
RETURN
END
```

```
      SUBROUTINE MPLOT (XX,YY,KD,NPLT,K,RATIO,LAST,ABCD,WXYZ)
C     K=1 CARTESIAN PLOT OF Y VS X
C     KX=NUMBER OF SETS OF X-Y PAIRS TO BE PLOTTED
      INTEGER KD(10),L(10)
      DIMENSION X(250),Y(250),BUFFER(10000)
      DIMENSION HEAD(20),TITLE(20),AB(20),ORD(20)
      DIMENSION XX(10,150),YY(10,150)
      DIMENSION LGND(20),LEGEND(2)
      DIMENSION ABC(6),WXY(6)
      COMMON U(42,3,6),N,I,J
      DATA BLANK/'    '/
      DATA L(1),L(2),L(3),L(4),L(5),L(6),L(7),L(8),L(9),L(10)/
     10,1,2,3,4,5,6,10,11,12/
      DATA HGL/0,10/
C     PREPARE GRAPH FOR NPLT(LE 10) CURVES
C     DETERMINE YLGH - LENGTH OF Y-AXIS IN INCHES
      IF(NPLT.LE.2)GOTO1000
      IF(NPLT.LE.4)GOTO1001
      IF(NPLT.LE.6)GOTO1002
      IF(NPLT.LE.8)GOTO1003
      YLGH=6.5
      GOTO1004
1000  YLGH=7.3
      GOTO1004
1001  YLGH=7.1
      GOTO1004
1002  YLGH=6.9
      GOTO1004
1003  YLGH=6.7
C     READ HEAD,TITLE,AB,ORD, & LEGEND
C     EACH LGND MUST HAVE LE 26 CHARACTERS
1004  YLGH=YLGH-.4
      READ100,(HEAD(I),I=1,20)
      READ100,(TITLE(I),I=1,20)
      READ100,(AB(I),I=1,20)
```

```
      READ100,(ORD(I),I=1,20)
100   FORMAT(20A4)
102   FORMAT(1X,20A4)
      IH=0
      IT=0
      IX=0
      IY=0
      DO1008I=1,20
      IF(AB(I).EQ.BLANK)IX=IX+1
      IF(ORD(I).EQ.BLANK)IY=IY+1
      IF(HEAD(I).EQ.BLANK)IH=IH+1
      IF(TITLE(I).EQ.BLANK)IT=IT+1
1008  CONTINUE
      IX=-(20-IX)*4
      IY=(20-IY)*4
      IH=(20-IH)*4
      IT=(20-IT)*4
      H=IH
      T=IT
      HGH=5.6/(H+1.E-07)
      HGT=5.6/(T+1.E-07)
      IF(HGH.GT.0.20)HGH=0.20
      IF(HGT.GT.0.20)HGT=0.20
C     FIND LARGEST & SMALLEST X & Y FOR SCALING LATER
C     ALL PLOTS TO SAME SCALE
1022  BIGY=YY(1,1)
      BIGX=XX(1,1)
      SMLX=XX(1,1)
      SMLY=YY(1,1)
      DO1009I=1,NPLT
      MAX=KD(I)
      DO1009J=1,MAX
      IF(YY(I,J).LT.SMLY)SMLY=YY(I,J)
      IF(YY(I,J).GT.BIGY)BIGY=YY(I,J)
      IF(XX(I,J).LT.SMLX)SMLX=XX(I,J)
```

```
      IF(XX(I,J).GT.BIGX)BIGX=XX(I,J)
1009  CONTINUE
C     DRAW HEAD,TITLE,LEGEND, & BOX PLOT
      DATA LEGEND/'LEGE','ND  '/
      CALL PLOTS(BUFFER,10000)
      IF(RATIO,NE,1,)CALL FACTOR(RATIO)
      CALL PLOT(10.,0.,-3)
      CALL PLOT(6.0,0.,2)
      CALL PLOT(6.0,9.0,2)
      CALL PLOT(0.,9.,2)
      CALL PLOT(0.,0.,2)
      CALL PLOT(0.,8.3,3)
      CALL PLOT(6.,8.3,2)
      DUM=IH*HGH
      XSH=(5.6-DUM)/2.+.2
      DUM=IT*HGT
      XST=(5.6-DUM)/2.+.2
      IF(IH.NE.0)CALL SYMBOL(XSH,8.7,HGH,HEAD,0.,IH)
      IF(IT.NE.0)CALL SYMBOL(XST,8.4,HGT,TITLE,0.,IT)
      CALL SYMBOL(.2,8.1,HGL,LEGEND,0.,8)
      CALL PLOT(0.,8.05,3)
      CALL PLOT(1.,8.05,2)
      KK=1
      YBGN=8.1
      DO1015I=1,NPLT
      GOTO(1010,1011),KK
1010  YBGN=YBGN-0.20
      LS=L(I)
      CALL SYMBOL(.10,YBGN,HGL,LS,0.,-1)
      READ100,(LGND(LL),LL=1,20)
      IL=0
      DO1012LL=1,20
1012  IF(LGND(LL).EQ.BLANK)IL=IL+1
      IL=(20-IL)*4
      CALL SYMBOL(.4,YBGN,HGL,LGND,0.,IL)
```

```
      PRINT102,(LGND(LL),LL=1,20)
      KK=2
      GOTO1015
1011  LS=L(I)
      CALL SYMBOL(3.1,YBGN,HGL,LS,0.,-1)
      READ100,(LGND(LL),LL=1,20)
      IL=0
      DO1013LL=1,20
1013  IF(LGND(LL).EQ.BLANK)IL=IL+1
      IL=(20-IL)*4
      CALL SYMBOL(3.4,YBGN,HGL,LGND,0.,IL)
      PRINT102,(LGND(LL),LL=1,20)
      KK=1
1015  CONTINUE
      YBGN=YBGN-0.1
      CALL PLOT(0.,YBGN,3)
      CALL PLOT(6.,YBGN,2)
      CALL PLOT(-1.5,0.,3)
      CALL PLOT(-1.5,1.,2)
      CALL PLOT(-1.5,9.,3)
      CALL PLOT(-1.5,10.,2)
      CALL PLOT(7.,0.,3)
      CALL PLOT(7.,1.,2)
      CALL PLOT(7.,9.,3)
      CALL PLOT(7.,10.,2)
C     PLOT & SCALE FOR CARTESIAN PLOT
1100  CALL PLOT(.5,.5,-3)
      DO1103I=1,NPLT
      TX1=XX(I,1)
      TX2=XX(I,KD(I))
      TY1=YY(I,1)
      TY2=YY(I,KD(I))
      XX(I,1)=SMLX
      XX(I,KD(I))=BIGX
      YY(I,1)=SMLY
```

```
      YY(I,KD(I))=BIGY
      MAX=KD(I)
      DO1101J=1,MAX
      Y(J)=YY(I,J)
1101  X(J)=XX(I,J)
      CALL SCALE(X,5,1,MAX,1)
      Y(MAX+1)=ABCD
      Y(MAX+2)=WXYZ
      X(MAX+1)=0.0E00
      MAX2=MAX+2
      PRINT2000,KD(I),YLGH
2000  FORMAT(1X,I3,2X,F6.2)
      X(1)=TX1
      X(KD(I))=TX2
      Y(1)=TY1
      Y(KD(I))=TY2
      XX(I,1)=TX1
      XX(I,KD(I))=TX2
      YY(I,1)=TY1
      YY(I,KD(I))=TY2
      LS=L(I)
      WRITE(6,9000) (X(J),Y(J),J=1,MAX)
      WRITE(6,9000) (X(J),Y(J),J=MAX,MAX2)
 9000 FORMAT(2(8X,E13.6))
1103  CALL  LINE(X,Y,MAX,1,10,LS)
      CALL PLOT(-.5,-.5,-3)
      MAX=KD(NPLT)
      CALL AXIS(.5,.5,ORD,IY,YLGH,90.,Y(MAX+1),Y(MAX+2))
      CALL AXIS(.5,.5,AB,IX,5.1,0.,X(MAX+1),X(MAX+2))
      CALL PLOT(0.,0.,-3)
      IF(LAST.EQ.1)CALL PLOT(0.,0.,999)
      RETURN
      END
```

```
 MODEL 1 CTX PDE'S BY PREDICTOR-CORRECTOR
 3.530E-02 4.000E-01 3.175E-01 5.200E-04 1.600E-00
                                                    1.00CE-01
 1.000E-05 3.040E-02 1.100E-03 6.100E+01 6.150E+02 6.150E+02
           1.000E+00 5.000E-01 1.000E-00 1.000E-00 6.400E+01 1.431E+02 1.595E+02
 2.500E-03 1.000E+01 4.100E+01 1.100E+03 6.000E-00 3.000E-00
 0.000E-00 3.00CE+02 2.500E+01 3.000E+02 2.500E+01 9.700E-01 5.000E-03
           5.200E-04 3.510E-01 2.280E-01 8.330E-05 3.040E-09 2.074E-01 8.140E-05
-3.130E+03 9.146E+06-1.350E+03 8.917E+14-1.350E+04 2.160E-03 1.310E-00 8.390E-04
 1.410E-00 3.690E-04 5.620E-01 3.710E-04 5.090E-01 2.610E-00-6.750E+04 7.410E-00
-1.386E+05 8.850E-05 4.450E-01
 FIGURE 13.    BED EFFICIENCY VERSUS ELAPSED TIME
  ..............    MODEL 1. RUN 13 (1/4  PELLETS)
 TIME  (MINUTES)
 BED EFFICIENCY

 FIGURE 14.   BULK GAS PHASE TEMPERATURE PROFILES
  ..............    MODEL 1. RUN 13 (1/4  PELLETS)
 TIME-DISTANCE CHARACTERISTIC
 BULK GAS TEMPERATURE  (DEG. C)
 INLET OF REACTOR
 1/3 DOWN THE REACTOR
 2/3 DOWN THE REACTOR
 OUTLET OF THE REACTOR
 FIGURE 15.   NORMALIZED OXYGEN PROFILE
  ..............    MODEL 1. RUN 13 (1/4  PELLETS)
 TIME-DISTANCE CHARACTERISTIC
 NORMALIZED OXYGEN CONCENTRATION
 INLET OF REACTOR
 1/3 DOWN THE REACTOR
 2/3 DOWN THE REACTOR
 OUTLET OF THE REACTOR
 FIGURE 21.   NORMALIZED SULFUR DIOXIDE PROFILE
  ..............    MODEL 1. RUN 13 (1/4  PELLETS)
 TIME-DISTANCE CHARACTERISTIC
```

NORMALIZED SULFUR-DIOXIDE CONCENTRATION
INLET OF REACTOR
1/3 DOWN THE REACTOR
2/3 DOWN THE REACTOR
OUTLET OF THE REACTOR
FIGURE 17. NORMALIZED OXIDATION REACTION SITE
•••• PENETRATION FOR RUN 13 (1/4 PELLETS)
TIME-DISTANCE CHARACTERISTIC
NORMALIZED CUPRIC OXIDE-CUPROUS OXIDE RADIUS
INLET OF REACTOR
1/3 DOWN THE REACTOR
2/3 DOWN THE REACTOR
OUTLET OF THE REACTOR
FIGURE 18. NORMALIZED SULFATION REACTION SITE
•••• PENETRATION FOR RUN 13 (1/4 PELLETS)
TIME-DISTANCE CHARACTERISTIC
NORMALIZED COPPER SULFATE-CUPRIC OXIDE RADIUS
INLET OF REACTOR
1/3 DOWN THE REACTOR
2/3 DOWN THE REACTOR
OUTLET OF THE REACTOR
FIGURE 22. PELLET TEMPERATURE PROFILES
•••••••••••••• MODEL 1. RUN 13 (1/4 PELLETS)
TIME-DISTANCE CHARACTERISTIC
PELLET TEMPERATURE (DEG. C)
INLET OF REACTOR
1/3 DOWN THE REACTOR
2/3 DOWN THE REACTOR
OUTLET OF THE REACTOR

APPENDIX D

ANALYTICAL SOLUTION COMPARISON ALGORITHM IN FORTRAN IV

```
**********  PLACE THESE STATEMENTS AFTER STATEMENT NUMBER  2600  IN   **********
********** THE MAIN PROGRAM OF THE PREDICTOR-CORRECTOR SOLUTION      **********
**********                      ALGORITHM                           **********
C                                                                   **********
C      CHECK ACCURACY OF NUMERICAL SOLUTION                         **********
C                                                                   **********
      CALL COMPAR(Y,NT,NTP)                                         **********


      SUBROUTINE COMPAR(Y,NT,NTP)
C
C      THIS SUBROUTINE COMPARES THE ANALYTICAL AND NUMERICAL SOLUTIONS FOR
C      MODEL 2 (DIFFUSION-CONTROLLED CASE) BY DETERMINING THE FRACTIONAL
C      DIFFERENCE BETWEEN THE COMPUTED AND ANALYTICAL VALUES FOR THE
C      INDEPENDENT VARIABLES (THE NORMALIZED DISTANCE CHARACTERISTIC AND THE
C      NORMALIZED TIME-DISTANCE CHARACTERISTIC).
C
C
C
C      Z IS THE ANALYTICAL VALUE FOR THE NORMALIZED DISTANCE CHARACTERISTIC.
C      ZI IS THE COMPUTED VALUE OF THE NORMALIZED DISTANCE CHARACTERISTIC.
C      T IS THE ANALYTICAL VALUE FOR THE NORMALIZED TIME-DISTANCE
C                                                CHARACTERISTIC.
C      TI IS THE COMPUTED VALUE FOR THE NORMALIZED TIME-DISTANCE
C                                                CHARACTERISTIC.
C      AZ IS THE FRACTIONAL ERROR IN THE DISTANCE CHARACTERISTIC.
C      AT IS THE FRACTIONAL ERROR IN THE TIME-DISTANCE CHARACTERISTIC.
C      VZ IS THE VARIANCE IN THE FRACTIONAL ERROR IN THE DISTANCE
C                                                CHARACTERISTIC.
C      VT IS THE VARIANCE IN THE FRACTIONAL ERROR OF THE TIME-DISTANCE
C                                                   CHARACTERISTIC.
C      Y IS THE MATRIX CONTAINING THE COMPUTED VALUES OF THE DEPENDENT
C                                                      VARIABLES.
C      W IS THE NORMALIZED UNREACTED-SHRINKING-CORE RADIUS.
```

```
C       S IS THE NORMALIZED SULFUR DIOXIDE CONCENTRATION.
C
C
      DIMENSION Y(4,101,6)
      DOUBLE PRECISION U,DZ,DT,AZ,AT,VZ,VT
      COMMON U(42,3,6),N,I,J
      COMMON /MSPC/ DZ,DT
      COMMON /MFPP/ G(50),Q(20),GG(25)
      DATA  AZ,AT,VZ,VT   /0.0D+00,0.0D+00,0.0D+00,0.0D+00/
C
C       FUNCTION STATEMENTS
C
      ATA(W)=C*ATAN2((2.0*W+1.0),(C))
      AL(W)=ALOG(ABS((W-1.0)/SQRT(1.0+W+W**2)))
C
C
      NSTAT=3*NT
      C=-SQRT(3.0)
      K=1
      C1=G(1)*G(3)*G(3)/3.0/(1.0-G(2))/G(4)/G(13)/G(20)
      C2=C1*G(5)*G(15)*1.5/G(2)/G(39)/G(19)*(1.0-G(2))
   10 DO100JI=2,4
      I=(JI-1)*14
      DO100 J=2,NT
      S=Y(JI,J,2)
      W=Y(JI,J,3)
      IF(W.GT.0.9999999) NSTAT=NSTAT-1
      IF(W.GT.0.9999999) GOTO100
      W1=(W**3-1.0)/S+1.0
      AA=SIGN(1.0,W1)
      W1=((AA*W1)**(1.0/3.0))*AA
      Z=ATA(W)
      Z1=ATA(W1)
      Z=Z-Z1+AL(W)
      Z1=AL(W1)
```

```
      Z=Z-Z1
      Z1=Q(10)*ALOG(ABS(S))
      Z1=Z+Z1
      Z=-C1*Z1
      Z1=(I-1)*DZ
      T=-C2*( W1**2 -1.0+2.0*Q(10)*(W**3-1.0)/3.0/S)
      T1=(J-1)*DT*NTP
      IF(K.EQ.2) GOTO50
      AZ=AZ+ABS((Z-Z1)/Z1)
      AT=AT+ABS((T-T1)/T1)
      GOTO100
   50 VZ=VZ+((Z-Z1)/Z1-AZ)**2
      VT=VT+((T-T1)/T1-AT)**2
  100 CONTINUE
      K=K+1
      IF(K.GT.2) GOTO110
      AZ=AZ/NSTAT
      AT=AT/NSTAT
      IF(K.EQ.2) GOTO10
  110 VZ=VZ/(NSTAT-1)
      VT=VT/(NSTAT-1)
      WRITE(6,150)
      WRITE(6,200) AZ,AT,VZ,VT
  150 FORMAT(1H1,27X,'LAMBDA',8X,'THETA'//)
  200 FORMAT(10X,'MEAN ERROR = ',2(2X,D16.8)/,3X,'VARIANCE IN ERROR = ',
     12(2X,D16.8))
      RETURN
      END
```

VITA

The author was born in Thibodaux, Louisiana on July 29.,1946. He attended public schools in Thibodaux and graduated from Thibodaux High School in 1964. After attending Nicholls State College for a year, he transferred to Louisiana State University where he received a B.S. degree in chemical engineering in 1968. In September, 1968 the author entered graduate school at Louisiana State University as a National Aeronautics and Space Administration Trainee and received an M.S. degree in chemical engineering in May 1970. He continued his graduate training and is presently a candidate for the Doctor of Philosophy degree in chemical engineering from Louisiana State University.

In August, 1968, the author married Loraine Sear of Thibodaux, Louisiana. They are anxiously awaiting the arrival of their first child within the next few months.

EXAMINATION AND THESIS REPORT

Candidate: Sidney V. Bourgeois, Jr.

Major Field: Chemical Engineering

Title of Thesis: Transient Analysis of Multiple Solid-fluid Reactions in an Adiabatic Fixed Bed Reactor: Removal of Sulphur Dioxide from Flue Gases

Approved:

Frank R. Groves Jr.
Major Professor and Chairman

Max Goodrich
Dean of the Graduate School

EXAMINING COMMITTEE:

Philip A. Bryant

Albert Herb

O. J. McClatchey

J. A. Blanchard

Leonard C. Adams

Date of Examination:

December 17, 1971